CHARACTERIZATION AND UTILIZATION POTENTIAL OF CLASS F FLY ASHES

A THESIS SUBMITTED TO
THE GRADUATE SCHOOL OF NATURAL AND APPLIED SCIENCES
OF
MIDDLE EAST TECHNICAL UNIVERSITY

BY

İLKER ACAR

IN PARTIAL FULFILLMENT OF THE REQUIREMENTS
FOR
THE DEGREE OF DOCTOR OF PHILOSOPHY
IN
MINING ENGINEERING

JANUARY 2013

Approval of the thesis:

CHARACTERIZATION AND UTILIZATION POTENTIAL OF CLASS F FLY ASHES

submitted by **İLKER ACAR** in partial fulfillment of the requirements for the degree of **Doctor of Philosophy in Mining Engineering Department, Middle East Technical University** by,

Prof. Dr. Canan Özgen   _____
Dean, Graduate School of **Natural and Applied Sciences**

Prof. Dr. Ali İhsan Arol   _____
Head of Department, **Mining Engineering**

Prof. Dr. Mustafa Ümit Atalay   _____
Supervisor, **Mining Engineering Dept., METU**

Examining Committee Members:

Prof. Dr. Gülhan Özbayoğlu   _____
Dean, Faculty of Engineering, Atılım University

Prof. Dr. Mustafa Ümit Atalay   _____
Mining Engineering Dept., METU

Prof. Dr. Özcan Gülsoy   _____
Mining Engineering Dept., Hacettepe University

Prof. Dr. Ali İhsan Arol   _____
Mining Engineering Dept., METU

Prof. Dr. Çetin Hoşten   _____
Mining Engineering Dept., METU

Date: <u>29.01.2013</u>

I hereby declare that all information in this document has been obtained and presented in accordance with academic rules and ethical conduct. I also declare that, as required by these rules and conduct, I have fully cited and referenced all material and results that are not original to this work.

Name, Lastname: **İlker, Acar**

Signature:

ABSTRACT

CHARACTERIZATION AND UTILIZATION POTENTIAL OF CLASS F FLY ASHES

Acar, İlker
Ph.D., Department of Mining Engineering
Supervisor: Prof. Dr. Mustafa Ümit Atalay

January 2013, 125 Pages

In this thesis, characterization of two class F fly ashes (FA) from Çatalağzı and Sugözü thermal power plants were carried out and their utilization potentials in three different fields were examined.

Characterization of sintered samples and determination of their utilization potentials in ceramic industry is the first research area in this thesis. For this purpose, the class F fly ash samples were first pressed into cylindrical specimen without the addition of any organic binders or inorganic additives, and then sintered to form ceramic materials. Effects of sintering temperature and time on sintering characteristics were investigated. In the experiments, the cylindrical specimens were first preheated to $300^{o}C$ for 1 h to remove moisture and any other gases. The specimens were then fired at the temperatures of $1000^{o}C$, $1050^{o}C$, $1100^{o}C$ and $1150^{o}C$ for the sintering times of 0.5, 1.0, 1.5 and 2.0 hours. Heating rate of $10^{o}C/min$ was kept constant throughout the experiments. Quality of sintered samples was evaluated in terms of ceramic specifications such as density, water absorption, porosity, shrinkage and splitting tensile strength. In addition, mineralogical and microstructural changes during sintering were determined with X-ray diffraction (XRD) and scanning electron microscopy (SEM) analyses. According to literature data, better microstructure, the highest density and strength with the lowest porosity, water absorption and shrinkage values are the indications of the optimum sintering conditions. Based on these specifications, Sugözü fly ash gave better results compared to Çatalağzı fly ash, and the optimum conditions were achieved at the sintering temperature of $1150^{o}C$ for the sintering time of 1.5 hours for both samples.

Pozzolanic reactivity of the fly ashes and their utilization potentials in civil engineering applications were also examined in detail during this study. For this purpose, Çatalağzı (CFA) and Sugözü (SFA) fly ashes were first subjected to a specific hydraulic classification process developed at CAER (University of Kentucky, Center for Applied Energy Research) to recover ultrafine fly ash particles. The overflow products with average particle sizes of 5.2 µm for CFA and 4.4 µm for SFA were separated from the respective as-received samples with average particle sizes of 39 µm and 21 µm. After the classification stage, the pozzolanic activities of these ultrafine fly ash fractions (UFA) and as-received samples were examined by preparing a number of mortar (mixture of Portland cement (PC), FA or UFA as partial cement replacement, sand and water) and paste (mixture of PC, FA or UFA as partial cement replacement and water) specimens. Control samples containing only PC were also prepared and tested through the experiments for the comparison of the results. In the mortar experiments, three different PC replacement ratios by FA and UFA (10%, 20% and 30%) were used to examine the effects of FA and UFA samples on the fresh and hardened mortar properties such as water requirement, compressive strength, drying shrinkage and water expansion. These mortar tests indicated that ultrafine fractions of Çatalağzı (CUFA) and Sugözü (SUFA) fly ashes provided more than 10% reduction in water demand compared to the control sample for 30% PC replacement. The mortar cubes containing CUFA and SUFA samples exhibited also higher strength development rates after 14 days compared to the ones with as-received samples and PC only. At the end of the curing age of 112 days, both CUFA and SUFA provided more than 40% increase in compressive strength compared to the control sample for the PC replacement ratios higher than 20%. As a comparison, SUFA gave better results than CUFA in both water demand and compressive strength tests. The mortar bars prepared with the both FA and UFA samples exhibited very

low shrinkage and expansion values. These values decreased generally with increasing PC replacement ratio especially after 14 days. In the paste experiments, thermogravimetric analyses (TGA) of the paste specimens prepared by using only with 20% PC replacement were carried out to determine pozzolanic reactivity of the samples. The difference between the remaining $Ca(OH)_2$ (portlandite) contents in the paste specimens containing the fly ashes and the reference PC paste was used as a measure of pozzolanic reactivity. After 112 days, 68.56% and 62.68% $Ca(OH)_2$ content of PC only pastes were obtained with the pastes containing CUFA and SUFA samples, respectively, corresponding to 11% and 13% more $Ca(OH)_2$ consumptions in reference to the respective as-received samples. X-ray diffraction (XRD) analyses were also performed for comparison of main portlandite peak intensities in the paste specimens containing FA or UFA with those in the PC only paste during cement hydration. According to these XRD analyses, portlandite content in PC/UFA pastes decreased significantly after 14 days compared to the PC only paste. All of these tests and analyses showed that a highly reactive lower cost pozzolan with very fine particle size and higher surface area compared to regular fly ash pozzolans can be produced from both Çatalağzı and Sugözü fly ashes using a relatively simple hydraulic classification technology.

Cenosphere recovery potentials from Çatalağzı and Sugözü fly ashes were also studied in this thesis. Determination of cenosphere content was done under optical microscope by particle counting on the basis of point and area. Based on the point-counting data, CFA and SFA samples originally contain 11.30% and 4.50% cenospheres, respectively. Variations of cenosphere contents in the fly ash samples were examined by using float-sink, screening and air classification tests. The results pointed out that cenosphere contents decreased with decreasing size and increasing density for both samples. According to the float-sink tests, Çatalağzı fly ash has much more floating products and more cenospheres than Sugözü fly ash for the same density interval. Based on the air classification results, cenospheres were concentrated in the underflow products, and cenosphere contents increased with increasing air pressure and decreasing motor speed for both samples. The most efficient cenosphere separation technique among the examined methods was screening. Cenosphere contents of CFA and SFA increased to 21.65% and 11.83%, respectively by only using simple screening through 38 µm.

Keywords: Class F fly ashes, characterization, utilization, sintering, ceramic, classification, ultrafine ash, pozzolan, pozzolanic reactivity, cenosphere.

ÖZ

F SINIFI UÇUCU KÜLLERİN KARAKTERİZASYONU VE KULLANIM POTANSİYELİ

Acar, İlker
Doktora, Maden Mühendisliği Bölümü
Tez Yöneticisi: Prof. Dr. Mustafa Ümit Atalay

Ocak 2013, 125 Sayfa

Bu tez kapsamında, Çatalağzı ve Sugözü termik santrallerinden kaynaklanan F sınıfı iki uçucu külün (FA) karakterizasyonu yapılmış ve bunların üç farklı alandaki kullanım potansiyelleri incelenmiştir.

Sinterlenmiş uçucu kül örneklerinin karakterizasyonu ve bunların seramik endüstrisindeki kullanım potansiyellerinin belirlenmesi bu tez kapsamındaki ilk çalışma alanıdır. Bu amaçla, ilk olarak F sınıfı uçucu kül numuneleri, hiçbir organik bağlayıcı veya inorganik katkı maddesi içermeksizin silindirik şekilde preslenmiş ve daha sonra sinterlenerek seramik formunda malzemeler elde edilmiştir. Sinterleme karakteristikleri, sinterleme sıcaklığı ve zamanına bağlı olarak incelenmiştir. Deneylerde preslenmiş silindirik numuneler öncelikle nem ve diğer gazların uzaklaştırılması amacıyla 300°C'de 1 saat boyunca ön ısıtma işlemine tabi tutulmuştur. Ön ısıtma sonrasında, sinterleme işlemi 1000°C, 1050°C, 1100°C ve 1150°C sıcaklıklar için 0,5, 1,0, 1,5 ve 2,0 saat sinterleme süreleri kullanılarak gerçekleştirilmiştir. Deneyler boyunca ısıtma hızı 10°C/dak olarak sabit tutulmuştur. Sinterlenmiş numunelerin kalitesi, yoğunluk, su emme kapasitesi, porozite, büzülme ve dayanım gibi seramik ölçütlerine göre değerlendirilmiştir. Buna ek olarak, sinterleme sırasında oluşan mineralojik ve mikroyapısal değişimler, sırasıyla X-ışını difraktometresi (XRD) ve taramalı elektron mikroskobu (SEM) yardımıyla belirlenmiştir. Literatür verilerine göre, daha kompakt mikroyapı, en yüksek yoğunluk ve dayanım ile en düşük porozite, su emme ve büzülme değerleri ideal sinterleme koşullarını işaret etmektedir. Bahsi geçen bu kriterlere göre, Sugözü uçucu külü, Çatalağzı uçucu külüne oranla daha iyi sonuçlar vermiştir. Ayrıca her iki numune için de ideal koşullara, 1150°C sinterleme sıcaklığı ve 1,5 saat sinterleme süresi kullanılarak ulaşılmıştır.

Bu çalışma kapsamında, uçucu kül (FA) örneklerinin puzolanik reaktiviteleri ve bunların inşaat mühendisliği uygulamalarındaki kullanım potansiyelleri de ayrıntılı bir şekilde incelenmiştir. Bu amaçla, Çatalağzı (CFA) ve Sugözü (SFA) uçucu külleri, öncelikle çok ince boyuttaki taneciklerin kazanımı amacı ile CAER (University of Kentucky, Center for Applied Energy Research) tarafından geliştirilen özel bir hidrolik sınıflandırma işlemine tabi tutulmuştur. Ortalama parçacık boyutları 39 µm ve 21 µm olan CFA ve SFA numunelerinden, sırasıyla 5,2 µm ve 4,4 µm ortalama parçacık boyutuna sahip olan üst akım ürünleri elde edilmiştir. Hidrolik sınıflandırma aşamasından sonra elde edilen bu çok ince boyuttaki uçucu kül fraksiyonları (UFA) ile esas numunelerin puzolanik aktiviteleri, bir çok harç (Portland çimentosu (PC), kısmi çimento ikamesi olarak FA veya UFA, kum ve sudan meydana gelen karışım) ve macun (PC, kısmi çimento ikamesi olarak FA veya UFA ve sudan meydana gelen karışım) örnekleri hazırlanarak incelenmiştir. Harç deneyleri boyunca elde edilen sonuçların karşılaştırılması amacıyla, FA ve UFA içermeyen kontrol numuneleri hazırlanmış ve test edilmiştir. Harç deneylerinde, FA ve UFA numuneleri üç farklı PC değişim oranında (%10, %20 ve %30) kullanılmış ve bunların su ihtiyacı, basma dayanımı, büzülme ve genleşme gibi taze ve sertleşmiş harç özellikleri üzerindeki etkileri incelenmiştir. Bu harç testleri, çok ince boyuttaki Çatalağzı (CUFA) ve Sugözü (SUFA) uçucu kül fraksiyonlarının, %30 PC değişimi için kontrol numunesine oranla, su ihtiyacında %10'dan fazla bir azalma sağladığını işaret etmiştir. CUFA ve SUFA içeren kübik harç numuneleri basma dayanımında, esas numuneler ve yalnızca PC içeren küplere oranla, 14 günden sonra daha yüksek bir artış hızı sergilemiştir. 112 günün sonunda ise, CUFA ve SUFA numunelerinin her ikisi de kontrol numunesine oranla, %20 ve üzeri PC değişim oranları

için, basma dayanımında %40'dan daha fazla bir artış sağlamıştır. SUFA, su ihtiyacı ve basma dayanımının her ikisi için de, CUFA'ya oranla daha iyi sonuçlar vermiştir. FA ve UFA numuneleri ile hazırlanan harç çubuklar, çok düşük değerlerde büzülme ve genleşme göstermişlerdir. Bu değerler, genellikle 14 günden sonra, artan PC değişim oranları ile azalmaktadır. Macun deneylerinde, FA ve UFA numunelerinin puzolanik reaktivitelerinin belirlenmesi için, yalnızca %20 PC değişim oranı ile hazırlanan macun örneklerinin termogravimetrik analizleri (TGA) yapılmıştır. Bu deneylerde, uçucu küller ve yalnızca PC katkısı ile hazırlanan macun örneklerindeki $Ca(OH)_2$ (portlandit) içeriğindeki fark, puzolanik reaktivitenin ölçüsü olarak kullanılmıştır. 112 günün sonunda, CUFA ve SUFA numuneleri içeren macun örneklerindeki $Ca(OH)_2$ içeriği, yalnızca PC içeren örneğe oranla, sırasıyla %68,56 ve %62,68 olarak bulunmuştur. Bu değerler de esas numunelere oranla, sırasıyla %11 ve %13 daha fazla $Ca(OH)_2$ tüketimine tekabül etmektedir. Uçucu küller ve yalnızca PC katkısı ile hazırlanan bu macun örneklerindeki portlandit içeriğindeki değişimin kıyaslanması amacıyla, aynı zamanda bu örneklerin X-ışını difraktometre analizleri (XRD) yapılmıştır. Bu XRD analizlerine göre, PC/UFA macun örneklerindeki portlandit içeriği yalnızca PC içerene oranla, 14 günden sonra önemli bir azalış göstermiştir. Tüm bu test ve analizlerden elde edilen sonuçlar, Çatalağzı ve Sugözü uçucu küllerinden, basit bir hidrolik sınıflandırma teknolojisi ile, sıradan uçucu kül puzolanlarından daha yüksek reaktivite ve yüzey alanına ve son derece küçük parçacık boyutuna sahip ucuz bir puzolanın elde edilebileceğini göstermiştir.

Çatalağzı ve Sugözü uçucu küllerinden senosfer kazanım potansiyeli de bu tez kapsamında araştırılmıştır. Senosfer içeriğinin belirlenmesi, parçacıkların optik mikroskop altında nokta ve alan bazında sayımıyla gerçekleştirilmiştir. Noktasal baz verilerine göre, CFA ve SFA numuneleri sırasıyla %11,30 ve %4,50 senosfer içeriğine sahiptir. Uçucu küllerdeki senosfer içeriğinin değişimi, yüzdürme-batırma, eleme ve havalı sınıflandırma testleri kullanılarak incelenmiştir. Elde edilen sonuçlar, senosfer içeriğinin, parçacık boyutundaki küçülme ve yoğunluktaki artış ile orantılı olarak azaldığını göstermektedir. Yüzdürme-batırma testlerine göre, Çatalağzı uçucu külü aynı yoğunluk aralığında, Sugözü uçucu külüne oranla çok daha fazla yüzen malzeme ve daha fazla senosfer içermektedir. Havalı sınıflandırma test sonuçlarına dayanarak, her iki numune için de senosferlerin alt-akım ürününde konsantre olduğu ve senosfer içeriği, hava basıncındaki artış ve motor hızındaki azalma ile orantılı olarak artmıştır. Eleme, incelenen bu metotlar arasındaki en etkin senosfer kazanım tekniğidir. CFA ve SFA'nın senosfer içerikleri, yalnızca 38 μm'lik bir elek kullanarak sırasıyla %21,65 ve %11,83'e yükselmiştir.

Anahtar Kelimeler: F sınıfı uçucu küller, karakterizasyon, kullanım, sinterleme, seramik, sınıflandırma, ultraince kül, puzolan, puzolanik reaktivite, senosfer.

TO MY FAMILY

ACKNOWLEDGEMENTS

TABLE OF CONTENTS

LIST OF TABLES

TABLES

FIGURES

LIST OF ABREVIATIONS

^oC	Degree Celsius
CAER	Center for Applied Energy Research, University of Kentucky
CFA	Çatalağzı fly ash
CUFA	Çatalağzı ultrafine ash
FA	Fly ash
GeoE	Department of Geological Engineering, METU
h	Hour
HUME	Hacettepe University, Department of Mining Engineering
ICP-MS	Inductively coupled plasma-mass spectroscopy
MetE	Department of Metallurgical and Materials Engineering, METU
min	Minute
MinE	Department of Mining Engineering, METU
mm	Millimeter
MPa	Megapascal
μm	Micrometer
O/F	Overflow
PC	Portland cement
psi	Pounds per square inch
rpm	Revolutions per minute
SCFA	Sintered Çatalağzı fly ash
SEM	Scanning electron microscopy
SFA	Sugözü fly ash
SP	Superplasticizer
SSFA	Sintered Sugözü fly ash
STS	Splitting tensile strength
SUFA	Sugözü ultrafine ash
TGA	Thermogravimetric analysis
UFA	Ultrafine ash
U/F	Underflow
XRD	X-ray diffraction
XRF	X-ray fluorescence

CHAPTER 1

INTRODUCTION

1.1 Field of research area

Coal has become a major source of energy with increasing demands to the generation of more electric power for more than eighty years although developed countries are nowadays trying to increase renewable energy (solar, wind and geothermal energy) usage in daily life (Erol *et al.*, 2007). According to US Energy Information Administration, in the USA, 42.3% of produced electricity was provided by coal combustion in 2011 (USEIA, 2012). Similarly, in 2010, 54.8% of total electricity production for 27 countries in the European Union was based on combustible fuel (EC, 2012). According to Turkish Ministry of Energy and Natural Resources, in 2011, 28.2% of total electricity production in Turkey was from coal combustion. Whereas 40.5% of worlwide electricity production was based on coal in 2008, it is expected to increase to 43% by the year 2035 because of availability and low cost of coal (EUAS, 2011).

Increasing energy demands for industrialization and desirable properties of coal like abundance, availability and cost effectiveness have brought about construction of many coal fired thermal power plants since 1920s. Thermal power plants exhaust huge amount of ash (mostly fly ash and low amount of bottom ash) and related by-products (gypsum and boiler slag) as a result of coal combustion. Today, worldwide annual production of coal ash is around 600 million tones, 75-80% of which is constituted by coal fly ash. Thus, the amount of combusted waste (mostly fly ash) resulting from factories and thermal power plants has been increasing throughout the world, and the disposal of this large amount of waste has resulted in serious environmental problems with technological and economic effects (Erol *et al.*, 2007; Ahmaruzzaman, 2010).

According to the American Coal Ash Association (ACAA) and European Coal Combustion Products Association (ECOBA), in 2010, total fly ash production in the USA was 67.7 million tons, while, in 2009, this fly ash production in Europe (EU-15 Countries) was 34.3 million tones. For the mentioned years, 37.9% of total produced fly ash was used in various applications in the USA, whereas this utilization was 44% in Europe (EU-15 Countries), the majority of which corresponded to cement and concrete industry, which is the main user of coal fly ash (ACAA, 2011; ECOBA, 2010). In addition to cement and concrete industry, fly ash has a number of uses and utilization areas including structural fill and cover material, waste solidification and stabilization, ceramic industry, metallurgy and valuable metal extraction, agriculture, environmental engineering and reclamation of damaged areas (Tuzcu, 2005). On the other hand, production rate of fly ash is obviously much more than its consumption despite the positive uses and utilization areas of fly ash mentioned above. Thus, for the remaining material, disposal practices are used involving holding ponds, lagoons, landfills and slag heaps, all of which can be considered as environmentally undesirable and a non-productive use of land resources. All of these factors have motivated researchers to look for alternative application areas for fly ash (Iyer and Scott, 2001).

1.2 Brief information about the application areas

1.2.1 Sintering of fly ash

The sintering process is a widely used technique in the production of conventional ceramic materials. Sintered ceramics have found a number of application areas in the construction sector. The ceramic industry demands large amounts of natural resources in the process as raw materials such as quartz, feldspar and clay. For instance, a medium size ceramic factory needs approximately 400 tons of natural raw materials in a day. It is vital important to supply these raw materials in sufficient amount to the ceramic industry. Thus, this situation has prompted researchers to look for alternative raw materials for the

ceramic industry due to economic and environmental reasons like the large amounts of raw materials necessity and the conservation of the natural sources (Erol *et al.*, 2008a).

Fly ash can be considered as a potential raw material for the ceramic industry because of its suitable chemical composition and physical state. Fly ash mainly consists of SiO_2, Al_2O_3, CaO and Fe_2O_3, which are the building stone of ceramic materials. Furthermore, very fine size of fly ash eliminates the grinding process and its high cost. In other words, it can be directly used into ceramic pastes with almost no pretreatment. In addition to these superior properties of fly ash, both consumption of natural raw materials and environmental pollution can be reduced using this waste product in the ceramic industry. As all of these factors are considered, it can be easily said that fly ash can be a good candidate for the ceramic industry as a raw material resource. Nevertheless, fly ash must be used without any material like organic binders or inorganic additives. Otherwise, the production process would not be economic and environmentally friendly (Erol *et al.*, 2008a).

1.2.2 Fly ash utilization as a high-quality pozzolan

Fly ash has been widely used in construction industry as a supplementary cementitious material due to its superior properties like contribution to the fresh concrete workability, microstructure formation and improvement in long term mechanical and durability properties. Utilization of fly ash in civil engineering applications also reduces cost of the concrete materials, and conserves energy and natural resources since less raw material is needed in the process with the use of fly ash. Furthermore, a considerable decrease in CO_2 emissions can be achieved in cement production. In addition to these benefits, less environmental pollution occurs in fly ash disposal area with the use of this waste in cement and concrete industry (Zeng *et al.*, 2011; Langan *et al.*, 2002).

According to ASTM Standard C 618, fly ashes are classified into two chemical types, Class F and Class C, in terms of their industrial applications. The low calcium Class F fly ashes including high amount of silica, alumina and iron oxide ($SiO_2+Al_2O_3+Fe_2O_3 \geq 70\%$) are generally resulted from the burning of higher-rank bituminous coals and anthracites. On the other hand, the Class C fly ashes ($SiO_2+Al_2O_3+Fe_2O_3 \geq 50\%$) are mostly produced from the burning of low-rank lignites and sub-bituminous coals (Vassilev and Vassileva, 2007). The Class F fly ashes are pozzolanic in nature, meaning that they form strength developing products (pozzolanic reactivity) when reacted with $Ca(OH)_2$ and water. For this reason, they are used in combination with Portland cement, producing $Ca(OH)_2$ during its hydration. These fly ashes provide various positive properties when they are used in concrete as a cement replacement, including low heat of hydration and high durability. In addition to these positive effects, they also provide concrete strength by pozzolanic and filler effects (Nochaiya *et al.*, 2010).

Despite all of these benefits of fly ash explained above, it has also some disadvantages related with using this material especially for early stages of aging because of its relatively low surface area and accompanying pozzolanic activity. In the early age, since pozzolanic reactivity of fly ash is relatively slow, the strength of concrete with a high volume of fly ash as a partial cement replacement is much lower than that of control concrete containing only cement. This pozzolonic reaction between fly ash and $Ca(OH)_2$ resulted from cement hydration does not provide a significant improvement to concrete properties up to several weeks after the start of hydration, bringing about slow strength development and inadequate strength although concrete may have higher strength and durability in the longer term compared to the control concrete (Langan *et al.*, 2002; Nochaiya *et al.*, 2010).

Silica fume and air-classified fly ash have been used for years to overcome the adverse effects of fly ash on the early age properties due to their very fine particle size and much higher surface area, especially for silica fume. However, limited supply and high cost of these materials have kept usage relatively low (Rathbone, 2004). Also, air classification is not feasible in most applications since it requires perfectly dry feed. On the other hand, it is not an easy task to achieve very fine size with conventional hydraulic classification systems. A special hydraulic classification technique may be used to recover very fine particle size with high surface area from fly ash, and then this ultrafine ash can be used as a high-performance pozzolan.

1.2.3 Cenosphere recovery potential from fly ash

Cenospheres, present in coal fly ash, are lightweight, thin-walled, inert and hollow ceramic microspheres. They are made up of silica, alumina and iron. Their quantity in fly ash depending on numerous factors related to coal characteristics and combustion type varies in the range 0.01-4.8%, and the common occurrence is 0.3-1.5%. Cenospheres gain their hollow spherical shape during cooling and solidifying around a trapped gas. This gas can be mostly CO_2 and N_2, and traces of CO, O_2 and H_2O. Mineralogical composition of cenospheres generally includes aluminosilicate glass, mullite, quartz, calcite, Fe oxides, Ca silicates and sulphates. The diameter of cenosphere varies from 5 to 500 μm, as the most common dimension is in the range 20-250 μm. Density ranges from 0.2 to 0.5 g/cm^3 and shell wall thickness is in the range 2-10 μm (Vassilev *et al.*, 2004; Kolay and Singh, 2001).

Cenospheres have a number of application areas because of their superior properties such as sphericity, low density, high strength, high energy absorption, protection against electromagnetic interference, inertness to some acids and high fusion temperatures. These application areas include ceramics, plastics, construction, recreation, automotive and energy and technology. Cenospheres are mostly used as lightweight fillers in these sectors due to improved properties and reduced cost of final product (Vassilev *et al.*, 2004; Kolay and Singh, 2001).

Since formation of cenospheres need specific conditions, the world average of cenosphere content is very low. Therefore, only some fly ashes include cenospheres. There are mainly two methods for cenosphere recovery from fly ashes, namely simple sedimentation and flotation. In the first method, cenospheres are recovered using their natural buoyancy in water because of their low bulk density. The other method for cenosphere recovery is flotation, one of the most widely used methods in mineral processing (Alcala *et al.*, 1987). Final product is obtained after cenosphere concentrate is subjected to drying and size classification (Kruger, 1996).

1.3 Aim and objectives of the thesis

The overall aim of this thesis was characterization of the fly ash samples in many ways by using a number of physical, chemical, microstructural and mechanical methods and investigation of their utilization potentials in three different fields. In order to do this, it was desired to set the following particular objectives:

I.   All available literature review to understand the range of methods used in the research areas

II. Physical, chemical and microstructural characterization of the fly ashes to explain their behavior in the research areas

III. Designation of initial experiments to determine the processing conditions to be used in the research areas

IV. Carrying out of the specific tests to:

    i.   Explain strength gaining mechanism and the relationship between sintered body density and strength in sintering

    ii. Evaluate utilization possibility of the fly ashes as high quality pozzolans in cement and concrete industry and determine their pozzolanic reactivity

    iii. Determine cenosphere recovery potential from the samples by using various processing techniques

1.4 Outline of the thesis

➢ Chapter 2 reviews all available background literature about characterization and utilization of fly ashes. Fly ash utilizations in the research fields examined in this thesis were also explained more specifically in this chapter.

➢ Chapter 3 gives the complete characterization of the fly ash samples used in this thesis.

➢ Chapter 4 explains all the methods used for the research fields examined in this thesis.

➢ Chapter 5 gives the overall results on investigation of sintering properties, pozzolanic reactivity assessment and cenosphere recovery potential of the samples. In this chapter, these results were also discussed in detail.

➢ Chapter 6 provides conclusions about the all results obtained from the studies of specific research areas.

CHAPTER 2

LITERATURE SURVEY

2.1 Coal fly ash

2.1.1 Definitions of coal fly ashes

Fly ash can be defined as "the main waste residue produced during the pulverized coal combustion and collected by electrostatic precipitators in a thermo-electric power station" (Vassilev *et al.*, 2003). According to ASTM C 618 standard, fly ash is defined as "the finely divided residue that results from the combustion of ground or powdered coal and that is transported by flue gasses" (ASTM, 2012). In another definition by BS EN 450-1 standard, fly ash can be described as "fine powder of mainly spherical, glassy particles, derived from burning of pulverized coal, with or without co-combustion materials, which has pozzolanic properties and consists essentially of SiO_2 and Al_2O_3, the content of reactive SiO_2 as defined and described in EN 197-1 being at least 25% by mass" (BSI, 2005). Coal properties, combustion conditions and storage methods determine the mineralogy, chemistry and physical properties of fly ash. Therefore, fly ash derived from burning of different type of coal (e.g., anthracite, bituminous and lignite coal) has different chemical compositions and physical properties (Jala and Goyal, 2006).

2.1.2 Characterization of coal fly ash

2.1.2.1 Physical properties

Physically, fly ash forms as fine particles of mainly spherical in shape. Fly ash has a wide-range of particle size varying from sub-micron to 500 µm. Specific gravity of fly ash varies in the range 2.1-2.6 g/cm^3 while bulk density ranges from 1 to 1.8 g/cm^3. Other desirable physical properties like shear strength and permeability increase fly ash usage in civil engineering applications. The color of fly ash can be varied from water-white to yellow orange to deep red or brown to opaque depending on its iron oxide content. Fly ash can also be used as a material for top soil in surface mine lands because of its dominance of silt size particles, leading to improvements in physical conditions of soil especially water holding capacity (Jala and Goyal, 2006).

2.1.2.2 Chemical composition

Chemically, fly ash includes major (>1%), minor (1-0.1%) and trace (<0.1%) elements. Since it is a combusted material, the major and minor elements are present as oxides. In order of decreasing amounts, these elements are commonly O, Si, Al, Ca, Fe, C, K, Mg, H, Na, Ti, N, P, and Ba. The other elements are mostly present in trace amounts in fly ash. The elements in fly ash do not exist in free form. Instead, they generally occur in both organic and inorganic matter, and each element has strong affinities with certain minerals and phases in fly ash (Vassilev and Vassileva, 2007). Sulfur content of the parent coal affects the pH of fly ash which is in the range 4.5-12.0. Generally, anthracite including high sulfur content forms acidic ash, whereas lignites containing low sulfur and high calcium contents produce alkaline ash (Jala and Goyal, 2006).

2.1.2.3 Mineralogical composition

Fly ashes include forming (>10%), major (1-10%), minor (0.1-1%) and accessory (<0.1%) minerals and phases. These minerals and phases in fly ashes except accessory species are mostly glass, mullite, quartz, char, hematite-magnetite, anhydritre-gypsum, feldspars, lime-portlandite, clay and mica minerals,

5

cristobalite-tridymite, calcite-ankerite, corundum, jarosite, and some Ca and Ca-Mg silicates. A number of trace and minor elements may also form accessory minerals and phases in fly ashes. The minerals and phases in fly ashes can be classified as original (primary) or newly formed (secondary and tertiary) in terms of their formations. Primary species are original coal minerals and phases in which no phase transformations occur during combustion. These species are generally materials with relatively high melting temperatures such as some stable silicates, oxides, sulfates, phosphates and carbonates. Secondary species are new phases formed during combustion. These are various silicates, oxides, sulfates, carbonates, sulfides, glass and char. Tertiary species are new minerals or phases formed during transport and storage of fly ash. These species are portlandite, brucite, gypsum, iron sulfate, calcite, dolomite, iron and aluminum hydroxides and amorphous material (Vassilev and Vassileva, 2007).

2.1.3 Classification of fly ash

In literature, there are various approaches used to classify coal fly ashes for their industrial applications. Today, one of the most widely used methods for worldwide fly ash classification is based on ASTM Standard C 618. According to this standard, fly ashes are classified into two chemical types, namely Class F and Class C. The low calcium Class F fly ashes including high amount of silica, alumina and iron oxide ($SiO_2+Al_2O_3+Fe_2O_3 \geq 70\%$) are generally resulted from the burning of higher-rank bituminous coals and anthracites. These fly ashes show pozzolanic property which means that they become hard when reacted with $Ca(OH)_2$ and water. However, the Class C fly ashes ($SiO_2+Al_2O_3+Fe_2O_3 \geq 50\%$) are mostly produced from the burning of low-rank lignites and sub-bituminous coals. This type of fly ashes shows pozzolanic and also cementitious properties due to its high calcium content. In other words, calcium oxide content which is varied by the combusted coal types is the main difference between Class F and Class C fly ashes (Vassilev and Vassileva, 2007). Table 2.1 summarizes chemical and physical requirements based on ASTM Standard C 618 for use in concrete (ASTM, 2012). According to the table, other important chemical and physical requirements are SO_3 contents, moisture content, loss on ignition, particle size and some criteria used in cement and concrete industry.

Table 2. 1 Classification of fly ash based on ASTM C 618 (ASTM, 2012)

Chemical requirements		Class	
		F	C
$SiO_2+Al_2O_3+Fe_2O_3$, min, %		70.0	50.0
SO_3, max, %		5.0	5.0
Moisture content, max, %		3.0	3.0
Loss on ignition, max, %		6.0	6.0
Physical requirements		F	C
Amount retained when wet sieved on 45 µm (No. 325) sieve, max, %		34	34
Strength activity index	With Portland cement at 7 days, min, % of control	75	75
	With Portland cement at 28 days, min, % of control	75	75
Water requirement, max, % of control		105	105
Autoclave expansion or contraction, max, %		0.8	0.8

Fly ashes can also be classified into three main categories based on the CaO concentrations, namely Type F (<8% CaO), Type CI (8-20% CaO), and Type CH (>20% CaO). According to the LOI contents, fly ashes are grouped into four types which are Type F (≤8% and up to 12% based on performance) and

Types C, CI and CH (≤6%). Another approach by the United Nations classifies fly ashes into four chemical groups in terms of some chemical and physical characteristics (Vassilev and Vassileva, 2007). These are:

    I.   Silico-aluminate fly ashes containing $SiO_2/Al_2O_3 \geq 2$ and CaO <15%

    II.   Alumino-silicate fly ashes including $SiO_2/Al_2O_3 < 2$, CaO <15% and $SO_3 < 3\%$

    III.   Lime-sulfate fly ashes with CaO>15% and $SO_3 > 3\%$

    IV.   Basic fly ashes with CaO>15% and $SO_3 < 3\%$

The European Union countries use EN 450 standard for fly ash classification. According to this standard, fly ashes are classified in terms of fineness (≤40.0% retained on 45 μm), LOI (≤5.0%), relative density, SO_3 (≤3.0%), free CaO (≤1.0%), total CaO (≤10.0% only for sub-bituminous fly ashes), reactive silica (≤25%), chloride (≤0.10%) and some characteristics used in cement and concrete industry such as water requirement, strength activity index and soundness (Vassilev and Vassileva, 2007).

2.1.4 Utilization of coal fly ash

Fly ash utilization has increased in recent years due to many economic, technologic and environmental reasons. First of all, lower disposal costs and less area requirement for disposal are provided. Secondly, less environmental pollution occurs with the utilization of fly ash in many applications. Thirdly, fly ash can be used as a partial replacement material for some important natural resources. Another important advantage is that fly ash is also used as an essential additive in some sector to improve the properties of final products, such as special pozzolanic additive in cement and concrete industry (Ahmaruzzaman, 2010).

According to the American Coal Ash Association (ACAA) and European Coal Combustion Products Association (ECOBA), in 2010, 37.9% of total produced fly ash was used in various applications in the USA, while, in 2009, this utilization was 44% in Europe (EU-15 Countries), the majority of which corresponded to cement and concrete industry, which is the main user of coal fly ash (ACAA, 2011; ECOBA, 2010). In addition to cement and concrete industry, fly ash has a number of uses and utilization areas including structural fill and cover material, roadway and pavement utilization, construction materials as a light weight aggregate, waste solidification and stabilization, ceramic industry, metallurgy and valuable metal extraction, agriculture and water and environmental improvement (Ahmaruzzaman, 2010; Tuzcu, 2005). Table 2.2 shows coal combustion products and utilization data by application areas in 2010 in the USA (ACAA, 2011).

2.1.4.1 Fly ash utilization in cement and concrete industry

Fly ash has been widely used in cement and concrete industry as a supplementary cementitious material. There are three main purposes of fly ash utilization in cement. First of all, fly ash can be used as partial replacement of cement in concrete. Secondly, it can also be utilized as a pozzolanic material in the production of pozzolanic cements. Thirdly, fly ash retards setting of cement as a replacement of gypsum (Ahmaruzzaman, 2010).

There are many beneficial effects of fly ash utilization in cement and concrete industry. Fly ash improves properties of the concrete products like the fresh concrete workability and microstructure formation, and it provides better long term mechanical and durability properties. In addition, fly ash reduces cost of the concrete materials and conserves energy and natural resources due to less raw material requirement in the process. Furthermore, a considerable decrease in CO_2 emissions can be achieved in cement production

with the utilization of fly ash. Also, less environmental pollution occurs in fly ash disposal area with the use of this waste in construction industry (Zeng *et al.*, 2011; Langan *et al.*, 2002).

Table 2. 2 Utilization of coal combustion products by application areas in 2010 in the USA (ACAA, 2011)

Beneficial utilization versus production (short tons)					
	Fly ash	**Bottom ash**	**Boiler slag**	**FGD product**	**FBC ash**
Total production	67,700,000	17,800,000	2,332,944	32,080,506	10,267,914
Total utilization	25,723,217	7,541,732	1,418,996	11,921,473	8,732,008
Use to production rate (%)	37.90	42.30	60.80	37.16	85.00
Utilization areas					
Concrete/Concrete products/Grout	11,016,097	615,332	0	37,892	0
Blended Cement/ Clinker feed	2,045,797	949,183	3,000	1,135,211	0
Flowable fill	135,321	52,414	0	13,998	0
Structural fills/ Embankments	4,675,992	3,124,549	78,647	1,237,030	0
Road base/Sub-base	242,952	715,357	3,128	3,018	0
Soil Modification/ Stabilization	785,552	162,065	0	19,189	0
Snow and ice control	0	549,520	41,194	0	0
Blasting grit/ Roofing granules	86,484	19,914	1,257,571	0	0
Mining applications	2,399,837	528,881	0	1,134,533	8,660,408
Gypsum panel products	109	0	0	7,661,527	0
Waste stabilization/ Solidification	3,528,825	41,233	0	39,283	71,600
Agriculture	22,220	4,674	0	481,827	0
Aggregate	6,726	555,031	27,155	0	0
Miscellaneous/Other	1,047,305	223,579	8,301	157,965	0

Utilization of class C fly ash seems to be quite suitable in Portland cement due to its high calcium and reactive glass contents. High-strength concretes can be made using class C fly ash and plasticizers. Class F fly ashes can also be used as raw material for the production of high-strength and high-performance concrete. Spherical shape of fly ash particles enhance pumpability of concrete and also result in a decrease in permeability and better packing. In addition, fly ash provides more dense paste and pozzolanic reaction. A lower heat of hydration compared to Portland cement control is achieved in the production of mass concrete by using especially class F fly ash with high cement replacement. Cement replacement ratios are generally 15-25% and 25-40% for class F and class C fly ashes, respectively. This replacement ratio can be increased to 75% for class C fly ash in the construction of parking lots, driveways and streets. Today, chemical admixtures are essential components in concrete making since they decrease water demand substantially without loss of workability. The hardening rates of fly ash can be accelerated using these chemicals to obtain good performance (Ahmaruzzaman, 2010).

High volume utilization of class C and class F fly ash for the construction of roadway paving was reported by Naik *et al.*, 1994. According to the results, class C and class F fly ashes can be utilized in high volume for the production of high-quality pavements with excellent performance. Siddique, 2004 investigated performance characteristics of high volume class F fly ash in concrete. The test results indicated that class F fly ash utilization can be feasible up to 50% of cement replacement in the construction of precast elements and reinforced concrete. The use of fly ash in concrete dam construction was studied by Pei-wei *et al.*, 2007. Based on the results, for the curing ages of 90 days, higher compressive strengths of dam concrete with 50% of fly ash were achieved compared to those with 30% of fly ash or cement control. Also, fly ash decreased shrinkage and expansive strain in significant amount. Coal combustion by-products (fly ash and bottom ash) utilization with stone quarries waste for the construction of lightweight concrete was studied by Nisnevich *et al.*, 2006 at the Research Authority of The College of Judea and Samaria (Ariel, Israel). According to the test results, the developed technology can be used for production of structural lightweight concrete with high enough strength and density.

2.1.4.2 Utilization of fly ash as lightweight aggregate

Utilization of fly ash as a lightweight aggregate provides important advantages to the manufacturer. The main advantage is the reduction in freight costs of shipping of the finished product compared to natural raw materials. Weight becomes more important if fly ash is used in brick manufacturing since fly ash bricks are approximately two-third lighter than conventional clay-fired bricks. Secondly, with the utilization of low cost fly ash in the process, environmental pollution can be decreased due to reduced solid waste and dust in the nature. Clay-fly ash bricks with better physical and mechanical properties like porosity, water absorption and compressive strength can be produced compared to those of clay bricks (Ahmaruzzaman, 2010).

The effect of fly ash with high clay replacement on brick's properties was investigated by Lingling *et al.*, 2005. Based on the test results, the fired bricks with high compressive strength, low water absorption, no cracking due to lime, no frost and high resistance to frost-melting were produced with the utilization of high volume ratio of fly ash. Utilization possibility of the mixtures with fly ash, sand and hydrated lime in the production of light weight bricks was reported by Cicek and Tanriverdi, 2007. The obtained results indicated that lightweight bricks with good quality can be produced using the mixtures with fly ash, sand and hydrated lime. In addition to brick products, fly ash can also be used in the production of lightweight roofing materials like rigid roofing tiles. The fly ash roofing tiles are lighter than the conventional ones and they have very good fire-proof property (class A fire-rating). This class A fire-rating property makes the fly ash roofing tiles a good candidate for the utilization in high fire danger areas (Ahmaruzzaman, 2010).

2.1.4.3 Fly ash use in road sub-base

Roadway embankment is another important utilization area of fly ash. Fly ashes have been largely utilized as raw material in soil stabilization, aggregate filler, pavement additive and mineral filler. Fly ash has several advantages as a soil stabilizer along roadway embankments. Firstly, fly ash can be used as plentiful supplies if fill and cover material are scarce in the area. However, thermal power plants should be close. Otherwise, this process would be uneconomic due to the high transportation cost. Availability and positive physical properties of fly ash are the other important advantages for soil stabilization. In addition, fly ash has generally higher shear strength, which is one of the most important properties for the fly ash utilization in soil stabilization, compared to the strength of soils generally used for embankments. Fly ash utilization in road works provides approximately 10-20% profit in construction cost (Ahmaruzzaman, 2010).

2.1.4.4 Fly ash utilization in mine backfill

Utilization of fly ash in mine back filling seems to be a good option for the power plants located near the coal mine. Underground mine back filling with fly ash is technically feasible and has large potentials for the areas where the cover material is scarce. Fly ash can also be used as land reclamation material for open cast mine. In the present day, fly ash is generally used in closed underground mining sites with the grout injection method. The main purpose of the injection process is to reduce acid mine drainage (AMD). Fly ash decreases AMD through two mechanisms, namely neutralization of existing AMD due to its alkaline nature and inhibition of AMD occurrence by preventing contact between water and pyritic materials (Ahmaruzzaman, 2010).

Prevention of AMD occurrence with fly ash addition to sulfide-rich residues in non-saturated column experiments was reported by Perez-Lopez, *et al.*, 2007. Based on the test results, a great improvement in the quality of the leachates was achieved due to pyrite dissolution at high pH as a consequence of the leaching of fly ash. Utilization potential of lignite fly ash for preventing acid generation from sulfidic tailings was investigated by Xenidis *et al.*, 2002. The test results indicated that increasing in pH of the leachates at values of 8.6-10.0 and reduction in the dissolved concentrations of contaminants, especially for Zn and Mn, were obtained with fly ash utilization.

2.1.4.5 Utilization of fly ash in agriculture

Effects of fly ash utilization on soil properties have been investigated by a numerous researchers. Acidic or alkaline nature of fly ashes depending on the coal types can be used to buffer pH of the soil. Fly ash also increases the electrical conductivity of soil. High lime contents in some fly ashes, especially lignite fly ash, provide release of nutrients in the soil such as S, B and Mo in the form and amount beneficial to crop plants. Fly ash utilization for the purposes of increasing the pH of acidic soils and improving soil texture was studied for agronomic benefits and improving the nutrient status of soil. One of the major limiting factors for fly ash use in agriculture is boron toxicity. Adverse effects of boron on soil microbes can be prevented by using a readily oxidizable organic substrate such as a highly carbonaceous acidic material. Promising changes in the soil properties, pH increasing and improved crop yield can be obtained using mixed application of fly ash, paper factory sludge and farmyard manure (Jala and Goyal, 2006).

2.1.4.6 Synthesis of zeolites from fly ash

Zeolites are alumino-silicate minerals, consisting of group I or II elements as counter ions. $[SiO_4]^{4-}$ and $[AlO_4]^{5-}$ tetrahedra constitute the main framework including a three-dimensional network with lots of voids and open spaces. These voids and open spaces provide the main property, adsorption of molecules in the huge internal channels. The substitution of Si^{4+} by Al^{3+} in the tetrahedra results in a negative charge of the structure, causing an increase in cation exchange capacity (CEC). As a result of their unique structure, zeolites have been widely used in ion exchange of Na^+, K^+ and Ca^{2+} for other cations on the basis of ion selectivity, selective adsorption of specific gas molecules and water adsorption (Querol *et al.*, 2002).

The methodology for synthesis of zeolite is based on dissolution of Al-Si phases in fly ashes with alkaline solutions (mainly NaOH and KOH solutions) and the subsequent precipitation of zeolitic material. In this process, the main limitation is the necessity of relatively high temperatures (125-200°C) to dissolve Si and Al from the fly ash particles. In literature, different hydrothermal activation methods have been applied to synthesize different types of zeolites from fly ashes (Querol *et al.*, 2002).

2.1.4.7 Uses of fly ashes as adsorbents for waste management

A considerable body of literature exists on fly ash utilization as adsorbents for cleaning of flue gas and removal of organic and inorganic components, toxic metals and dyes from wastewater. Activated carbon has largely been used to oxidize reduced sulfur compounds due to its superior adsorptive property. On the

other hand, for the utilization of large scale applications, it is too costly. Coal fly ash can be used as a cheap adsorbent for dry type flue gas desulfurization (FGD). Some promising results have been obtained for recycling of fly ash in the desulfurization process (Ahmaruzzaman, 2010). Adsorption properties of fly ash for NO_x removal from flue gases were investigated by Lu and Do, 1991. According to the test results, adsorption capacity of fly ash particles can be improved by using controlled gasification of the unburned carbon.

Fly ashes have wide variety of applications in wastewater treatment due to their suitable physical properties and chemical composition. Furthermore, the alkaline nature provides neutralizing property to the fly ash. In this process, it is vital important to adjust the pH of wastewater by using lime and sodium hydroxide to maximize the adsorption efficiency (Ahmaruzzaman, 2010).

2.1.4.8 Utilization of fly ash in composite materials

Utilization of fly ash in plastic and metal composites, especially in aluminum, has been increased in recent years. Competitive products can be obtained with similar or higher hardness and elastic moduli and improved wear abrasive resistance by using aluminum fly ash composites which are considered as potential materials for components like pulleys, oil pans, intake manifolds and valve covers. Better wear resistance of nickel fly ash composite coatings was obtained compared to plain nickel coatings. It was considered that better wear resistance property probably resulted from the excellent bonding between fly ash particles and the nickel (Iyer and Scott, 2001). Due to their hollow spherical particles, cenosphere, some fly ashes can also be used to reduce the density of metal composites with better insulation properties, reduced shrinkage and warpage values (Wandell, 1996).

2.1.4.9 Production of glass-like materials from fly ash

Fly ash mainly consists of SiO_2, Al_2O_3, CaO and Fe_2O_3 depending on coal types. These oxide resources have been generally accepted as a low cost raw material for the production of glass and glass-ceramic. In addition to its suitable chemical composition, since fly ash is physically presented as fine particles, high cost grinding operation is eliminated in most cases. Utilization of fly ash in glass and glass-ceramic production includes three major advantages. Firstly, a zero cost raw material is used in the process if the power plant is close to production unit. Secondly, natural resources can be conserved by fly ash use as a raw material. Thirdly, environmental pollution can be decreased by the elimination of this waste product (Erol *et al.*, 2008b). The obtained glass can be evaluated as a secondary raw material in construction industry. Glass-ceramic materials can be produced from heat treatment process of vitrified coal fly ashes. This process provides better microstructural, mechanical and physical properties to the waste glasses, making them to find more application areas (Erol *et al.*, 2007).

2.1.4.10 Valuable metal extraction from coal fly ash

Coal fly ash is mainly consists of low value species such as silica, alumina, iron oxide and calcium oxide. This major matrix contains very low concentration of valuable metals including boron, lithium, vanadium, gallium and germanium (Tsuboi *et al.*, 1991). Fly ash can be considered as a source of the valuable metals. Therefore, recovery potential of valuable metals from this waste should be studied. This research area has promised with increasing ash generation throughout the world (Tsuboi *et al.*, 1990). Since these high value metals have very low concentrations in commercial minerals, recovery and purification of several rare metals from fly ash have been investigated. For example, bauxite is the main mineral source of gallium and its gallium content is in the range 0.003-0.008%. The gallium contents of coals vary widely and come from the inorganic components. As a result of combustion process, gallium contents are concentrated into the combustion by-products. Fly ash contains gallium concentrations of 0.001-0.3%. For this reason, gallium recovery from fly ash seems to be an interesting alternative to disposal if the present price of gallium is considered as \$400 kg^{-1} (Gutierrez *et al.*, 1997).

In literature, there are several studies about recovery of gallium, germanium, vanadium and boron from fly ash. These studies mainly includes the methods of leaching and extraction of gallium with commercial extractants (Gutierrez *et al.*, 1997), ion flotation of germanium from aqueous leachate with complexating agent and a surfactant as collector (Hernandez-Exposito *et al.*, 2006) and boron leaching with dilute sulfuric acid and its further treatment with solvent extraction (Tsuboi *et al.*, 1990).

2.2 Characterization of sintered coal fly ashes and their utilization potentials in ceramic industry

Fly ash can also be considered as a potential low cost raw material for the ceramic industry as it is used for the production of glass and glass-ceramic due to its suitable chemical composition and physical state. Fly ash mainly consists of SiO_2, Al_2O_3, CaO and Fe_2O_3, which are the building stone of ceramic materials. In addition, very fine size of fly ash eliminates the grinding process which needs the highest cost in mineral processing applications. In other words, it can be directly used into ceramic pastes with almost no pretreatment for most of the times. In addition to these suitable properties of fly ash, like utilization in glass and glass-ceramic, both consumption of natural raw materials and environmental pollution can be reduced using this waste product in the ceramic industry. As all of these environmental, economic and process advantages are considered, it can be easily said that fly ash can be a good candidate for the ceramic industry as a low cost raw material resource (Erol *et al.*, 2008a).

2.2.1 Sintering

Sintering is a worldwide processing technique used for metal and ceramic powders in order to produce density-controlled materials and components using thermal energy. In fact, it is one of the oldest human technologies, dating back to the prehistoric era with the firing of pottery. Sintering was also used to produce some tools from sponge iron. However, sintering was studied fundamentally and scientifically after the 1940s. Sintering science has been developed significantly from that time. Today, fabrication of sintered parts for all kind of materials, including powder-metallurgical parts and bulk ceramic components is one of the most common utilization areas of sintering (Kang, 2004).

General fabrication pattern of sintered products can be seen from Figure 2.1. In this pattern, each production step contains various processing variables. For example, according to the shape and properties necessity for the end product, various shaping techniques including simple die compaction, isostatic pressing, slip casting and injection molding can be used in the process. Sintering conditions and sintered body properties may vary remarkably depending on the techniques used for shaping. Similarly, there are many techniques and processing variables in the sintering step, resulting in variations in sintered body properties. General aim of sintering is to manufacture sintered products with reproducible and designed microstructure by controlling processing variables. Microstructural control is generally achieved by controlling particle size, sintered density and size and distribution of pores. The main purpose of microstructural control is to prepare a sintered product with the properties of high density and fine grain structure (Kang, 2004).

2.2.1.1 Definitions and categories of sintering

Sintering can be defined as "a thermal treatment for bonding particles into a coherent, predominantly solid structure via mass transport events that often occur on the atomic scale. The bonding leads to improved strength and lower system energy" (German, 1996). According to Rahaman, 2008, "the heat treatment process in which a powder or a porous material, already formed into a required shape, is converted to a useful solid is referred to as sintering". Based on the ISO, sintering can be described as "the thermal treatment of a powder or compact at a temperature below the melting point of the main constituent, for the purpose of increasing its strength by bonding together of the particles" (http://www.azom.com/article.aspx?ArticleID=1725).
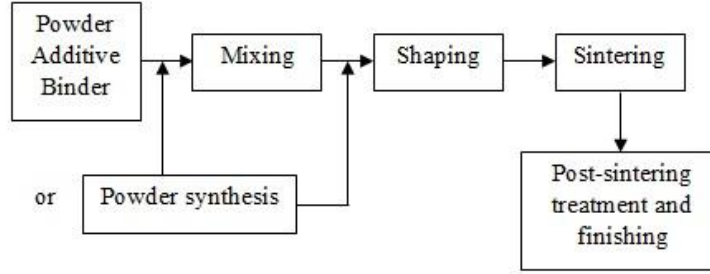
Figure 2. 1 General fabrication pattern of sintering process (Kang, 2004)

Sintering process is mainly divided into two types, namely solid state sintering and liquid phase sintering. The first one occurs as the powder compact becomes totally dense in a solid state at the sintering temperature. On the other hand, liquid phase sintering occurs when densification occurs with the presence of a liquid phase during sintering. Generally, easy control of microstructure and reduction in processing cost can be achieved with liquid phase sintering compared to solid state sintering. However, it has some adverse effects on material properties like mechanical properties. Conversely, many specific products can only be produced by using liquid phase sintering due to the required properties of the grain boundary phase (Kang, 2004).

2.2.1.2 Driving force and basic phenomena in sintering

The main driving force of sintering process is the reduction of the total interfacial energy in the system. The total interfacial energy of a powder compact (γA) depends on the specific surface energy (γ) and the total surface area of the compact (A). The reduction of the total energy can be defined as

$$\Delta(\gamma A) = \Delta\gamma A + \gamma\Delta A \tag{2.1}$$

Where the change in interfacial energy ($\Delta\gamma$) is resulted from densification and the change in interfacial area is caused by grain coarsening. The change in interfacial energy in solid state sintering is dependent on the replacement of solid/vapor interfaces by solid/solid interfaces. Figure 2.2 illustrates schematically the basic phenomena of sintering, namely densification and grain coarsening (Kang, 2004).

Three forces, namely the curvature of the particle surfaces, externally applied pressure and chemical reaction provide the main driving force of sintering. The schematic diagram illustrating the driving forces in sintering can be seen in Figure 2.3 (Rahaman, 2008).

2.2.1.3 Stages of sintering

Figure 2.4 shows three main stages of sintering, initial stage, intermediate stage and final stage (http://www.ipmd.net/Introduction_to_powder_metallurgy/Sintering). This figure clearly illustrates that the initial open pore structure and high porosity of the green samples are consumed by inter-particle neck growth, grain coarsening and pore shrinkage. As a result, mainly spherical closed pores form in the final stage of sintering (German, 1996).
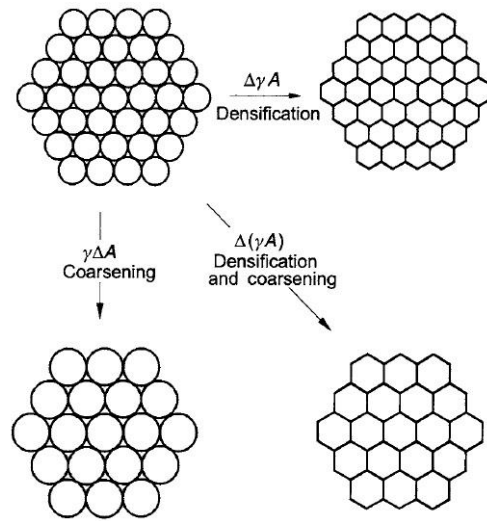
Figure 2. 2 Basic phenomena of sintering (Kang, 2004)
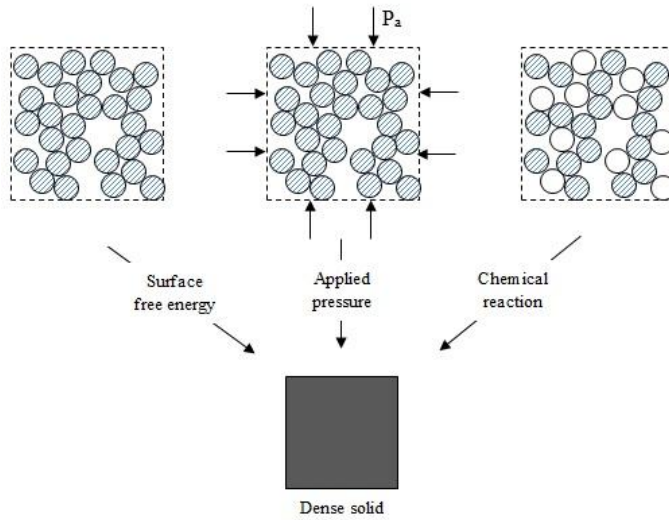
Figure 2. 3 Driving forces in sintering process (Rahaman, 2008)
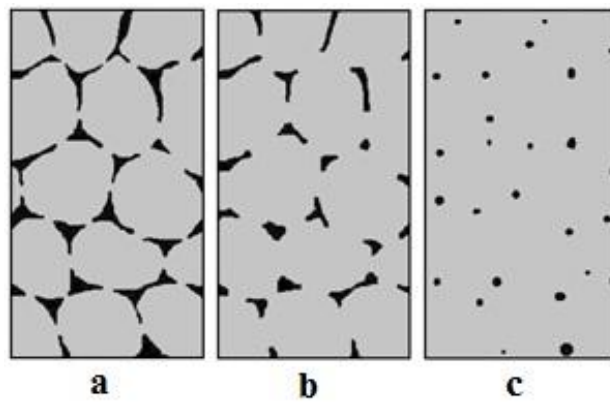
Figure 2. 4 Three main stages of sintering; (a) initial stage, (b) intermediate stage and (c) final stage

The main processes and property changes during sintering are summarized in Table 2.3. According to Table 2.3, in initial stage, the contacts grow in size and extensive loss of surface area occurs with sintering. After that, intermediate stage occurs. This stage is characterized by a tubular and rounded pore structure which is open to the compact surface. The grain boundaries are generally connected to the open pore structure in a crystalline material. In the final stage of sintering, the pores shrink and have no connection with the compact surface (German, 1996).

Table 2. 3 Processes and changes in material properties during sintering (German, 1996)

Stage	Process	Surface area loss	Densification	Coarsening
Initial	Neck growth	Significant, up to 50%	Small at first	Minimal
Intermediate	Pore rounding and elongation	Near total loss of open porosity	Significant	Increase in grain size and pore size
Final	Pore closure and final densification	Negligible further loss	Slow and relatively minimal	Extensive grain and pore growth

2.2.1.4 Variables of sintering process

The major variables affecting sintering of a powder compact are divided into two categories, namely material variables and process variables. Table 2.4 shows the all variables resulted from both raw material and sintering conditions.

Table 2. 4 Variables affecting sintering process (Kang, 2004)

Raw material variables	*Powder:* shape, size, size distribution, agglomeration, mixedness, etc.
	Chemistry: composition, impurity, non-stoichiometry, homogeneity, etc.
Process variables	Temperature, time, pressure, atmosphere, heating and cooling rate, etc.

Raw material variables contain powder size, powder shape, powder size distribution, degree of powder agglomeration, chemical composition of powder compact, etc. which influence the powder compressibility, densification and grain growth. Process variables are mostly thermodynamic variables like temperature, time, atmosphere, pressure, heating and cooling rate (Kang, 2004).

2.2.2 Previous studies on sintering of fly ash

In literature, there are many studies on sintering of fly ash with the addition of natural raw materials, various waste products and organic binders. However, limited studies are present with the use of coal fly ash alone. On the whole, these researches were focused on the relationship between green body properties like density, particle size, mineralogy and chemistry and crystallinity, microstructure and physical and mechanical properties of sintered products. Furthermore, effects of various processing conditions like compaction pressure, milling, sintering temperature and sintering time were investigated on the physical and mechanical properties, microstructure and mineralogy of sintered products (Mangialardi, 2001; Benavidez *et al.*, 2003; Ilic *et al.*, 2003; Erol *et al.*, 2008a; Erol, *et al.*, 2008b; Biernacki *et al.*, 2008; Furlani *et al.*, 2008; Chandra *et al.*, 2008; Acar and Atalay, 2012).

Particle size of starting fly ash is an important material's property in the sintering process. The effects of particle size on sintered material properties like density, water absorption, shrinkage, strength and microstructure were investigated by Ilic *et al.*, 2003. Based on the test results, the higher density and strength with the lower linear shrinkage and water absorption were observed for finer ash due to the increasing surface area of the particles as a result of milling.

The effects of compaction pressure on the sintered body properties were studied by Mangialardi, 2001. According to the results, an increase in the compaction pressure provides the higher compressive strength with the lower water absorption as a consequence of a reduced initial porosity of the as received fly ash.

The effects of main processing conditions, namely sintering temperature and sintering time on the physical, mechanical and microstructural properties of sintered coal fly ashes were studied by Ilic *et al.*, 2003; Biernacki *et al.*, 2008; Chandra *et al.*, 2008; Furlani *et al.*, 2008; Acar and Atalay, 2012. In these studies, with increasing sintering temperature, generally, a sintered product including the properties of the higher density and strength with lower shrinkage, water absorption and porosity and better microcrystalline structure was obtained.

Ilic *et al.*, 2003 investigated the effects of sintering temperature varies from 1130-1190°C on the density, water accessible porosity, mineralogy and microstructure of a sintered lignite fly ash. The test results indicated that density reached the maximum value for 1170°C and then decreased probably because of the softening of glassy phase and evolution of gases, resulting in the formation of pores.

Sintering characteristics of a class F fly ash was studied by Biernacki *et al.*, 2008 as a function of sintering temperature (1050-1200°C) and sintering time (0-90 min) with the addition of corn syrup as a binder. Sintering efficiency was measured with the physical and mechanical tests generally used in the ceramic industry. According to the results, complete carbon removal was found to be inhibited by premature densification and both internal and external mass transfer conditions play important roles in carbon combustion.

Sintering of the mixture of fly ash and low alkali pyrophyllite as a function of sintering temperature and different mixture composition with the addition of sodium hexa meta phosphate (SHMP) as a complex activator for the aim of wall tile manufacturing was studied by Chandra *et al.*, 2008. Based on the test results, wall tiles with low strengths were produced by fly ash alone with SHMP in the temperature range 925-1050°C. With the addition of pyrophyllite, an increase in impact strength was observed. According to the regulations set by the Indian Standards Institute for wall tiles, satisfying results were obtained with the use of more than 40% pyrophyllite in the mixtures.

Characterization of sintered powders obtained from coal fly ash and paper mill sludge was investigated by Furlani *et al.*, 2008 as a function of sintering temperature between 1130 and 1190°C. Various physical and mechanical properties like density, water absorption, shrinkage on firing, crystal structure, microstructure, strength, hardness and toughness were evaluated as a measure of sintering efficiency. The test results indicated that a sintered product with best overall properties was obtained with the use of material containing 25% of coal fly ash and 75% of powder from paper sludge.

The effects of sintering temperature and sintering time on two class F fly ashes from Çatalağzı and Sugözü thermal power plants in Turkey were studied by Acar and Atalay, 2012. Quality of sintered samples was evaluated in terms of ceramic specifications such as density, water absorption, porosity, shrinkage and splitting tensile strength. In addition, mineralogical changes and microstructural evolution during sintering were determined with X-ray diffraction (XRD) and scanning electron microscopy (SEM) analyses. Overall results indicated that Sugözü fly ash seems to be a better candidate for ceramic industry due to the better microstructure, higher density and strength with the lower porosity, water absorption and shrinkage values.

Possible utilization of both fly ash and bottom ash as raw material for the ceramic industry was analyzed by Benavidez *et al.*, 2003. The starting samples were prepared by mechanical mixing of both kinds of ashes and evolution of density through packing, pressing and sintering was investigated. According to the

results, raw materials containing higher fly ash content showed higher packing density which provided compacts with improved green and sintered densities probably due to the more spherical morphology and smaller particles of fly ash. Furthermore, preheating at temperatures above $600^{o}C$ resulted in an increase in the green and sintered densities.

The effects of fly ash addition on the properties of fired clay bricks with the purpose of high replacing ratio were studied by Lingling *et al.*, 2005. Based on the test results, with increasing of replacing ratio of fly ash, a substantial decrease was observed in the plasticity index of mixture of fly ash and clay. Additive A (not specified) was used to improve the plasticity index of mixture. Although improved properties were obtained by fly ash addition with high replacing ratio, the sintering temperature of bricks was increased by about $50-100^{o}C$ higher than that of pure clay bricks. The results also indicated that the properties of fired bricks were further improved with the utilization of pulverized fly ash.

Utilization potential of fly ash from Çayırhan thermal power plant in brick making was also examined by Tütünlü, 2000 using high brick clay replacing ratio. Bricks containing 40%, 50% and 60% fly ash and clay only bricks were compacted and then fired at $750^{o}C$, $850^{o}C$ and $950^{o}C$. Quality of bricks was evaluated by using various physical and mechanical tests such as shrinkage, water absorption, firing loss, plasticity water and compressive strength. These test results indicated that competitive bricks with reasonably good properties can be produced by using Çayırhan fly ash for the clay replacing ratio of up to 60%.

The effects of three different binders, namely cement, lime and bentonite on the properties of sintered fly ash aggregate was reported by Ramamurthy and Harikrishnan, 2006. According to the results, improved properties of sintered fly ash aggregate like higher strength and lower water absorption were obtained with the use of bentonite compared to lime and cement probably due to the high content of very fine organic matter present in the bentonite. Although the three binders did not change the chemical composition, they affect the microstructure, leading to improvements in the properties of aggregates.

Kinetics and the densification mechanisms of fly ash sintering on the bases of the linear shrinkage and sintering time were studied by Mangialardi, 2001. The test results showed that the sintering can be modeled kinetically by an intermediate-stage liquid-phase sintering, and liquid phase diffusion and grain shape accommodation are the main process to control the densification.

Mineralogy and microstructure of sintered fly ashes were investigated by several researchers as a function of processing conditions. The phases in sintered products changes mainly based on the as received samples. With sintering process, some of the phases in as received samples remain the same, some are changed in their amount, and some new phases are formed. In point of microstructure, sintering leads to coalescence of fly ash particles in some degree depending on the processing conditions. A considerable amount of interaction among the particles is achieved with high enough sintering temperature and time, forming more compact products with much smoother surfaces (Ilic *et al.*, 2003; Biernacki *et al.*, 2008; Chandra *et al.*, 2008; Furlani *et al.*, 2008; Erol *et al.*, 2008a; Acar and Atalay, 2012).

2.3 Utilization potential of class F fly ashes as high-quality pozzolans in construction industry

In recent decades, fly ashes have been widely used in construction industry as supplementary cementitious material due to their various technical, environmental and economic benefits. Contribution to the fresh concrete workability, microstructure formation and improvement in long term mechanical and durability properties can be counted as some of fly ashes' technical benefits. Less environmental pollution occurs in fly ash disposal area with the use of these wastes in cement and concrete industry. Further environmental and economic benefits are achieved by reducing CO_2 emissions in cement production and decreasing cost of the concrete materials due to less raw material need, leading to the conservation of energy and natural resources in construction industry (Zeng *et al.*, 2011; Langan *et al.*, 2002; Islam, 2012).

The low calcium Class F fly ashes are pozzolanic in nature. In other words, they form strength developing products (pozzolanic reactivity) when reacted with $Ca(OH)_2$ and water. Accordingly, this type of fly ashes is used in combination with Portland cement, producing $Ca(OH)_2$ during its hydration. Various positive properties like low heat of hydration and high durability can be added to the product when the class F fly ashes are used in concrete as cement replacement. Furthermore, they also provide concrete strength by pozzolanic and filler effects (Nochaiya *et al.*, 2010). Although fly ashes have various technical, environmental and economic benefits, they have also some adverse effects especially for early stages of aging due to their relatively low surface area and accompanying pozzolanic activity. The pozzolonic reaction between fly ash and $Ca(OH)_2$ does not provide a significant improvement to concrete properties up to several weeks after the start of hydration, bringing about slow strength development and inadequate strength although concrete may have higher strength and durability in the longer term compared to the control concrete (Langan *et al.*, 2002; Nochaiya *et al.*, 2010).

In order to overcome these disadvantageous properties of fly ashes on the early age related to low surface area and accompanying pozzolanic activity, silica fume and air-classified fly ash have been used for years due to their very fine particle size and much higher surface area. On the other hand, limited supply and high cost of these materials have kept usage relatively low (Rathbone, 2004). In addition to this, perfectly dry feed necessity of air classification limits its use significantly. Conventional hydraulic classification systems have also some serious disadvantageous for the acceptable recovery with very fine size. A high-performance pozzolan with improved pozzolanic reactivity may be produced using a special hydraulic classification technique by recovering of very fine particle size from the as received fly ash.

2.3.1 Pozzolans

2.3.1.1 Definition of pozzolan

Pozzolans can be defined as silicious or silicious and aluminous material which have little or no cementitious value, but in finely divided form and in the presence of moisture, they chemically react with calcium hydroxide (CH) at ordinary temperatures to form compounds with cementitious properties such as calcium silicate hydrates (C-S-H) and calcium sulfoaluminate hydrates (C-A-S-H) gels (Dunstan, 2011 and Yilmaz, 2003). Both natural and artificial materials have pozzolanic properties and they are generally used in cement and concrete industry as supplementary cementitious materials. Artificial pozzolans are mostly resulted from high-temperature processes as waste or by-products like fly ashes from thermal power plants and silica fume from silicon smelting. On the other hand, they can also be produced intentionally, for instance by thermal activation of kaolin-clays to metakaolin. Today, the most widely used pozzolans are fly ash, silica fume, highly reactive metakaolin and burned organic matter residues rich in silica like rice husk ash. Natural pozzolans are concentrated in certain locations and they are widely used in Italy, Germany, Greece and China as an addition to Portland cement. Today, the most commonly used natural pozzolans are volcanic ashes and pumices which are largely composed of volcanic glass (http://en.wikipedia.org/wiki/Pozzolan).

2.3.1.2 Supplementary cementitious materials

Artificial pozzolans like fly ash, ground granulated blast-furnace slag and silica fume, and natural pozzolans such as calcined shale and calcined clay are materials which contribute to the properties of both fresh and hardened concrete through hydraulic and/or pozzolanic activity. Figure 2.5 illustrates supplementary cementitious materials in use today. In the figure, class C fly ash, calcined clay (metakaolin), silica fume, class F fly ash, slag and calcined shale are shown from left to right (http://www.ce.memphis.edu/1101/notes/concrete/PCA_manual/Chap03.pdf).

In literature, pozzolans and slags are usually classified as supplementary cementitious materials or mineral admixtures. Applicable categories, and chemical compositions and basic properties of these materials are listed in Tables 2.5 and 2.6 (http://www.ce.memphis.edu/1101/notes/concrete/PCA_manual/Chap03.pdf).

Figure 2. 5 Supplementary cementitious materials in use today
(From left to right: class C fly ash, calcined clay, silica fume, class F fly ash, slag and calcined shale)

Table 2. 5 Categories of supplementary cementitious materials

Ground granulated iron blast-furnace slags-ASTM C 989 (AASHTO M 302)	
Grade 80	Slags with a low activity index
Grade 100	Slags with a moderate activity index
Grade 120	Slags with a high activity index
Fly ash and natural pozzolans-ASTM C 618 (AASHTO M 295)	
Class N	Raw or calcined natural pozzolans including: Diatomaceous earths Opaline cherts and shales Tuffs and volcanic ashes or pumicites Calcined clays including metakaolin and shales
Class F	Fly ash with pozzolanic properties
Class C	Fly ash with pozzolanic and cementitious properties
Silica fume-ASTM C 1240	

Table 2. 6 Chemical compositions and basic properties of typical pozzolans

	Class F fly ash	Class C fly ash	Ground slag	Silica fume	Calcined clay	Calcined shale	Metakaolin
SiO_2, %	52	35	35	90	58	50	53
Al_2O_3, %	23	18	12	0.4	29	20	43
Fe_2O_3,%	11	6.0	1.0	0.4	4.0	8.0	0.5
CaO, %	5.0	21	40	1.6	1.0	8.0	0.1
SO_3, %	0.8	4.1	9.0	0.4	0.5	0.4	0.1
Na_2O, %	1.0	5.8	0.3	0.5	0.2	-	0.05
K_2O, %	2.0	0.7	0.4	2.2	2.0	-	0.4
Total Na eq. alk., %	2.2	6.3	0.6	1.9	1.5	-	0.3
LOI, %	2.8	0.5	1.0	3.0	1.5	3.0	0.7
Blaine fine., m^2/kg	420	420	400	20,000	990	730	19,000
Relative density	2.38	2.65	2.94	2.40	2.50	2.63	2.50

2.3.1.3 Benefits and advantages of pozzolan utilization

There are mainly three benefits of pozzolan utilization in cement and concrete industry. Firstly, partial replacement of the Portland cement by cheaper pozzolans provides an important economic gain. Secondly, environmental pollution is decreased due to less greenhouse gases resulted from cement production. Thirdly, pozzolans also enhance the durability of the final product. Today, pozzolans can be used as replacement material for Portland cement in the concrete mix up to 40% by weight depending on required specifications of the end products. If the concrete mix is prepared properly, a final concrete product can be obtained with competitive compressive strength and other performance characteristics. The final product properties mainly depend on the development of the binder microstructure which is affected by distribution, type, shape and dimensions of both reaction products and pores. Improved properties of the final product with pozzolan utilization are mostly attributed to the pozzolanic reaction between pozzolan and Portland cement. As a result of this reaction, a more compact product is obtained by filling of the reaction products in pores, leading to a reduction in permeability (http://en.wikipedia.org/wiki/Pozzolan).

Utilization of pozzolans also provides increased chemical resistance to the harmful action of some aggressive solutions which results in an improvement in the durability of the final concrete product. The lowered lime content available for deleterious expansive reactions due to the pozzolanic reaction is one of the main reasons for increased durability. In addition, the entrances of harmful ions like chlorine or carbonate are hindered due to the reduced permeability. Furthermore, the pozzolanic reaction changes the binder pore solution, leading to the reduced risk of alkali-silica reactions by lowering the solution alkalinity. Increasing alumina content in pozzolans also improves chemical resistance of the end product (Chappex and Scrivener, 2012).

2.3.2 Pozzolanic reactivity of fly ash

Pozzolanic reactivity can be described as "the ability of natural or by-product materials to produce components having binding property as a result of their reaction with calcium hydroxide (CH) in presence of moisture" (Uzal *et al.*, 2010). The utilization of pozzolanic materials in cement and concrete products has become almost unavoidable because of various technical, environmental and economic advantages. The performance of pozzolans in cement and concrete products varies mainly depending on the material properties like particle size, size distribution and specific surface area. These material properties have important effects on water requirement, rheology and pozzolanic reactivity. Hardened concrete properties

such as compressive strength, permeability and chemical durability are affected by pozzolanic reactivity (Uzal *et al.*, 2010).

Some specifications of the requirements which cover properties of fly ash have been imposed by various standards. Historical development of fly ash specifications provided by various organizations is summarized in Table 2.7.

Table 2. 7 Historical developments of fly ash specifications in various standards (Islam, 2012)

Specification		LOI, (max, %)	Fineness Specific surface (min, m²/kg)	Fineness 45 µm sieve residue, (max, %)	Water req., (max, %)	Pozzolanic activity index (min, %)
Davis et al., 1937		7.0	250	12.0	103	min 5 N/mm² with lime
US Bureau of Rec., 1951		5.0	300	12.0	103	-
Nebraska State, 1952		10.0	-	-	-	-
ASTM C 350, 1954		12.0	280	-	-	100
BS 3892, 1965	Zone A		125-275			
	Zone B	7.0	275-425	-	-	-
	Zone C		> 425			
ASTM C 618, 1968		12.0	650	-	105	85
Tennessee Valley Auth. G-30, 1968	Class I	6.0	650	< 12.0	-	85
	Class II	6.0	500	12.0-22.0	-	75
	Class III	6.0	-	22.0-32.0	-	75
ASTM C 618, 1969		12.0	-	12.0	105	75
ASTM C 618, 1971		12.0	-	34.0	105	75
BS 3892, 1982		7.0	-	12.5	< 95	85 (7 d)[a]
EN 450, 1995		5.0	-	40.0	-	75 (28 d)
						85 (90 d)
BS 3892, 1997		7.0	-	12.0	< 95	80 (28 d)
EN 450, 2005	Cat. A	0-5	-	< 12 (Cat. S)	< 95	75 (28 d)
	Cat. B	2-7	-	< 40 (Cat. N)	-	85 (90 d)
	Cat. C	4-9	-	-	-	
ASTM C 618, 2012	Class N	10.0	-	34.0	115	75 (7 d)
	Class F	6.0[b]	-	34.0	105	75 (28 d)
	Class C	6.0	-	34.0	105	

[a] 5 days in 20ºC, following this 46 hours in 50ºC and finally 2 hours in 20ºC
[b] can be approved by the user if it satisfies other requirements

According to the table, in addition to loss on ignition (LOI), fineness and water requirement, most standards have the specification on "pozzolanic activity index" which measures reactivity of fly ash based on compressive strength measurements of the mortars with fly ash and Portland cement reference (Islam,

2012). The term "strength factor" was used as pozzolanic activity index in the standard BS 3892-1. Based on this standard, in mortar preparation, fly ash level was 30% and variable water content was used to obtain equal flowability (BSI, 1997). In the current European standard BS EN 450-1, pozzolanic activity index was expressed by "activity index". According to this standard, 25% fly ash and equal water content (w/c=0.5) was used in mortar preparation, resulting in variable flowability (BSI, 2005). "Strength activity index" is used as a measure of fly ash reactivity in the ASTM standard C618. Similar to the standard BS 3892-1, variable water content is used to obtain same flowability in this standard. However, this time fly ash replacement ratio is 20% (ASTM, 2012).

All of these tests defined above are based on the strength measurements of mortar cube containing fly ash for a definite curing age (e.g. 7, 28 and 90 days) and comparison with the ones containing only Portland cement. This approach can be affected by particle size distribution which is directly related to packing of materials. Therefore, evaluation of fly ash reactivity with this method can be accepted as an indirect way. Also, the long residence time necessity to obtain test results is the other disadvantage for this method (Islam, 2012). Determination of $Ca(OH)_2$ consumption in PC/fly ash paste (mixture of Portland cement, fly ash and water) by thermogravimetric analysis (TGA) is another method for evaluation of fly ash reactivity as a pozzolan. This $Ca(OH)_2$ consumption can be accepted as a measure of fly ash reactivity due to the pozzolanic reaction between fly ash and lime. In contrast to the pozzolanic activity index based on strength measurements, packing influence is minimized in this method (Islam, 2012).

2.3.2.1 Hydration of Portland cement paste

In the anhydrous state, there are four main types of minerals present in Portland cement, namely alite (tricalcium silicate, Ca_3SiO_5), belite (dicalcium silicate, Ca_2SiO_4), aluminate (tricalcium aluminate, $Ca_3Al_2O_6$) and a ferrite phase (tetracalcium aluminoferrite, $2(Ca_2AlFeO_5)$). In cement chemistry notation, oxides are referred to by their first letter meaning that CaO, SiO_2, Al_2O_3, Fe_2O_3 and H_2O are represented by "C", "S", "A", "F" and "H", respectively. According to this notation, alite ($3CaO.SiO_2$) thus becomes C_3S. Similarly, belite, aluminate and ferrite phases become C_2S, C_3A and C_4AF, respectively. In addition to these phases, Portland cement also contains small amounts of clinker sulfate (sulfates of sodium, potassium and calcium) and gypsum generally added during grinding of clinker (Winter, 2005).

The cement hydration process consists of two main stages. The cement dissolves in the first stages, releasing ions into the mix water. For this reason, this step is called as dissolution. The mix water becomes an aqueous solution with a variety of ionic species, which is called as pore solution. In the pore solution, gypsum and the anhydrous cement minerals C_3S and C_3A are highly soluble and dissolve quickly immediately after cement and water are mixed, resulting in a rapid increase in the concentrations of ionic species. As the concentrations of these ionic species are achieved to the supersaturation point in which energetically favorable conditions occur for the formation of new solid phases from the ionic species, the second step of hydration called as precipitation starts. These new precipitated solid phases are called as hydration products. Precipitation of new solid phases is very important and makes dissolution of the starting minerals continue so cement hydration becomes a continuous process (http://iti.northwestern.edu/cement/).

2.3.2.1.1 Hydration reactions and products

In the cement hydration, the starting anhydrous minerals have different reaction rates and they form different solid phases. Unlike individual reactions, all anhydrous minerals dissolve into the same pore solution during the real cement hydration process, making the process very complicated due to the interactions between the hydration products. Nevertheless, evaluation of the hydration reactions individually let the process easy to understand (http://iti.northwestern.edu/cement/).

2.3.2.1.1.1 Hydration of the silicate minerals

In Portland cements, tricalcium silicate (C_3S) which provides most of the early strength development to the cement paste is the most important and abundant mineral. The hydration reaction of C_3S can be expressed as:

$$C_3S + (1.3 + x)\ H \longrightarrow C_{1.7}SH_x + 1.3CH \tag{2.2}$$

where $C_{1.7}SH_x$ is called as calcium silicate hydrate (C-S-H) gel phase. In cement chemistry notation, CH represents calcium hydroxide, which has the mineral name portlandite. This reaction takes place very high in the first few days, resulting in a considerable increase in strength and reduction in capillary porosity. Similarly, the hydration of C_2S can be considered as:

$$C_2S + (0.3 + x)\ H \longrightarrow C_{1.7}SH_x + 0.3CH \tag{2.3}$$

In this reaction, less CH forms compared to hydration of C_3S since C_2S is much less soluble than C_3S. In spite of little contribution to the early strength, the hydration of dicalcium silicate leads to a substantial increase in strength of cement paste and concrete for the later curing ages (http://iti.northwestern.edu/cement/).

2.3.2.1.1.2 Hydration of the aluminate and ferrite minerals

In Portland cement hydration, aluminate and ferrite minerals have more complex reactions than those of the silicates. The presence of sulfate ions in the pore solution determines the reactions which take place. C_3A is a very soluble mineral and hydrates according to:

$$2C_3A + 21H \longrightarrow C_4AH_{19} + C_2AH_8 \longrightarrow 2C_3AH_6 + 9H \tag{2.4}$$
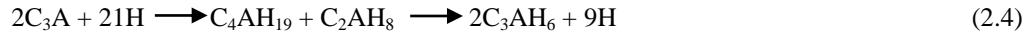
The second reaction occurs more slowly than the first one. Hydrogarnet (C_3AH_6) forms as the final product. In the presence of gypsum ($C\check{S}H_2$) which is normally added to the Portland cement to prevent the condition of flash set, due to its high solubility, calcium and sulfate ions rapidly release into the pore solution. Another reaction occurs as:

$$C_3A + 3C\check{S}H_2 + 26H \longrightarrow C_6A\check{S}_3H_{32} \tag{2.5}$$

This is the main hydration reaction for C_3A because all Portland cements have gypsum. Ettringite mineral ($C_6A\check{S}_3H_{32}$) forms as the final product. In the lack of gypsum, ettringite becomes unstable and reacts with C_3A according to:

$$C_3A + C_6A\check{S}_3H_{32} + 4H \longrightarrow 3C_4A\check{S}H_{12} \tag{2.6}$$

Almost all of the ettringite is converted to monosulfoaluminate ($C_4A\check{S}H_{12}$) during the first two days due to the insufficient gypsum. Similar to C_3A, the hydration of ferrite mineral (C_4AF) occurs as:

$$C_4AF + 3C\check{S}H_2 + 21H \longrightarrow C_6(A,F)\check{S}_3H_{32} + (F,A)H_3 \tag{2.7}$$

$$C_4AF + C_6(A,F)\check{S}_3H_{32} + 7H \longrightarrow 3C_4(A,F)\check{S}H_{12} + (F,A)H_3 \tag{2.8}$$
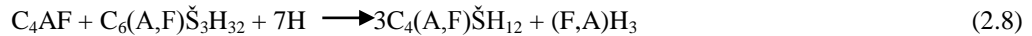
The main difference between aluminate and ferrite hydration is that iron takes the place of some of the aluminum in the reaction products. In the reactions of 2.7 and 2.8, (A,F) and (F,A) represent aluminum with variable substitution of iron and vice versa, respectively. Amorphous $(F,A)H_3$ phase forms in small amounts as results of the reactions of 2.7 and 2.8. The main reaction products, $C_6(A,F)\check{S}_3H_{32}$ and $C_4(A,F)\check{S}H_{12}$, are not pure ettringite and monosulfoaluminate, respectively due to the substituted iron. They are called as AFt and AFm phases, respectively, where "t" represents trisulfate and "m" represents monosulfate. In the actual condition, AFt and AFm phases are the main hydration products of Portland

cement since the reaction products always include iron in some extent (http://iti.northwestern.edu/cement/).

2.3.3 Pozzolanic reactivity determination of fly ash

Fly ash generally consists of a significant amount of amorphous glassy phase (50-70%), which provides most of its pozzolanic reactivity and crystalline phases like quartz, mullite, hematite and magnetite. Also, the crystalline phases can contribute to the reactivity with physical effects such as nucleation sites. Reactions of the phases of silicates and aluminates released from the glassy phase of fly ash with the calcium hydroxide produced during cement hydration result in the formation of C-S-H and C-A-S-H gels. These produced phases contribute to the microstructural properties and provide strength development especially for the later ages due to the slower pozzolanic reactions compared to Portland cement (PC) hydration. There are a number of test methods to evaluate pozzolanic reactivity of fly ash (Islam, 2012). Some of these tests are activity index based on BS EN 450-1 (BSI, 2005), strength factor based on BS 3892-1 (BSI, 1997), strength activity index based on ASTM C618 (ASTM, 2012) and ASTM C311 (ASTM, 2011), K-value from Ferét's law and assessed pozzolanic activity index based on API method (Yamamoto *et al.*, 2006) and potential pozzolanic index (PPI) (Hubbard and Dhir, 1984).

2.3.3.1 Pozzolanic reaction

Pozzolanic reaction can be defined as the reaction of pozzolans with calcium hydroxide resulted from cement hydration under moist conditions. Although pozzolanic reaction begins with hydration of silicate minerals in the cement which occurs in the first few hours, the major effects of this lime-pozzolan reaction is seen mostly after 28 days due to the very low reaction rate. This reaction can be simply expressed as follow (Yilmaz, 2003):

$$2(Al_2O_3.2SiO_2) + 7\ Ca(OH)_2 \longrightarrow 3CaO.2SiO_2.H_2O + 2(2CaO.Al_2O_3.SiO_2.H_2O) \qquad (2.9)$$
$$\text{(Pozzolan + Hydrated Lime} \longrightarrow 3CS_2H + 2C_2ASH)$$
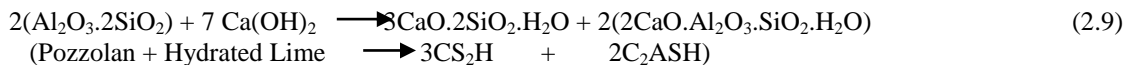
Pozzolanic reaction can also be expressed as a simple acid-base reaction between calcium hydroxide and silicic acid (H_4SiO_4, or $Si(OH)_4$) formed by pozzolan hydration. Simply, this acid-base reaction can be considered as follow (http://en.wikipedia.org/wiki/Pozzolanic_reaction):

$$Ca(OH)_2 + H_4SiO_4 \longrightarrow CaH_2SiO_4.2H_2O \qquad (2.10)$$
$$\text{(CH + SH} \longrightarrow \text{C-S-H)}$$

2.3.3.1.1 Pozzolanic reactions of fly ash with hydrated lime

In literature, there are several approaches for the pozzolanic reaction of fly ash with hydrated lime. Helmuth, 1987 expresses this reaction mainly as the interaction between silica content of fly ash and hydrated lime. Simply, this reaction can be considered as follow:

$$xCH + yS + zH \longrightarrow C_xS_yH_{x+z} \qquad (2.11)$$

In this reaction, depending on the concentration of fly ash and lime, the ratio of lime to silica (x/y) varies in the range 0.0-2.0. In addition to C-S-H gel phase, this reaction can also produce gehlenite hydrate (C-A-S-H gel phase). The below reaction can occur in the case of fully reacted lime as (Islam, 2012):

$$AS_2 + 3CH + zH \longrightarrow C_xS_yH_{x-5} + C_2ASH_8 \qquad (2.12)$$

According to Bentz and Remond, 1997, pozzolanic reactions can occur as follows:

$$1.1CH + S + 2.8H \longrightarrow C_{1.1}SH_{3.9} \qquad (2.13)$$

$$2CH + AS + 6H \longrightarrow C_2ASH_8 \tag{2.14}$$
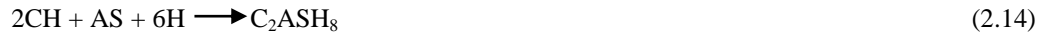
Based on these reactions, amorphous C-S-H phase and gehlenite hydrate form as the reaction products.

2.3.3.2 Previous studies on pozzolanic reactivity assessment of fly ash

In literature, considerable amount of studies exists on pozzolanic reactivity assessment of fly ash. These studies are focused on the effects of physical properties and chemical composition of fly ash such as fineness, particle size distribution, specific surface area, active silica content and glassy phase content. The effects of accelerated test methods on the pozzolanic properties of mortar and concrete containing fly ash were also studied. Furthermore, empirical and analytical models for the estimation of compressive strength development were designed by some researchers (Paya *et al.*, 1995; Lilkov et al., 1997; Paya *et al.*, 2000; Hanehara *et al.*, 2001; Hwang *et al.*, 2004; Antiohos and Tsimas, 2005; Rathbone *et al.*, 2005; Antiohos and Tsimas, 2006; Yamamoto *et al.*, 2006; Stevens *et al.*, 2009; Uzal *et al.*, 2010).

The effects of curing temperature and different sized fractions of fly ash on mortar's compressive and flexural strengths were investigated by Paya *et al.*, 1995. Four different size fractions were obtained using an air classifier. According to the test results, a significant increase in strength was observed with increasing curing temperature. In addition, the amount of fly ash with particle size less than 10 μm plays an important role in compressive strength development of mortars. It was also observed that the results of strength and particle mean size were well agreements for the 60% of cement replacement by fly ash.

Rathbone *et al.*, 2005 studied the pozzolanic reactivity of a ponded class F fly ash from a central Kentucky power plant. In order to increase reactivity of as received fly ash, they used a hydraulic classification technology and recovered the particles with mean diameter in the range 3.0-7.4 μm, which are called as ultrafine ash (UFA). According to the mortar tests, the UFA provided an approximately 10% decrease in water demand compared to the cement control. Also, for 20% and 40% cement replacement, the UFA contributed to the strength development considerably compared to typical class F and class C fly ash. Based on the test results, a strong positive relationship was present between strength gain and decreasing particle size.

The effects of size reduction of fly ash by grinding on the strength development of mortars for different curing temperatures were also studied by Paya *et al.*, 2000. The test results indicated that compressive strength increased significantly with curing temperature for the curing age of 3 days. On the other hand, the highest strength was not coincident with the highest temperature for 28 days. Based on the strength measurements, the higher reactivity was achieved using ground fly ash compared to the as received samples. For the curing ages of 3 days, mathematical equations were designed for the estimation of the compressive and flexural strengths of mortars with fly ash (15-60% replacement) for the curing temperatures in the range of 20-80°C.

The pozzolanic reaction of fly ash in cement paste was examined by Hanehara *et al.*, 2001 as a function of mix proportion and curing temperature. Based on the results, for the curing temperature of 40°C, the water to powder ratio of 50% and 40% cement replacement by fly ash, the reaction ratios of fly ash were found as 12% and 32% for the curing ages of 7 days and 1 year, respectively. The test results also indicated that the reaction ratio of fly ash increased with the increasing curing temperature and ratio of water to powder. The minimum requirements in order to start pozzolanic reaction were obtained as the curing temperature of 20°C and the curing age of 28 days.

The early age (first 24 hours) effects of fly ash, silica fume or both on blended cement pastes were studied by Lilkov et al., 1997. For determination of the pozzolanic activity, DTA, XRD and IRS analyses were conducted. The pozzolanic effects of fly ash and silica fume were determined in terms of total amount of hydration products and remaining portlandite content. According to the results, fly ash and silica fume actively affected the early hydration of cement. Coarse fly ash particles served as nuclei of hydration

products whereas silica fume contributed to the cement hydration and provided a connection between hydrating cement grains.

Uzal *et al.*, 2010 investigated pozzolanic activity of a commonly used natural zeolite mineral, clinoptilolite compared to silica fume, fly ash and a non-zeolitic natural pozzolan. Pozzolanic activity was evaluated as a measure of physical, chemical and mineralogical properties. Pozzolanic activity of lime-pozzolan pastes was determined with various test methods. The test results indicated that although clinoptilolite has a pozzolanic reactivity which was comparable to silica fume and higher than fly ash and a non-zeolitic natural pozzolan, relatively poor strength developments were observed with clinoptilolite. According to the researchers, the high reactivity was attributed to the specific surface area and reactive silica content of the clinoptilolite while low strength development was releated to the larger pore size distribution of the clinoptilolite-lime pastes compared to the lime-fly ash system.

Stevens *et al.*, 2009 studied the cementitous and pozzolanic properties of fly ash from Fluidized Bed Combustion (FBC). Although this FBC fly ash cannot be categorized depending on ASTM C618, its relatively high surface area, glassy silicates inclusion and high lime content provide both pozzolanic and cementitious properties. In addition to the as received fly ash, classified samples by screening and hydraulic classification were also tested. Mortar cubes were prepared to determine compressive strength and water demand. For shrinkage and expansion tests, mortar bars were prepared. According to the results, although the FBC fly ash initially retarded compressive strength development, it contributed to the strength significantly, achieving 94% strength index of the cement control for the curing age of 7 days.

The effects of active silica content of two class C fly ashes on cement hydration mechanism were investigated by Antiohos and Tsimas, 2005. The high-calcium fly ashes containing different reactive silica contents and ratios of silicon to calcium oxides were used to prepare mixes with Portland cement up to 30% by volume. The Portland cement-fly ash blends were tested for microstructural development, remaining calcium hydroxide and compressive strength. Based on the test results, the key factor for the hardening process was found as soluble silica of fly ashes especially after the first month. However, in addition to active silica content, additional material properties such as fineness and glass content were also important to estimate the final contribution of fly ashes to the blend product.

Antiohos and Tsimas, 2006 further studied the effects of active silica content of two fly ashes different in calcium content and their three mixtures for determination of pozzolanic reactivity in Portland cement-fly ash system. In this work, fly ashes were ground to the same size before utilization in the paste in order to remove the effect of specific surface area. According to this study, reactive silica is the vital factor affecting pozzolanic activity and future strength development of cement-fly ash system can be correlated with the reactive silica if it is precisely measured. In different from the previous work, this time reactive silica content was determined according to the European standard EN 450-1. Validity of the developed model was also confirmed using various kinds of fly ashes.

Hwang *et al.*, 2004 derived an equation to estimate compressive strength development of concrete with fly ash based on the test results. This equation can be expressed as:

$$f_c(t) = A(t)\left(\frac{\propto FA + C}{W}\right) + B \tag{2.15}$$

In this equation, $f_c(t)$ defines compressive strength (N/mm^2) at a definite "t" days, $A(t)$ is function of age (days), α is contribution of fly ash to strength and depends on various factors such as curing age, fly ash ratio (FA, kg/m^3) and Blaine specific surface area. C, W and B express cement content (kg/m^3), unit water content (kg/m^3) and a constant, respectively. Both of the increases and decreases in the early strengths due to fly ash addition can be explained by using this equation. According to the equation, the former condition is resulted from partial replacement of fine aggregate by fly ash whereas the second one is due to fly ash in place of part of cement. This model also explains the long-term strength increases and the effects of fly ash replacement and Blaine specific surface area on the strength.

Yamamoto *et al.*, 2006 studied the pozzolanic reactivity of fly ash in mortar by using a K-value from Feret's law. The test results indicated that the diffusion kinetic played a vital role on the pozzolanic reaction. Water content was an important parameter and directly influenced the diffusion constant. In this study, the relationship between K-value, which is a useful tool for the pozzolanic reactivity estimation, and pozzolanic activity index obtained using accelerated chemical test based on API method was also investigated. According to the results, due to the good relationship with K-value, API is one of the convenient acceleration approaches for the estimation of the pozzolanic reactivity.

2.4 Cenosphere recovery from fly ash

2.4.1 Definition of cenosphere

The ceramic particles in fly ash can be classified into three main structures, namely precipitators, cenospheres and plerospheres. Precipitator is defined as the solid spherical particles of fly ash while the hollow fly ash particles with density less than 1 g/cm^3 are called as "cenosphere". On the other hand, plerospheres can be defined as the large size hollow particles containing smaller size precipitators and cenospheres in their interiors (http://en.wikipedia.org/wiki/Cenosphere). The name "cenosphere" comes from two Greek words, which are kenos (hollow) and sphaira (sphere). Cenospheres can be described as lightweight, inert and hollow spheres, which are filled with air or gases, mostly including silica and alumina resulted from the combustion of pulverized coal at thermal power plants. Their hollow spherical shape is due to the cooling and solidifying of ash particles around a trapped gas, which are generally CO_2 and N_2 during combustion (Kolay and Singh, 2001). In literature, cenospheres can also be called as hollow spheres, microspheres, microballoons, hollow ceramic microspheres and glass beads. Due to their superior properties such as hollow spherical shape, wide-range of particle size varies from sub-micron to millimeters, ultra-low density, low thermal conductivity, high particle strength, resistant to chemicals and low water absorption, cenospheres find a number of uses and utilization areas in various industries (http://www.apitco.org/Profiles/Cenospheres%20from%20fly%20ash.pdf). Figure 2.6 shows general structures of precipitators (http://en.wikipedia.org/wiki/File:Fly_Ash_FHWA_dot_gov.jpg), cenospheres (www.flyashcenosphereexportindia.com/) and plerospheres (geoinfo.nmt.edu/staff/hoffman/flyash.html).
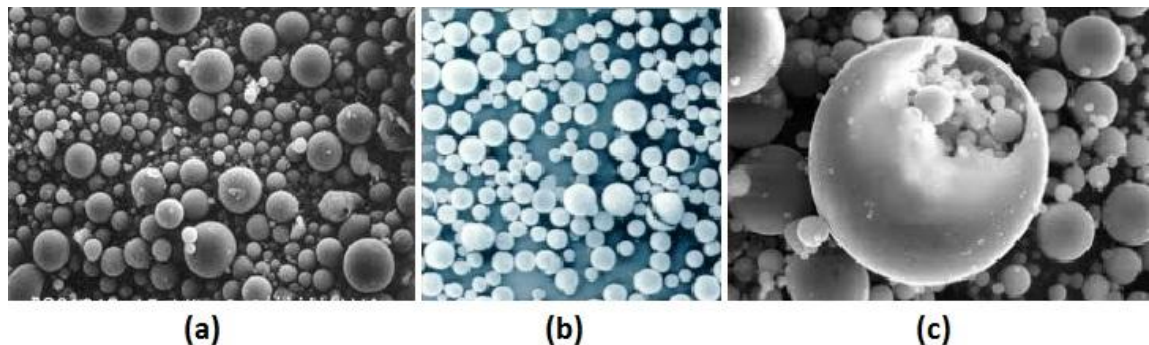
Figure 2. 6 General structures of precipitators (a), cenospheres (b) and plerospheres (c)

2.4.2 Physical, chemical and mineralogical characteristics of cenospheres

Cenosphere formation in thermo electric power stations needs a special condition and depends on a number of factors related to fuel characteristics and combustion type. Therefore, the common occurrence of cenospheres in fly ashes is very low, 0.3-1.5%. The major minerals and phases in cenospheres are alumino-silicate glass, mullite, quartz, calcite, iron oxides and calcium silicates and sulfates (Vassilev *et al.*, 2004). Chemically, similar to fly ash, cenospheres mainly include SiO_2 (55-65%), Al_2O_3 (27-33%) and

Fe_2O_3 (1-6%). Trapped gases in cenospheres are generally carbon dioxide (70%) and nitrogen (30%). The main physical properties of cenospheres are given in Table 2.8.

Table 2. 8 Basic physical properties of cenospheres (http://www.cenoash.com/products.htm)

Physical properties	Values
Average particle density	0.6-0.8 g/cm^3
Average bulk density	0.35-0.45 g/cm^3
Packing factor	60-65%
Hardness	Mohs-scale: 5-6
Wall thickness	5-10 % of sphere diameter
Melting temperature	1200-1600°C
Thermal conductivity	0.11 W/mK
Loss on ignition, (max.)	2.0%
Max. surface moisture	0.3%
Max. crush strength	105-210 kg/cm^2
Oil absorption	16-18 g oil/100 g cenosphere
Particle size	Grade 1: 5-500 μm
	Grade 2: 5-300 μm
	Grade 3: 5-150 μm

2.4.3 Advantages of cenospheres

The main advantageous properties of cenospheres can be summarized as follows:

➢ **Sphericity:** Spherical shape of cenosphere, which has the lowest surface area compared to its volume, mainly provides such a wide variety of application areas in comparison to the other lightweight fillers. Generally, spherical fillers give the final product with various superior properties such as excellent flow, reduced shrinkage, improved workability and lower binder necessity as a result of their shape. For these reasons, spheres are generally used as excellent fillers in order to keep the volume constant as much as possible.

➢ **Light-weight:** Cenospheres' second main advantage is resulted from their ultra-light weight. All the automotive, marine and aerospace industries need the materials with very low density to be used in plastic parts, sealants, putties etc. Although cenospheres have approximately 25% of the density of other mineral fillers, they also exhibit high strength in most applications. Therefore, they are commonly used in the construction industry as light-weight fillers.

➢ **High melting point:** Since cenospheres' melting temperature, 1200-1600°C, is considerably higher than synthetic glass microspheres, they can be used in almost all high temperature applications as refractories and fire resistant coatings and panels.

➢ **Inert:** Cenospheres' chemical composition, alumino-silicate spheres with very low reactivity, exhibits strong resistant to alkalis and acids.

➢ **Free flowing:** It means that cenospheres can be easily transported via pumps in a dry form.

➢ **Insulating:** Due to their low thermal conductivity, cenospheres find a variety of applications in insulating refractories, oil pipe-line insulation, geothermal cements, external wall insulation and many other uses.

- **Hard:** Cenospheres have a hard surface with a Mohs hardness of 5-6. As a result of this, they show high resistant to erosion. Also, their glassy shell gives the property of impermeability for liquids and gases.

- **Electrical properties:** Cenospheres can be used in electrical encapsulation and solenoids because of their excellent electrical properties as lightweight insulation additives.

- **Low oil absorption:** Cenosphere have the property of very low oil absorption because of their spherical shape with low surface area and the glassy, smooth and impermeable shell. Therefore, cenospheres seem to be a good candidate for the applications required low binder level without high viscosity increase.

- **Good packing factor:** Due to the small difference between their bulk and true density, cenospheres show a very high packing factor of 60-65%, resulting in a huge profit in transportation and storage costs (http://www.cenoash.com/products.htm).

2.4.4 Manufacturing process of cenospheres

Cenospheres naturally float in the wet discharging area, such as ponds and lagoons due to their low density and hollow spherical particles. The float cenospheres can be easily collected by simple skimming. The float product is then subjected to froth flotation process. After drying, a tribo electric separator is used to remove cenospheres from carbon and iron. The final cenosphere product is then specified in terms of different market requirements such as strength, density, size and color (http://www.apitco.org/Profiles/Cenospheres%20from%20fly%20ash.pdf).

2.4.4.1 Flotation

Alcala *et al.*, 1987 studied cenosphere recovery from fly ash by using two methods, namely flotation and simple sedimentation. Four different frothers, MIBC, two polypropilen glycol and pine oil were used throughout the experiments. According to the test results, the best results were obtained with MIBC frother. However, the cleanest cenosphere concentrate were achieved using simple sedimentation. In order to increase the settling rate of fly ash particles, four different flocculants were used through the sedimentation experiments.

2.4.4.2 Tribo-electrostatic separation

Electrostatic separation is based on the differences in electrical charges of the materials to be separated. This process mostly depends on the methods of charging and the particle characteristics such as electrical conductivity and surface contamination. There are mainly three charging mechanisms for commercial applications of electrostatic separation processes, namely ion or electron bombardments, conductive induction and contact or friction charging (tribo-charging). Tribo-electrostatic separation is based on the process that two materials should be charged oppositely when a third material is appropriately selected to be the contacting surface and then subjected to an electrical field for the separation of the materials (Yoon, 1999).

Gurupira *et al.*, 2001 investigated possibility of the selective separation of cenosphere, defined as particles with bulk density less than 2 g/cm^3 from fly ash by using tribo-electrostatic separation. According to this study, a specially designed air piping was used to transport fly ash, leading to a high surface charge on the fly ash particles. As a result of this, the polarity of the ash becomes negative whereas the carbon attains a positive charge. Since cenospheres have similar composition with fly ash, they also attain negative charge, resulting in effective carbon separation from the cenospheres when an electrical field applied after charging. Figure 2.7 shows the schematic of tribo-electrostatic separation process used by Li *et al.*, 1999.
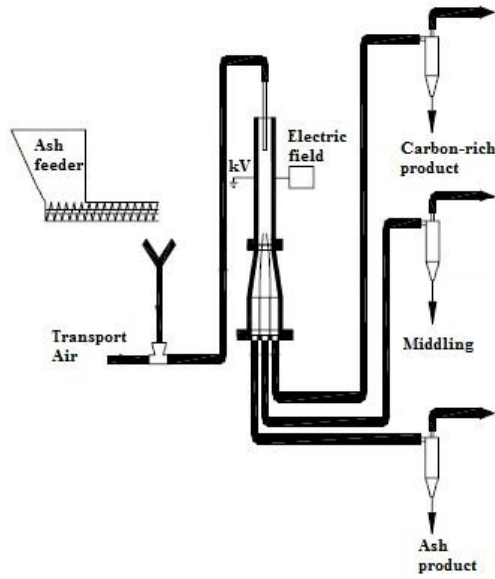
Figure 2. 7 Schematic of tribo-electrostatic separation process (Li *et al.*, 1999)

2.4.5 Grading of cenospheres

Today, there are a lot of producers of cenospheres due to their superior properties. These companies call special name for their own products with general properties of cenospheres. Grading of cenospheres are most widely done in terms of size. In addition, cenospheres are also specified by density, strength and color for different market requirements (http://www.cenosphereindia.com/grades.html).

2.4.6 Uses and utilization areas of cenospheres

Cenospheres have a number of uses and utilization areas in industry which are given in Table 2.9 (http://www.apitco.org/Profiles/Cenospheres%20from%20fly%20ash.pdf).

Table 2. 9 Uses of cenospheres in different markets (http://www.apitco.org)

Market	Product
Ceramics	Refractories, castables, tile, fire bricks, aluminum cement, insulating materials and coatings
Plastics	BMC, SMC, injection molding, extruding, PVC flooring, film, nylon, high density polyethylene, low density polyethylene and polypropylene
Construction	Specialty cements, mortars, grouts, stucco, roofing materials, acoustical panels, coatings, shotcrete and gunite
Recreation	Marine craft, flotation devices, bowling balls, surf boards, kayaks, golf equipment, footwear, lawn and garden decor
Automotive	Composites, undercoatings, tires, engine parts, brake pads, trim molding, body fillers, plastics and sound proofing materials
Energy and Technology	Oil well cements, drilling muds, industrial coatings, grinding materials, aerospace coatings and composites, explosives and propeller blades

2.4.7 Previous studies on cenosphere separation from fly ash

In literature, there are very few studies on separation of cenospheres from fly ash. The traditional cenosphere separation depends on wet processes where cenospheres float on the water due to their very low density as a result of disposal of fly ash in ponds or lagoons. In this condition, simple skimming is enough for the extraction of cenospheres from fly ash. This cenosphere product can be further concentrated using froth flotation (Alcala *et al.*, 1987; Hirajima *et al.*, 2010).

Alternative definitions of cenosphere were made by several scientists (Ghosal and Self, 1995; Gurupira *et al.*, 2001; Ramme *et al.*, 2008). According to these definitions, cenosphere was described as any particle in fly ash containing hollow spaces with density generally up to 2.0-2.2 g/cm^3. The density of cenosphere was not limited to 1 g/cm^3 in this new definition since the lowest density oxide in fly ash, crystalline silica, has a density of 2.2 g/cm^3. For this reason, particles with density greater than 1 g/cm^3 could also have gas bubbles in their interior and based on this new definition, these particles were also indicated as cenospheres. These heavier cenospheres containing less hollow space could also have high-value applications in construction industry as fillers and reinforcements because their greater wall thicknesses contribute to the strength of the final product. On the other hand, as high-value applications of cenospheres are mostly depending on their very low density, this new definition was not generally accepted by the considerable body of literature (Blissett and Rowson, 2012).

An alternative selective separation method of cenospheres, defined as particles with bulk density less than 2 g/cm^3, from fly ash was used by Gurupira *et al.*, 2001 with a specially designed pneumatic transport, tribo-electrostatic separation. Product density was especially evaluated using He pycnometry as a processing efficiency. Also, laser granulometry and optical and scanning electron microscopy were used for further characterization of the products. The test results indicated that products with density of 1.6 g/cm^3 could be obtained by the tribo-electrostatic separator, meaning that these products seems to be used as light-weight filler in ceramic and construction industry.

Hirajima *et al.*, 2010 investigated the performances of wet and dry separations for recovery of industrial cenospheres from coal fly ash by using the terminal velocity concept. Size and density measurements of both industrial cenospheres and fly ash were done to calculate the terminal velocity of the particles which were then used for performance estimation. According to this estimation, similar efficiencies were obtained for both wet and dry separations. Furthermore, in wet separation, cenospheres were concentrated in the overflow product due to their positive buoyancy, so separation was dependent on density in this condition. On the other hand, cenospheres were concentrated in the underflow product for dry separation since both the industrial cenospheres and the fly ash have densities much higher than air. Unlike to the wet separation, this process was based on size in this case. In order to check the estimation of dry process, a micron separator designed by Hosokawa Micron Co. was used. The test results indicated that cenospheres were also obtained in the underflow product with very close recovery in comparison to the theoretical one.

According to the same research group, wet separation techniques of cenospheres have some disadvantages such as consumption of large amounts of water and water pollution because of leaching possibility of heavy metals from fly ash. The researchers thought that air classification can be a good alternative. In this experimental study, separation efficiencies of two types of air classifiers, the closed-type pneumatic separator and the micron separator, were investigated. Based on the test results, the micron separator gave much better separation efficiency compared to the closed-type pneumatic separator. However, both separators were considerably less efficient than their estimated efficiencies. After the air classification, the cenosphere product of the micron separator (underflow) was subjected to a sink-float test where 87.8% reduction in fly ash weight was obtained with 80% of cenosphere recovery. Overall results suggested that air classification can be used for recovery of cenospheres with obtaining large reduction in water amount (Petrus *et al.*, 2011).

2.5 Fly ash utilization in Turkey

Total annual fly ash production in Turkey is approximately 15 million tones, most of which is resulted from burning of lignite (Alkaya, 2009). A very small amount of fly ash produced finds application mostly in cement industry. Therefore, fly ash disposal seems to be a significant problem for Turkey. However, fly ash utilization has been increasing day by day in Turkey (Alkaya, 2009; Tuzcu, 2005).

2.6 Worldwide fly ash utilization

According to the American Coal Ash Association (ACAA) and European Coal Combustion Products Association (ECOBA), in 2010, total fly ash production in the USA was 67.7 million tons, while, in 2009, this fly ash production in Europe (EU-15 Countries) was 34.3 million tones. 37.9% of total produced fly ash was used in various applications in the USA, whereas this utilization was 44% in Europe (EU-15 Countries) for the mentioned years (ACAA, 2011; ECOBA, 2010).

CHAPTER 3

MATERIAL CHARACTERIZATION

3.1 Materials

In this study, the coal fly ash samples were obtained from Çatalağzı and Sugözü thermal power plants of Turkey. Both of the fly ashes are resulted from burning of bituminous coals.

3.1.1 Çatalağzı thermal power plant

Çatalağzı thermal power plant is located near the Doğancılar and Kazköy villages of Zonguldak and 2 km away from the Çatalağzı Town. General information about the power plant is given in Table 3.1 (http://www.catestermik.com/index/cates.html).

Table 3. 1 General information about Çatalağzı thermal power plant

Installed power	2 x 150 MW
Annual production	2 x 966,000,000 kWh
Main fuel	Bituminous coal from heavy medium separation tailing (Low heating value = 3,300 kcal/kg)
Annual fuel consumption	Bituminous coal = 1,600,000 tons Fuel-oil = 7,200 tons, diesel-oil = 480 tons

3.1.2 Sugözü thermal power plant

Sugözü thermal power plant is located near the Yumurtalık town of Adana. Table 3.2 shows general information about the power plant (http://www.isken.com.tr/tr/index.asp).

Table 3. 2 General information about Sugözü thermal power plant

Installed power	2 x 660 MW
Annual production	9,000,000,000 kWh
Main fuel	Imported bituminous coal (Low heating value = 6,000 kcal/kg)

3.2 Characterization of the fly ash samples

3.2.1 Chemical compositions

The major chemical constituents of Çatalağzı and Sugözü fly ash samples were determined with Spectro IQ X-ray fluorescence (XRF) spectrometer shown in Figure 3.1. The major chemical constituents of the samples are presented in Table 3.3.

Figure 3. 1 Spectro IQ X-ray fluorescence (XRF) spectrometer (METU MinE Lab.)

Table 3. 3 Major chemical constituents of the samples

Constituents (%)	Çatalağzı	Sugözü
SiO_2	57.09	63.35
Al_2O_3	27.46	22.01
Fe_2O_3	6.56	7.90
CaO	1.97	1.45
MgO	2.38	2.31
Na_2O	0.31	0.79
K_2O	3.89	1.95
P_2O_5	0.11	0.16
TiO_2	1.13	0.91
SO_3	<0.01	<0.01

Table 3.3 indicates that SiO_2, Al_2O_3 and Fe_2O_3 are the major chemical constituents of the samples. According to ASTM C618 (ASTM, 2012), both samples meet the chemical requirements to be a class F fly ash with high amounts of silica, alumina and iron oxide and low amount of calcium oxide.

Heavy metal contents of the samples were also determined using microwave-assisted acid digestion (MW-AD) followed by inductively coupled plasma (ICP)-mass spectroscopy (MS) shown in Figure 3.2. A combination of HNO_3, HCl and HF was used for digestion of the samples due to their aluminosilicate compositions. Leachability characteristics of the same elements were further investigated in deionized water using the Turkish standard test (TS EN 12457-4) (TS EN, 2004).

Figure 3. 2 Perkin Elmer DRC II model ICP-MS (METU Central Lab.)

The heavy metal contents and the leachability characteristics of these metals from the fly ash samples are given in Table 3.4. In this table, toxicity limits of these metals based on the regulation of hazardous waste in Turkish standard, storage criteria of solid wastes (Appendix 11-A) can also be clearly seen (TS, 2005). Table 3.4 indicates that leaching capacities of all the metals are far from being considered as hazardous waste and most of these metals have the leaching capacities below the toxicity limits for non-hazardous waste.

Table 3. 4 Heavy metal contents and leachability characteristics of the samples

Element	Heavy Metal Contents (mg/kg)		Solubility, Leaching Test (mg/l) (TS EN 12457-4)		Toxicity Limits (mg/l) Regulation of Hazardous Waste in Turkish Standard, Storage Criteria of Solid Wastes (Appendix 11-A)		
	Çatalağzı	Sugözü	Çatalağzı	Sugözü	IW[a]	NHW[b]	HW[c]
Cd	3.77	5.73	0.004	0.008	≤ 0.004	0.004-0.1	< 0.1-0.5
Co	36.80	28.42	0.04	0.05	NI[d]	NI[d]	NI[d]
Cr	169.41	167.05	0.19	0.30	≤ 0.05	0.05-1	< 1-7
Cu	87.19	57.66	0.01	0.01	≤ 0.2	0.2-5	< 5-10
Ni	74.04	67.66	0.06	0.07	≤ 0.04	0.04-1	< 1-4
Pb	105.55	103.77	0.03	0.04	≤ 0.05	0.05-1	< 1-5
Zn	113.30	148.43	0.005	0.009	≤ 0.4	0.4-5	< 5-20
Mn	621.84	493.71	0.01	0.009	NI[d]	NI[d]	NI[d]

[a] Inert waste.
[b] Non-hazardous waste.
[c] Hazardous waste.
[d] Not included.

3.2.2 Mineralogical compositions of the samples

X-ray powder diffraction (XRD) was utilized to determine the mineralogical compositions of the fly ash samples. XRD patterns of the as-received samples were recorded using a Rigaku MiniFlex X-ray diffractometer shown in Figure 3.3. The X-ray diffractometer utilizing Cu Kα radiation was operated at 40 kV and 40 mA with a 2θ range of 5-80°. Analyses of the resulting XRD patterns were done by comparing the peak positions and intensities of the fly ash samples with those in the Joint Committee on Powder Diffraction Standards (JCPDS) data files. Figures 3.4 and 3.5 illustrate the XRD patterns of Çatalağzı and Sugözü fly ashes, respectively. The two figures show that the main crystalline phases for both samples are quartz, mullite and hematite.

Figure 3. 3 Rigaku MiniFlex X-ray diffractometer (http://mcc.lsu.edu/)
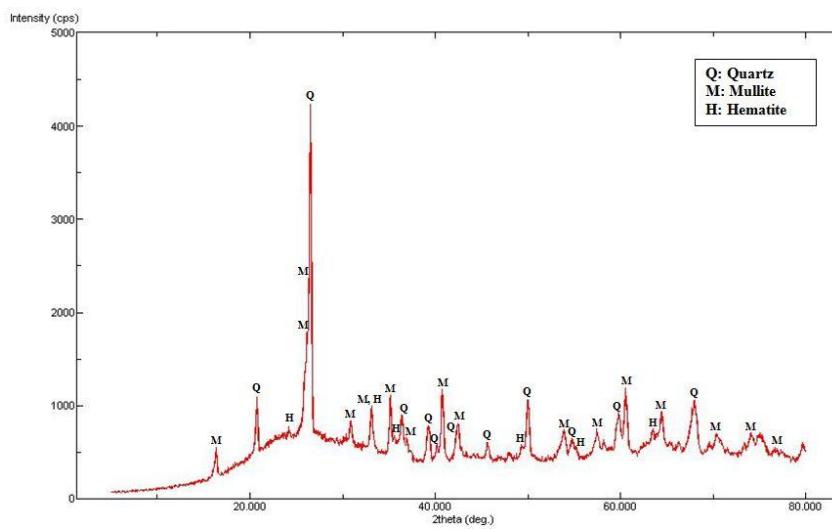
Figure 3. 4 Mineralogical composition of Çatalağzı fly ash
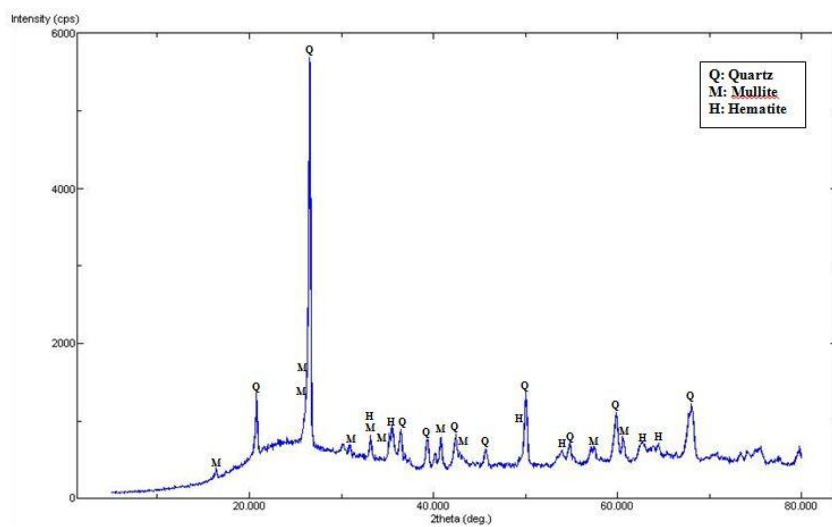
Figure 3. 5 Mineralogical composition of Sugözü fly ash

3.2.3 Microstructural characteristics of the fly ashes

Scanning electron microscopy (SEM) was used to observe the microstructural properties of the samples. SEM investigations of the fly ashes were done using JEOL JSM-6400 and Hitachi S-4800 shown in Figures 3.6 and 3.7, respectively.

Figure 3. 6 JEOL JSM-6400 scanning electron microscopy (METU MetE Lab.)

Figure 3. 7 Hitachi S-4800 scanning electron microscopy (CAER Lab.)

Figures 3.8 and 3.9 show the general views of Çatalağzı and Sugözü fly ashes with different magnifications, respectively. As seen from the figures, both fly ashes consist of generally small and glass like particles with spherical shape and also larger irregularly shaped particles. Wide variations in size and shape of particles can also be seen from the SEM images. In addition to some amorphous and crystalline phases, hollow spherical particles (cenospheres) and particles containing micro spheres in their interior (plerospheres) are also present in both samples. Opaque amorphous particles are generally resulted from coal particles which were not subjected to complete combustion while opaque spheres mostly consist of iron oxides (hematite and magnetite) alone or along with silicates.
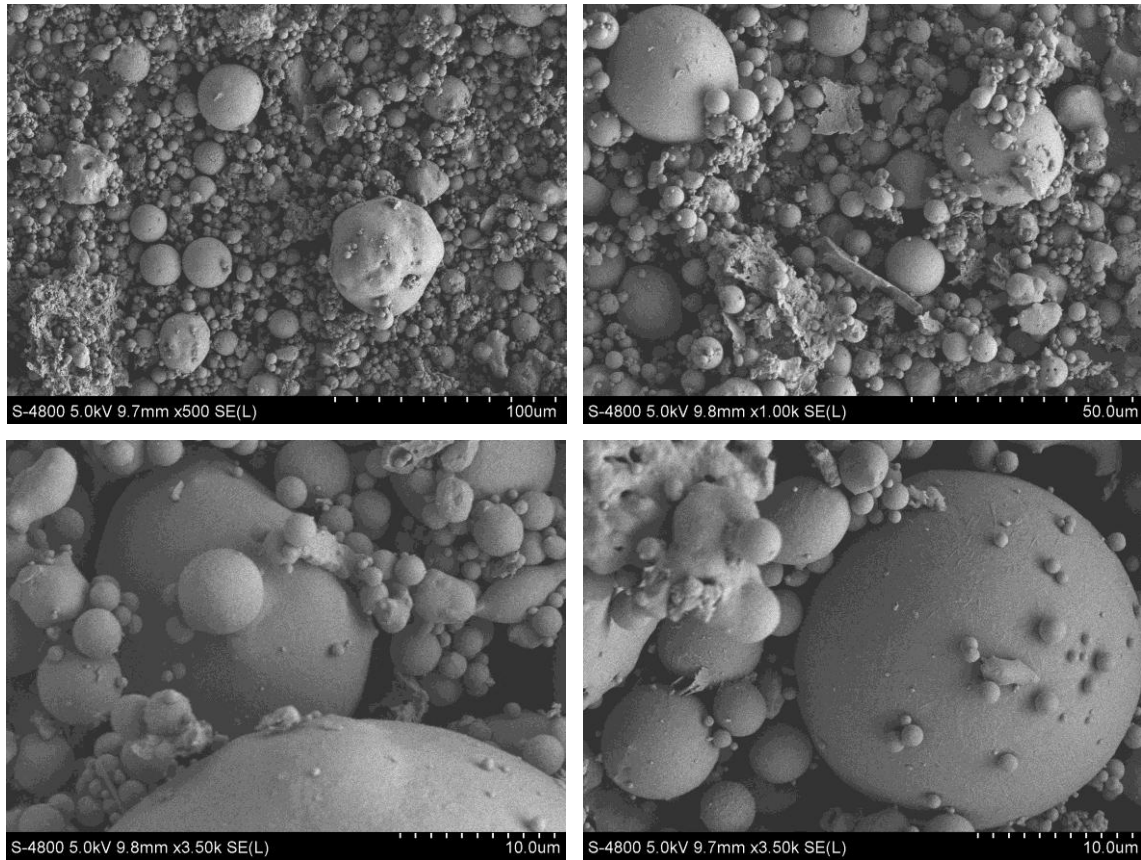
Figure 3. 8 General views of Çatalağzı fly ash with different magnifications

Figures 3.8 and 3.9 also indicate that Sugözü fly ash has more amounts of finer particles and opaque spheres compared to Çatalağzı fly ash. On the other hand, Çatalağzı fly ash includes much more non-opaque cenospheres than Sugözü fly ash. Figures 3.10 and 3.11 show the SEM image of a non-opaque cenosphere particle in Çatalağzı fly ash and its elemental analysis by means of energy-dispersive X-ray spectroscopy (EDX), respectively. As seen from these figures, aluminosilicate contents constitute major components of the cenosphere particle. Similarly, Figures 3.12 and 3.13 illustrate the SEM image of an irregularly shaped opaque particle in Sugözü fly ash and its elemental analysis by EDX, respectively. According to Figures 3.12 and 3.13, the irregularly shaped particle consists of almost totally silicates with very little amount of alumina.
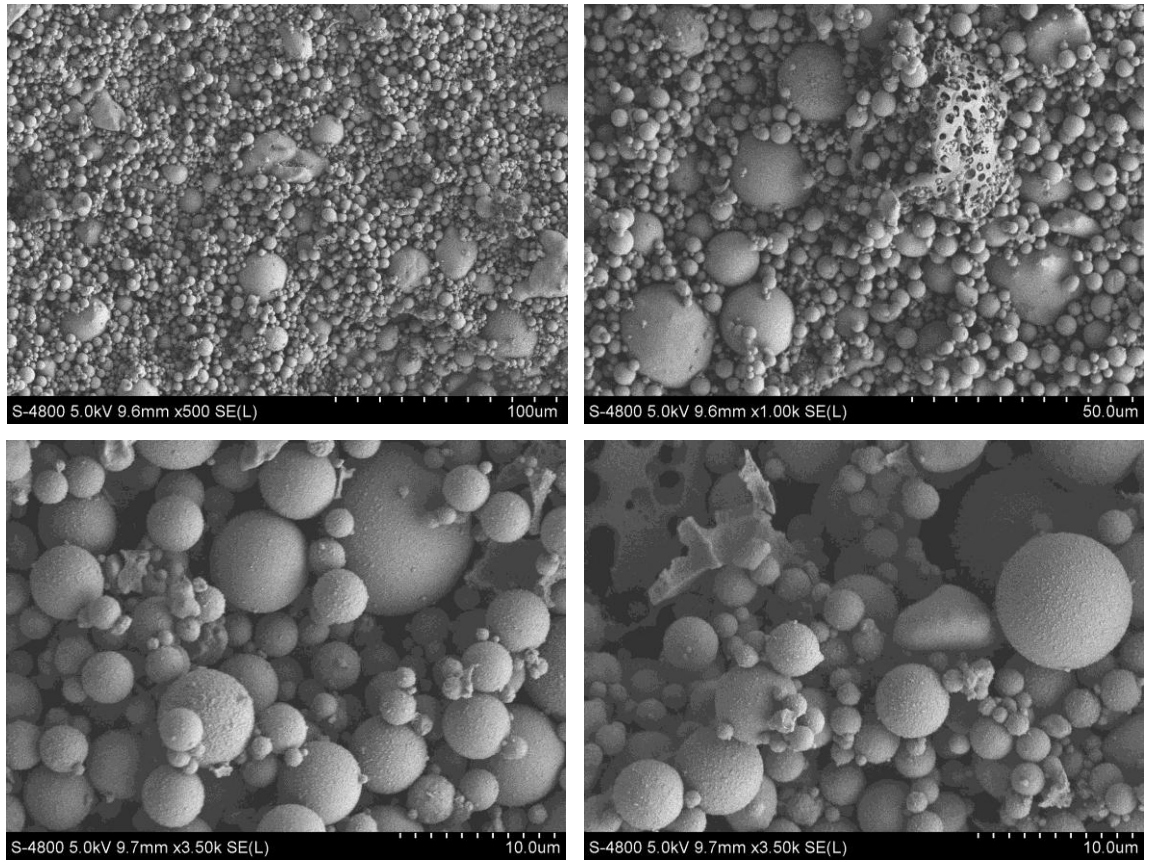
Figure 3. 9 General views of Sugözü fly ash with different magnifications
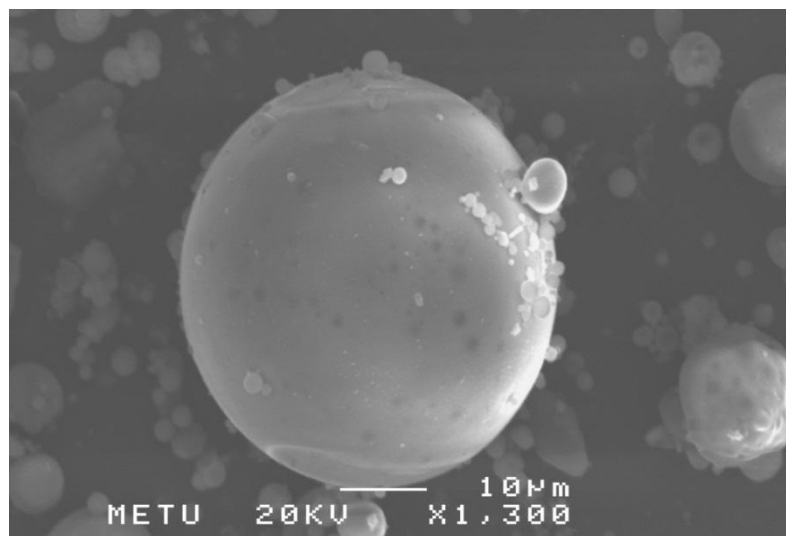
Figure 3. 10 SEM image of a spherical cenosphere particle in Çatalağzı fly ash
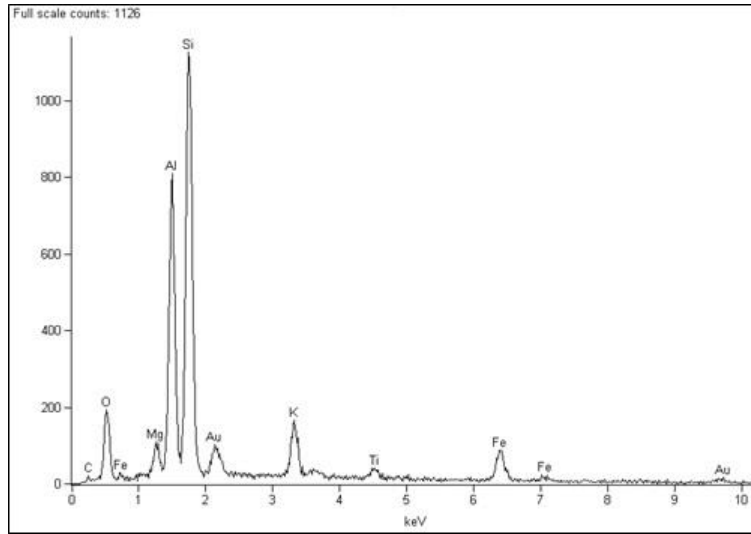
Figure 3. 11 Elemental analysis of the cenosphere particle in Çatalağzı fly ash
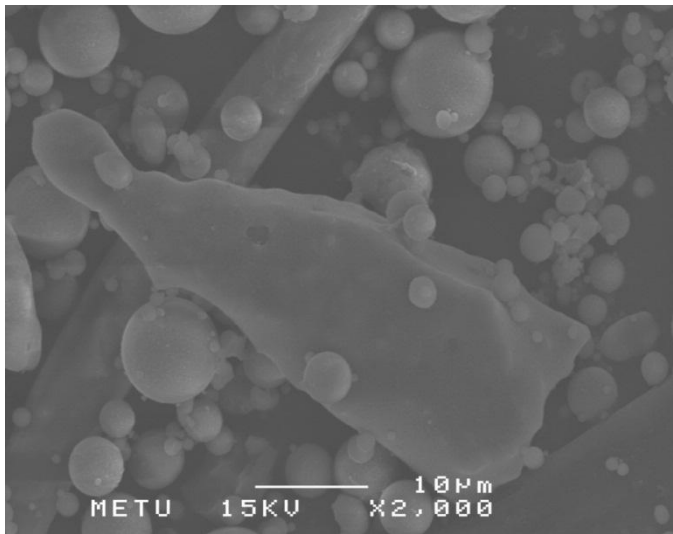
Figure 3. 12 SEM image of an irregularly shaped opaque particle in Sugözü fly ash
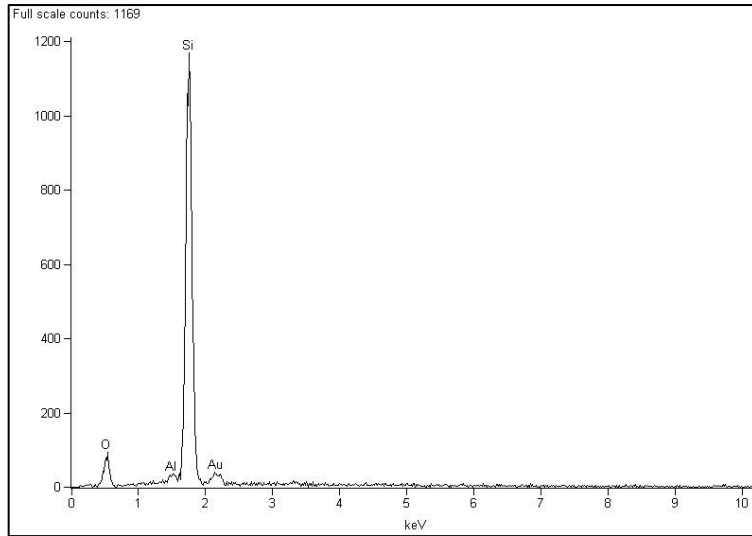
Figure 3. 13 Elemental analysis of the irregularly shaped particle in Sugözü fly ash

3.2.4 Particle size analysis

Particle size measurements of Çatalağzı (CFA) and Sugözü (SFA) fly ashes were done by both wet sieving and laser size analysis.

3.2.4.1 Wet sieving

Wet sieving analyses were performed using Tyler sieve series from 300 µm down to 38 µm. Table 3.5 shows wet sieving results of the samples. According to the table, average particle size of CFA is much coarser than that of SFA.

Table 3. 5 Wet sieving results of the fly ash samples

Nominal aperture size	Cumulative Weight of Undersize (%)	
(µm)	CFA	SFA
300	96.46	99.41
212	90.75	99.25
150	81.05	98.89
106	73.62	96.13
75	64.60	89.16
53	54.85	82.50
38	48.85	69.26

3.2.4.2 Laser size analysis

Laser size analyses of the samples were also done by using Malvern Mastersizer 2000 Particle Size Analyzer (Figure 3.14). Particle size distributions of the samples in volumetric basis based on laser size analyses were given in Figure 3.15. As seen from Figure 3.15, 50% passing sizes (d_{50}) of CFA and SFA in volumetric basis are approximately 40 µm and 23 µm, respectively.

Figure 3. 14 Malvern Mastersizer 2000 Particle Size Analyzer (METU Central Lab.)
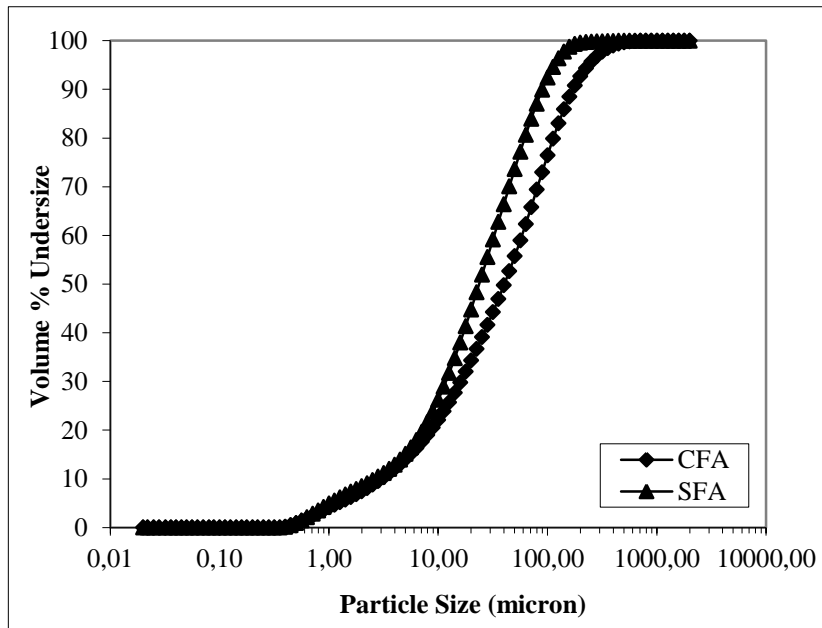
Figure 3. 15 Particle size distributions of the samples based on laser size analyses

3.2.5 Specific gravity determination

Specific gravities of the coal fly ash samples were measured with water pycnometer. Firstly, the empty pycnometer was weighed (P_1). The fly ash sample was then put into the pycnometer and weighed (P_2). In the next step, the pycnometer including sample was filled up with distilled water and weighed (P_3). In the final step, the pycnometer filled up with only distilled water was weighed (P_4) and the following equation was used to calculate specific gravities of the samples.

$$Specific\ Gravity = \frac{(P_2 - P_1)}{(P_2 + P_4) - (P_1 + P_3)} \tag{3.1}$$

For each measurement, the above procedure was repeated three times and the average value of these was accepted as the specific gravity of the sample. The specific gravities of the fly ash samples and the relationship between specific gravity and size are given in Table 3.6. As seen from the table, CFA has a lower specific gravity than SFA and specific gravity values increase with decreasing in particle size for both samples.

Table 3. 6 Specific gravity values of the fly ash samples

CFA	Specific Gravity	SFA	Specific Gravity
Original Sample	2.04	Original Sample	2.31
+150 µm	1.36	+106 µm	1.96
-150+75 µm	1.68	-106+75 µm	2.06
-75+38 µm	1.89	-75+38 µm	2.15
-38 µm	2.35	-38 µm	2.38

3.2.6 Density measurements

Density measurements were done using helium pycnometer. Each measurement was repeated three times and average value was accepted as the density of sample. The obtained density results are given in Table 3.7. Specific gravities of the samples were confirmed by the density measurements.

Table 3. 7 Density of the fly ash samples

Sample	Density (g/cm^3)
CFA	2.0765
SFA	2.3648

3.2.7 Porosity measurements of the samples

Porosity measurements of the fly ashes were done using Quantachrome Poremaster-60 Mercury Porosimeter (Figure 3.16). In the measurements, due to the powder compositions of the samples, the macro pores cannot be determined. In other words, only the values of micro pores (<10 µm) and total porosities can be obtained. The measurement is based on the physical principle that until a certain amount of pressure, a non-wetting liquid cannot be penetrated into the fine pores.

The mercury penetration data is generally used to plot volume distribution as a measure of pore diameter. Figures 3.17 and 3.18 illustrate the pore size distributions of CFA and SFA, respectively. The test results also indicate that total porosity value of CFA is 19.99% while this value is 6.97% for SFA.

Figure 3. 16 Poremaster-60 Mercury Porosimeter (http://www.quantachrome.com/)
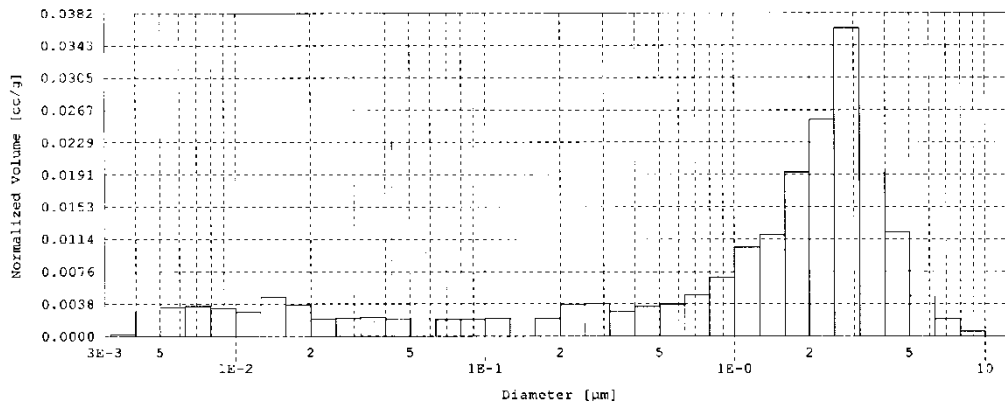
Figure 3. 17 Normalized volumes as a measure of pore size for CFA
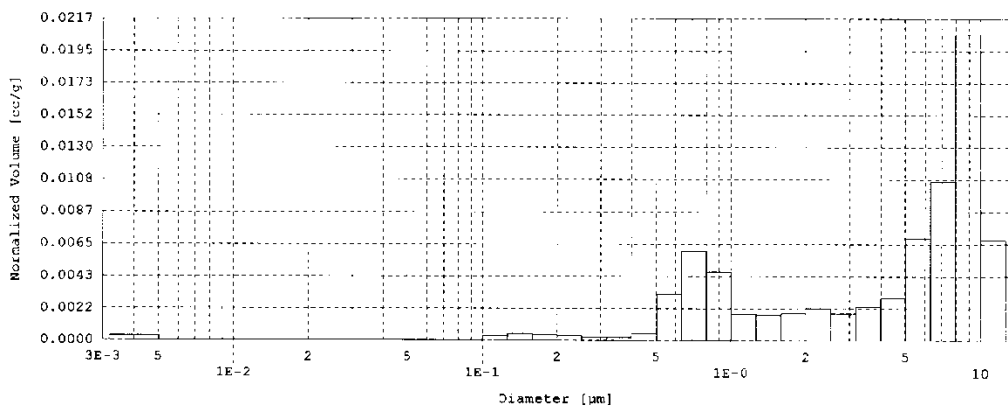
Figure 3. 18 Normalized volumes as a measure of pore size for SFA

3.2.8 Specific surface area measurements of the samples

The specific surface areas of the fly ash samples were measured using BET and Blaine methods. Sample preparation and specific surface area determination by BET method were done with the equipment of ASAP 2020 Micromeritics Specific Surface Analyzer (Figure 3.19). In addition to BET nitrogen adsorption method, the surface areas of the samples were also determined with Blaine air permeability apparatus in University of Dundee, Concrete Technology Unit. The specific surface area results of single point and BET measurements based on nitrogen adsorption and Blaine measurements are summarized in Table 3.8. According to this table, SFA has a higher surface area compared to CFA due to its finer particle size. BET method gave higher surface area values for both samples compared to Blaine method because of the higher adsorption rate of nitrogen used in BET.

Table 3. 8 Results of the specific surface area measurements

Method	Surface area (m^2/g)	
	CFA	SFA
Single point method at P/Po = 0.300718474	0.7960	1.1298
BET method	0.8284	1.1715
Blaine method	0.3850	0.4290

Figure 3. 19 ASAP 2020 Micromeritics Specific Surface Analyzer (CAER Lab.)

3.2.9 Loss on ignition (LOI) determination

Table 3.9 shows the loss on ignition of the two samples and the relationships between loss on ignition and size. As seen from the table, CFA has a lower loss on ignition than SFA. This table also indicates that loss on ignition decreases with decreasing in particle size for both samples. Coarse size fractions of the samples have higher loss on ignition values since the unburned carbon particles are concentrated in coarse size fractions especially for SFA sample.

Table 3. 9 LOI values of the fly ash samples

CFA	LOI (%)	SFA	LOI (%)
Original Sample	1.45	Original Sample	2.05
+150 µm	3.60	+106 µm	10.26
-150+75 µm	2.23	-106+75 µm	7.19
-75+38 µm	2.08	-75+38 µm	3.06
-38 µm	1.15	-38 µm	1.57

3.2.10 Float-sink experiments

Float-sink experiments were performed to observe the relationship between material density and amount of floating products. In these experiments, the fly ash samples were placed in beakers with water or heavy medium solutions (solid-liquid ratio 1:10) at ambient temperature. $ZnCl_2$ solutions were used to prepare heavy medium for the specific gravities from 1.10 to 1.80. Suspensions were periodically stirred for half an hour. After the residence time of 24 hours, floating products were separated from the solutions by decantation and filtration through membrane filters. After washing and drying in a furnace, final float products were obtained. The results of float-sink experiments are given in Table 3.10. According to the table, as expected from the specific gravity and density measurements, CFA has much more amounts of floating products compared to SFA probably due to its high amount of hollow spheres.

Table 3. 10 Float-sink experiments of the fly ashes

Specific gravity	Cumulative float weight (%)	
	CFA	SFA
1.00	1.43	0.08
1.10	1.94	0.13
1.20	4.04	0.70
1.30	6.14	1.04
1.40	8.15	1.25
1.50	10.88	1.64
1.60	15.24	1.88
1.70	19.76	2.13
1.80	24.71	4.30

CHAPTER 4

METHODS

4.1 The methods of sintering experiments

The methods used in sintering experiments of CFA and SFA samples can be divided into two main categories, namely preparation of green (unsintered compacted) and sintered samples and characterization of the sintered samples.

4.1.1 Preparation of sintered materials

The fly ash samples (a total of 20 grams per a SFA pellet and 17.2 grams per a CFA pellet) were well mixed with 5% distilled water and then uniaxially pressed at 65 MPa as the circular pellets of 31.30 mm diameter by using a pellet die and a press. The die and the press used for preparation of the pellets are illustrated in Figures 4.1 and 4.2, respectively.

Figure 4. 1 Pellet die used for preparation of the pellets (METU MinE Lab.)

Figure 4. 2 Ele Autotest 3000 compression machine (METU MinE Lab.)

In the second stage, the green specimens were preheated to 300^oC for 1 h to remove moisture and any other gases prior to sintering at high temperature. The specimens were then fired at the temperatures in the range of $1000\text{-}1150^oC$ with 50^oC intervals for the sintering times of 0.5, 1.0, 1.5 and 2.0 hours. Heating rate of $10^oC/min$ was kept constant throughout the experiments. For each set of operating conditions (temperature-time pairs), 15 samples were prepared and then fired in a single run using a furnace with programmable controller (Figure 4.3).

Figure 4. 3 Protherm heat treatment furnace (METU MinE Lab.)
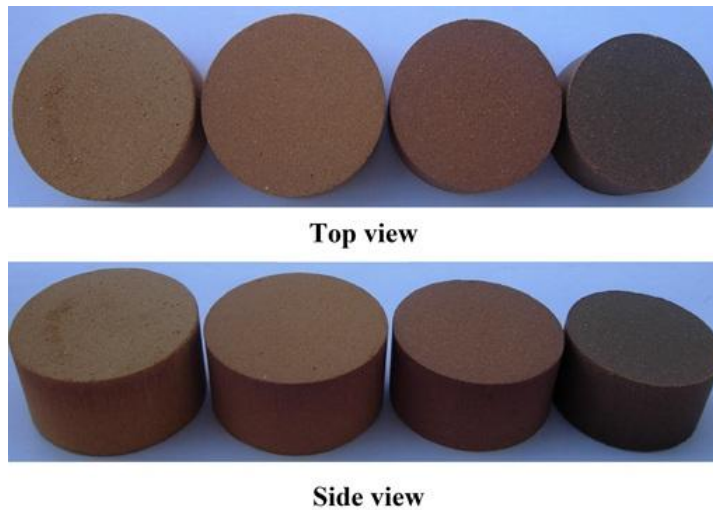
Figure 4. 4 Sintered CFA pellets processed for different sintering temperatures
(From left to right: 1000^oC, 1050^oC, 1100^oC and 1150^oC for the sintering time of 1.5 hours)

Figures 4.4 and 4.5 illustrate the sintered CFA and SFA pellets processed. In these figures, from left to right, temperature was 1000^oC, 1050^oC, 1100^oC and 1150^oC for both samples.
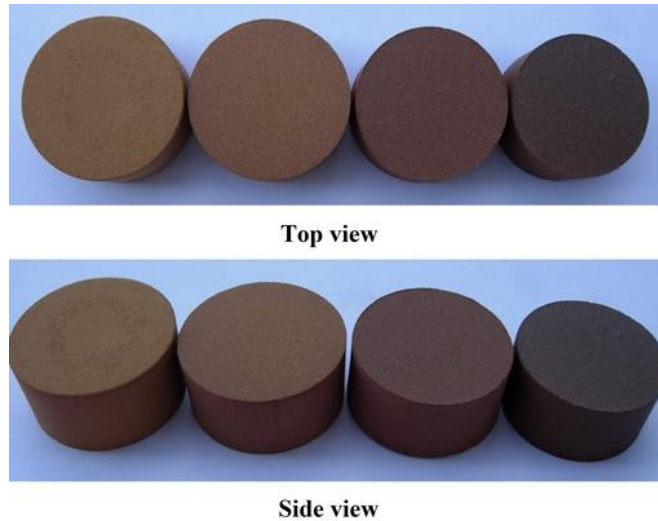
Figure 4. 5 Sintered SFA pellets processed for different sintering temperatures
(From left to right: 1000°C, 1050°C, 1100°C and 1150°C for the sintering time of 1.5 hours)

4.1.2 The methods for characterization of the samples

4.1.2.1 Measurements of physical and mechanical properties

The sintered class F fly ashes were characterized for a number of physical and mechanical properties used in ceramic industry. Bulk density, axial and radial shrinkage, water absorption and porosity analyses were carried out as physical measures of sintering efficiency (Acar and Atalay, 2012). Bulk density was calculated from the measured weight and specimen dimensions according to ASTM C134 (ASTM, 2005). Axial and radial shrinkage was measured based on ASTM C326 from the reduction in the height and diameter of the specimen, respectively (ASTM, 2003). Water absorption and apparent porosity were measured according to ASTM Standard C20 (ASTM, 2005). With regard to this standard, water absorption was determined from the increase in weight after the sample was subjected to 2 hours-boiling and 12 hours residence time in distilled water. Apparent porosity expresses as the ratio of the volume of the open pores in the specimen to exterior volume of the specimen.

Figure 4. 6 Tinius Olsen compression testing machine (METU MinE Lab.)

In addition to these physical specifications, mechanical characterization was performed on the basis of ASTM D3967 by the measurement of diametrical compression strength from which the splitting tensile strength (STS) was calculated (ASTM, 2008). Figure 4.6 shows the test machine used for determination of STS of the sintered samples.

4.1.2.2 Microstructural characterization of the sintered samples

Phase developments and microstructural changes due to sintering process were determined with X-ray diffraction (XRD) and scanning electron microscopy (SEM) analyses. The sintered fly ash samples were analyzed by XRD to determine the mineralogical changes in crystalline phases. XRD patterns were recorded by using a Rigaku MiniFlex X-ray diffractometer operated at 40 kV and 40 mA utilizing Cu Kα radiation with a 2θ range of 5-80°, at a step size of 0.02 and a dwell time of 2 s per step. A software package program was utilized to analyze the resulting patterns. Analyses of the patterns were done by comparing the peak positions and intensities of the samples with those in the Joint Committee on Powder Diffraction Standards (JCPDS) data files. SEM investigations were performed by using JEOL Model JSM-6400 operated at 20 kV to observe the microstructural changes in the sintered samples. The microstructures were examined to observe the degree of interactions among the particles, surface roughness and the amount of pore structures in the sintered samples as a function of processing conditions (Acar and Atalay, 2012). In the SEM observations, a couple of images were taken for each sample.

4.2 The methods used for determination of pozzolanic reactivity and utilization potentials of the samples as a high quality pozzolan

In the first stage of this study, ultrafine particles were tried to be recovered from Çatalağzı and Sugözü fly ashes using a hydraulic classification technology developed at CAER (Center for Applied Energy Research, University of Kentucky). In the second stage, the pozzolanic properties of these ultrafine fly ash products and as received samples were examined for their utilization potentials as high quality cement replacement materials. To accomplish this, the properties of mortar, both in the fresh and the hardened state, were tested based on ASTM standards for compressive strength and durability. Furthermore, paste experiments were designed to better understand the pozzolanic reactivity of the as received and classified fly ash samples during cement hydration.

4.2.1 The methods used for classification experiments

The classification experiments were performed in two stages. Since fly ashes have a high tendency to be flocculated in water, settling experiments were first designed for both samples by using two different dispersants in order to determine the more effective one and its optimum dosage. In the second stage, the hydraulic classification experiments were conducted on the basis of these settling experiments.

4.2.1.1 Settling experiments

Hydraulic classification is mainly based on the size and density of a material. In hydraulic classification systems, fly ash generally tends to flocculate and these flocs are considerably stable even for high pH values. In literature, some known chemicals such as sodium silicate and potassium hydroxide have been used to disperse the flocs. However, these attempts have not given satisfying results for the classification of fly ash. Some good results have been obtained with potassium metaphosphate and pyrophosphate (Robl and Groppo, 2003). On the other hand, these results have been erratic and highly substrate dependent. Therefore, it is required to find another dispersants producing high yield.

Some chemicals known as "superplasticizers" (SP), which are a group of organic water soluble polymers with long molecules of high molecular mass, are largely used in the cement and concrete industry because of their contributions to dispersion and water reduction properties. According to some projects, these chemicals can also be used as effective dispersing agents for separation of ultrafine particles (Robl and Groppo, 2003; Robl and Groppo, 2011).

4.2.1.1.1 Chemistry and working mechanism of superplasticizers

Superplasticizers (SP), commonly used in cement and concrete industry, provide many advantageous, in that they assist in the effective dispersion of cement particles, leading to an improvement in the workability of concrete. The main purpose of SP utilization in cement paste is to reduce the water to cement ratio, which results in reduced permeability, increased strength and improved durability in concrete. The strength of concrete also increases with SP addition. According to most of the literature data, an optimum dosage of SP was found as 2.0-2.5% of cement by weight in the paste, mortar or concrete systems. Beyond this level, a decrease in compressive strength was observed. However, some researchers reported that strength increased up to the SP dosage of 1.0% of cement by weight (Khatib and Mangat, 1999).

Today, commonly used superplasticizers are polynapthalene sulphonate, polymelamine sulphonate, carboxylated synthetic polymers, polyacrylates and aqueous sodium naphthalene sulphonate formaldehyde condensate (NSF) (Robl and Groppo, 2003). In the SP based on melamine and naphthalene sulphonate polymers, cement particle surfaces are covered by these chemicals within the first stage of concrete mixing. Sulphonic groups of these polymers lead to an increase in negative charge of the particle surfaces, forming electrostatic repulsion forces among the particles. Particle dispersion is enhanced as the result of this electrostatic repulsion mechanism, leading to improved concrete workability with less amount of water in the mixture. On the other hand, hydration begins as soon as cement particles contact with water, causing rapidly growing hydration phases on the particle surfaces. This changing in the surfaces prevents free dispersion of the cement particles due to the less interaction between the particles and superplasticizers. New technology carboxylate based SP polymers were developed to solve this problem. Electrostatic repulsion mechanism is also valid at the start of mixing like in melamine and naphthalene sulphonate polymers. In addition to this, dispersion of cement particles is stabilized with the help of the chains bound on polymer backbone which form a steric hindrance, resulting in a higher fluidity with less water (http://www.basf-yks.com.tr).

4.2.1.1.2 The methodology of settling experiments

Two different types of the SP polymers based on sulphonate (NSF, Disal) and carboxylate (Glenium 7500) were used in the settling experiments. Unlike NSF dispersant (Disal), Glenium 7500, which is a high range water reducing admixture, is based on the next generation of polycarboxylate technology (http://www.caribbean.basf-cc.com). Dispersant dosages of 0.5, 1.0, 1.5, 2.0, 2.5 and 3.0 mg/g of fly ash were tested in these experiments. Also, control experiments were done without dispersants to observe the differences. In these experiments, pulps with 1.5% solid content were prepared in a 250 ml graduated cylinder. After the required amount of dispersant was added to the fly ash pulp, the graduated cylinder was well mixed for a minute. The pulp was taken down to 100 ml level using a vacuum pump after 5 minutes of settling time. After the filtration and drying, the sample was weighed. Weight percentages of solid in the floating products were used as the measure of dispersant efficiency.

4.2.1.2 Classification experiments (Ultrafine ash process)

Today, hydrocyclone and hydraulic classifiers are the most widely used classifiers in mineral processing. For the separation of fine particles, hydrocyclones are commonly used in most applications down to 75 μm and smaller size cyclones can be used to separate fine particles down to a few microns. However, in addition to the problem of plugging due to small openings of the cyclone, the capacity is also reduced in

this condition. On the other hand, conventional hydraulic classifiers are usually designed to obtain clean coarse fractions without slimes. Hydraulic classifiers have a major disadvantage known as "blanket settling" which can be defined as the hindering of smaller particles' upward movements due to coarser particles. As expected, hydraulic classifiers generally have very low yield and recovery for the separation of very fine particles (Robl and Groppo, 2011).

The hydraulic classification technology used in this research is based on a method for cross-flow of particles in slurry for selective separation of fine particles. The method includes preparing dispersant added slurry of solids and establishing a cross-flow between the slurry and particles in which the movements of slurry and particles are perpendicular to each other. The interior dividers are also provided for effective removing of coarse particles from the system by increasing the settling area. The bottom of the classifier is separated into four underflow discharge areas for selective removal of particles with sequentially decreasing size. This classifier also provides cenosphere recovery if fly ash containing cenospheres are used as feed (Robl and Groppo, 2011). The hydraulic classifier used in this research for recovering of ultrafine particles from CFA and SFA samples is schematically illustrated by Figure 4.7.
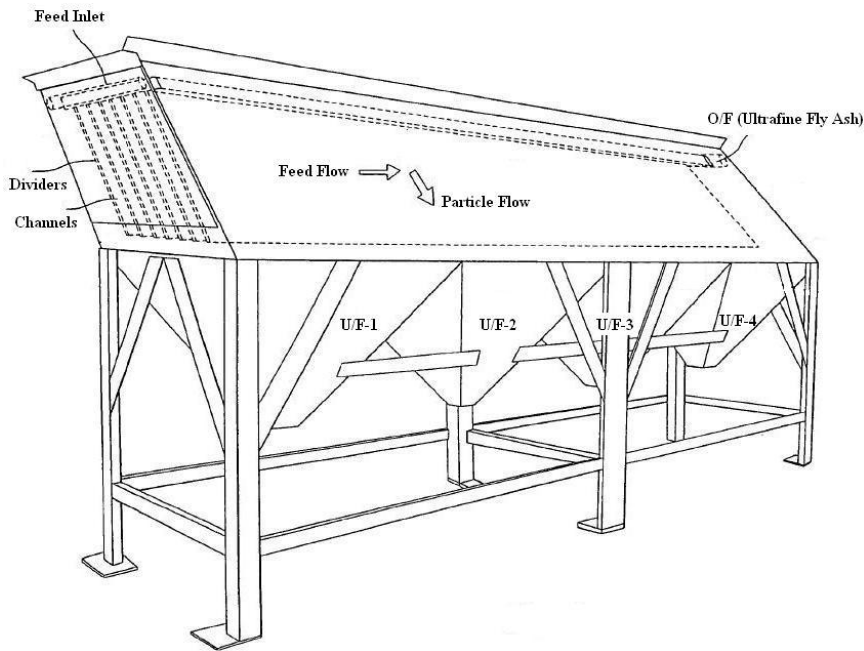
Figure 4. 7 Schematic representation of the hydraulic classifier used in the experiments

Figure 4. 8 Malvern Hydro 2000S Particle Size Analyzer (CAER Lab.)

In this hydraulic classification process, the important process parameters are feed pulp density, feed rate, underflow discharge rates, dispersant type and its dosages and divider spacing. Prior to each experiment, slurry feed rates and dispersant dosages were carefully adjusted to the desired values. Then, the classifier was filled with water up to the level of discharge pipe, and discharge rates of underflows were adjusted to remove the coarse particles from the system. After that, the classification process was started. Slurry and mass flow rates of feed, overflow (product) and underflows were checked two times by taking the samples from each for a definite period of time during the process. After the experiment, percentage of solids and loss on ignition (LOI) values of feed, overflow and underflows were measured via the samples taken during the experiment. Particle sizes of the all fractions were measured by using Malvern Hydro 2000S Particle Size Analyzer shown in Figure 4.8.

Figure 4. 9 Hydraulic classifier used during the experiment (CAER Lab.); (a) Front view, (b) Top view

In this process, the product grade was defined as the mean particle size of the overflow on volumetric basis. In addition to overflow mean size, yield and recovery were also calculated as measures of processing efficiency according to Equations 4.1 and 4.2, respectively. Figure 4.9 shows the hydraulic classifier used during the experiment.

$$Product\ yield = \frac{Mass\ of\ product\ solids}{Mass\ of\ feed\ solids} \qquad (4.1)$$

$$Product\ recovery = \frac{Mass\ of\ product\ solids\ finer\ than\ 5\mu m}{Mass\ of\ feed\ solids\ finer\ than\ 5\mu m} \qquad (4.2)$$

4.2.2 Mortar experiments

In these experiments, 10%, 20% and 30% of Portland cement (PC) replacement by as received fly ashes (FA) and their ultrafine fractions (UFA) were used for the mortar preparation. Control samples containing only PC were also prepared and tested through the experiments in order to observe the differences. Based on the applicable ASTM standards, mortar cubes and mortar bars were prepared and tested for their compressive strengths, drying shrinkages and water expansions which are commonly used criteria in construction industry to determine quality of mortar and concrete.

4.2.2.1 Determination of water demand and compressive strength

In this set of experiments, mortar mix containing PC, FA or UFA as partial cement replacement material, sand and water was prepared and tested to determine both the fresh and hardened mortar properties. Figure 4.10 illustrates the mixers used for mortar preparation.

Figure 4. 10 The mortar mixers with stainless steel bowl applicable to ASTM C305 (CAER Lab.)

Mortar mix was prepared using ASTM Standards C109 (ASTM, 2011) and C305 (ASTM, 2012). According to these standards, the proportions of PC to graded standard sand were used as 1 to 2.75 by weight. The amount of water was adjusted to obtain a mortar mix with a flow of 110 ± 5. In mortar

preparation for the control sample, mixing water was first placed in the bowl. After that, PC was added to the water, and the PC-water mixture was then mixed at the slow speed (140 ± 5 rpm) for 30 s. The entire quantity of sand was then added slowly through 30 s during the slow mixing. After that, the mixer was stopped and changed to medium speed (285 ± 10 rpm) followed by mixing for 30 s. Then, the mixer was stopped and the mortar mix was let stand for 90 s. In the first 15 s, the mortar mix was quickly scraped down into batch, and then the bowl was covered with the lid for the remainder time. This procedure was completed by mixing at the medium speed for 60 s. In preparation of the PC/FA and PC/UFA mortars, FA and UFA samples were used as 10%, 20% and 30% PC replacements in the mortar mix, and the same procedure explained above was used.

Based on ASTM Standards C230 (ASTM, 2008) and C1437 (ASTM, 2007), the mortar flow tests were conducted immediately after the mortar preparation by means of the flow table shown in Figure 4.11. In these tests, varying percentages of water were used to obtain a flow of 110 ± 5 in 25 drops of the flow table in 15 seconds. The procedure started with placing of the flow mold at the center of the flow table. Then, a layer of mortar with about 25 mm in thickness was placed in the mold and tamped 20 times with the tamper. After that, the mold was filled with the mortar followed by tamping as specified for the first layer. Then, the mortar in the flow mold was cut off from the top with the straight edge of a trowel. The flow mold was lifted away from the mortar after 60 s. The flow table was immediately dropped 25 times in 15 s. The resulting increase in base diameter of the mortar was measured by a caliper from four equal spaced intervals. These four readings were added and the total of these was recorded as flow of the mortar. If this value was in the range 110 ± 5, the flow test was ended, and the water amount used was accepted as water demand of the mortar. Otherwise, percentages of the water were varied until the specified flow was achieved. Water reductions provided by the FA and UFA samples were then calculated as percentages compared to the control sample.

Figure 4. 11 The flow table, flow mold and caliper applicable to ASTM C230 (CAER Lab.)

According to ASTM C109 (ASTM, 2011), the mortar on the flow table was returned to the bowl immediately after the flow test, and then scraped down into the batch. After that, the mortar was remixed at the medium speed for 15 s. Molding procedure was then started. The 2-inch cube mold set used to make mortar cubes for the compressive strength tests is shown in Figure 4.12. In the molding procedure, a layer of mortar with about 25 mm in thickness was placed in all of the cube compartments of the mold, and then each compartment was tamped 32 times in about 10 s in 4 rounds. After that, the mold was filled with the mortar followed by tamping as specified for the first layer. Then, the mortar in the cube mold was

smoothed off by drawing the flat side of the trowel. Excess mortar on the mold was cut off from the top with the straight edge of the trowel with a sawing motion over the length of the mold.
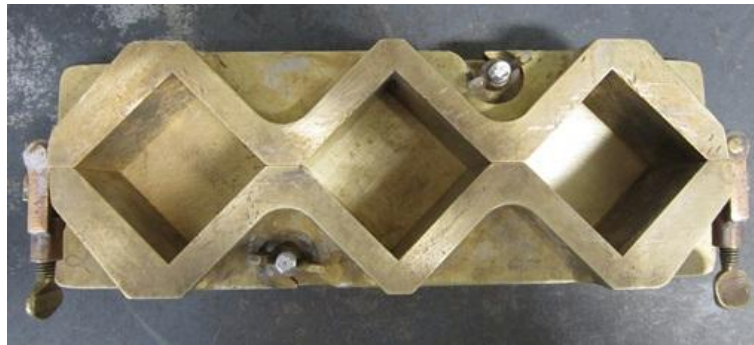
Figure 4. 12 The 2-inch cube mold set applicable to ASTM C109 (CAER Lab.)

Immediately after completion of the molding, the test specimens were placed in the moist room. Figure 4.13 shows the moist curing room applicable to ASTM C511 (ASTM, 2009). The prepared mortar cubes were taken from the moist room and removed from their molds after 24 hours. Then, the mortar cubes to be tested for the compressive strength of 1 day were separated from the others which were then labeled with a marker and put back into the moist room until the definite ages for the compressive strength tests.

Figure 4. 13 The moist curing room applicable to ASTM C511 (CAER Lab.)

According to ASTM C109 (ASTM, 2011), compressive strengths of the mortar cubes were measured for the curing ages of 1, 7, 14, 28, 56 and 112 days. Until these definite test ages, the mortar cubes were stored in the moist curing room with 100% relative humidity and a constant temperature of $23 \pm 2^{o}C$. Figure 4.14 illustrate the mortar cubes immediately after being removed from their molds (left) and in moist room (right). At a definite test age, the mortar cubes were removed from the moist room. Then, they were wiped to a surface dry condition, and any loose material was removed from the surfaces. Perpendicular two edges on a surface that will not be contacted with the bearing blocks of the testing machine were measured as millimeter (mm) and these values were entered into the software that is connected with the testing machine. After that, the cube was placed into the testing machine, and the load was applied to the cube. Compressive strength was then automatically calculated by the computer as megapascal (MPa) from the total maximum load indicated by the testing machine and the specimen

dimensions. For the each age, three cubes from a single batch were tested and the average value was taken as the compressive strength value. The compressive strength test machine can be seen from Figure 4.15.

Figure 4. 14 The cubes after being removed from their molds (left) and in the moist room (right)

Figure 4. 15 Satec Instron compressive strength testing machine (CAER Lab.)

4.2.2.2 Dimensional stability experiments

Dimensional stability is another important specification for any construction material. In order to test dimensional stability, expansion and shrinkage values of mortar bars prepared with the same procedure used for the cubes were examined according to ASTM C157 (ASTM, 2008) standard test method. Based on this method, for the expansion tests, the mortar bars were stored in lime-saturated water and measured immediately after being removed from their molds for the curing ages of 4, 7, 14, 28, 56 and 112 days. On the other hand, the bars were placed in air storage for the shrinkage tests and they were measured for the same curing ages with the expansion tests. In a similar way to the compressive strength tests, control bars containing only PC were also prepared and tested. For the expansion tests, lime-saturated water containing 3 g/l of $Ca(OH)_2$ was prepared on the basis of ASTM C511 (ASTM, 2009). For the shrinkage tests, the mortar bars were stored in the drying room at the temperature of 23 ± 2^oC and the relative humidity of $50 \pm 4\%$. Figure 4.16 shows mortar bar preparation mold used in the experiments. The bars stored in lime-saturated water and drying room can be seen from Figures 4.17 and 4.18, respectively.

Figure 4. 16 The mortar bar mold applicable to ASTM C490 (CAER Lab.)
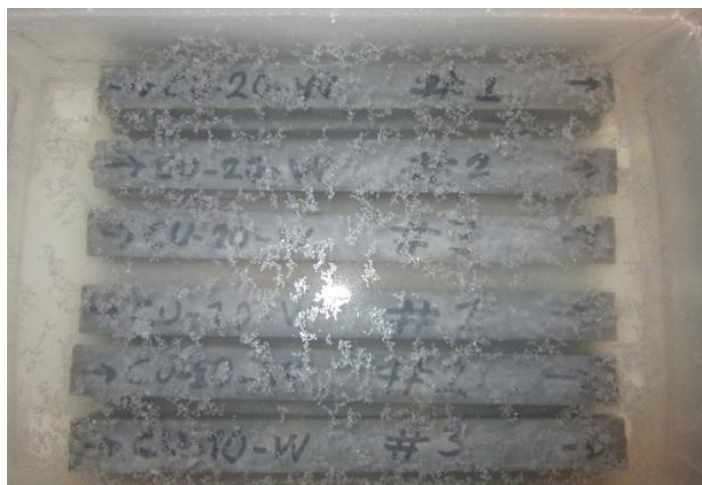
Figure 4. 17 The mortar bars stored in lime-saturated water applicable to ASTM C511 (CAER Lab.)

Figure 4. 18 The mortar bars stored in the drying room applicable to ASTM C157 (CAER Lab.)

4.2.2.2.1 Procedure used for calculating length change

In order to determine the length changes occurred in the bars precisely, a digital comparator was used with regard to ASTM C490 (ASTM, 2011). According to this standard, length change was calculated by using the equation given below. Figure 4.19 illustrates a digital comparator used for the measurement of length change in mortar bars.

$$L = \frac{(L_x - L_i)}{G} \ x \ 100 \tag{4.3}$$

In this equation; L: Change in length at x age (%)

L_x: Comparator reading of specimen at x age minus comparator reading of reference bar at x age (mm)

Li: Initial comparator reading of specimen minus comparator reading of reference bar at that same time (mm)

G: nominal gauge length (250 mm)

Figure 4. 19 The digital comparator applicable to ASTM C490 (http://testinternational.co.uk/)

4.2.3 Paste experiments

In this set of experiments, paste specimens containing Portland cement (PC), as received fly ashes (FA) or their ultrafine fractions (UFA) and water were prepared in small plastic bottles with 20% cement replacement. In the paste preparation, the required amounts of PC, FA or UFA and water were well mixed in a bottle, and then the bottle was sealed and kept at the temperature of 23 ± 2^oC. In a similar way to the mortar experiments, a PC control mix was also prepared. The proportions of water to PC and mixtures of PC/FA and PC/UFA were same as those in the mortar tests. At the respective test ages, fragments from the sample's core were collected and ground. After that, the ground sample was washed with isopropanol twice followed by drying in oven at 40^oC in order to stop hydration reactions in the sample. The dried samples were stored in a desiccator containing silica gel for the thermogravimetric (TG) and X-ray diffraction (XRD) analyses.

4.2.3.1 Thermogravimetric Analysis (TGA)

In TG analyses of the paste specimens, pozzolanic reactivity of FA and UFA samples were directly measured from the remaining $Ca(OH)_2$ contents determined by using the TG plots. As explained clearly in the literature survey, pozzolanic reaction can be defined as the reaction of pozzolans with calcium hydroxide which is resulted from cement hydration under moist conditions (Yilmaz, 2003). According to this definition, the difference between the remaining $Ca(OH)_2$ contents in the FA or UFA paste specimens and the reference PC paste can be used as the measure of pozzolanic reactivity. In thermogravimetric analysis, 10-20 mg sample was placed in an alumina cup, inside the TG instrument. The sample was then heated in the range of 50-1000°C with the heating rate of 20°C/min under nitrogen (100 ml/min) atmosphere. The $Ca(OH)_2$ quantity remaining in the samples was calculated from the TG plot and following equation:

$$Ca(OH)_2 \longrightarrow CaO + H_2O \qquad (4.4)$$
(74 g/mol)   (56 g/mol)   (18 g/mol)

$$\%Ca(OH)_2 = \frac{Mass\ Loss}{18} \times 74 \qquad (4.5)$$

The mass loss in the temperature ranges of 420-500°C (dehydroxylation region) is resulted from $Ca(OH)_2$ removed from the system (Islam, 2012). Thermogravimetric analyses of the samples were carried out using SDT Q600 thermal analysis instrument shown in Figure 4.20.

Figure 4. 20 SDT Q600 thermal analysis instrument (CAER Lab.)

Figure 4.21 shows the weight and derivative weight curves of the PC only paste as a function of temperature for the curing age of 1 day. As seen from the figure, mass loss due to $Ca(OH)_2$ removing from the system was calculated by using the following TG curves.
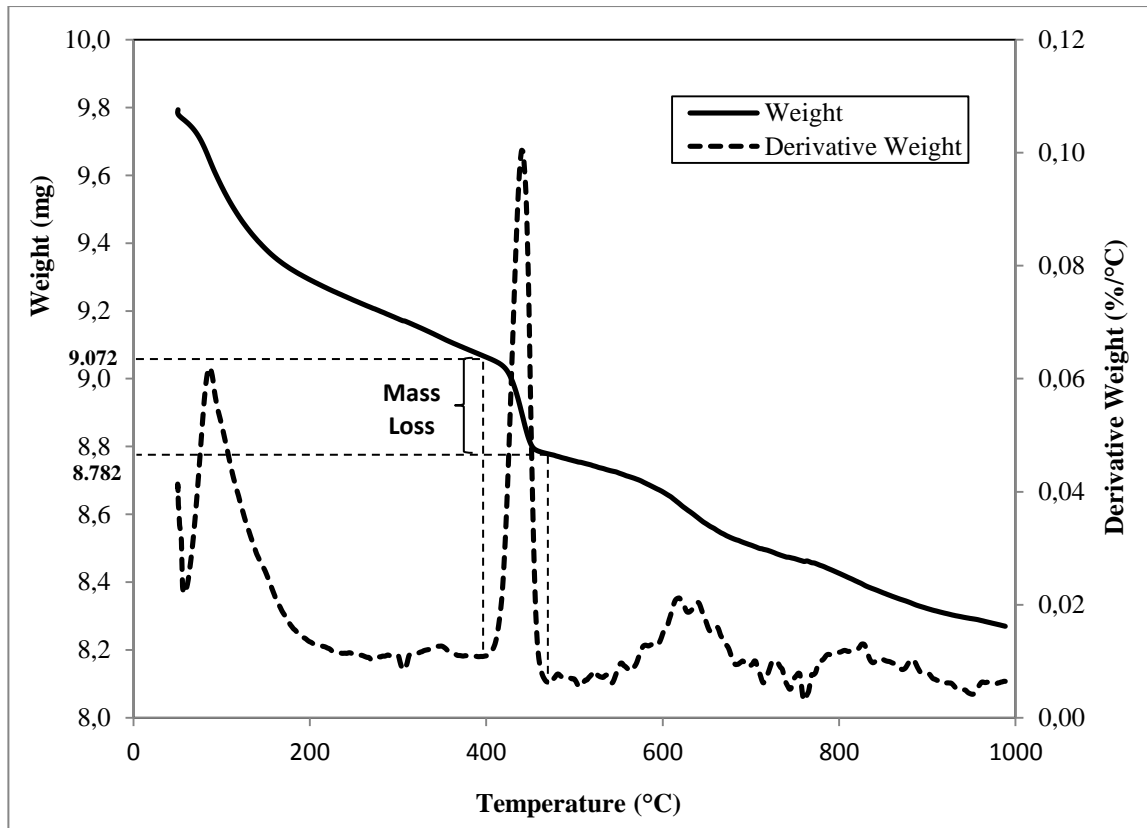
Figure 4. 21 TG curves of the PC only paste after 1 day

4.2.3.2 X-ray diffraction (XRD) analysis

Microstructural changes in the PC/FA and PC/UFA pastes during hydration were determined using Philips Analytical X'Pert PRO PW 3040 X-ray Diffractometer (Figure 4.22).

Figure 4. 22 Philips Analytical X'Pert PRO PW 3040 XRD (CAER Lab.)

PC only paste was also analyzed to determine mineralogical changes between the paste specimens of FA/UFA blended and PC only. A software package program was utilized to analyze the resulting patterns.

Analyses of the patterns were done by comparing the peak positions and intensities of the samples with those in the Joint Committee on Powder Diffraction Standards (JCPDS) data files.

4.3 The methods used for cenosphere recovery potentials from the fly ashes

Cenosphere contents of the samples were determined by using two different methods, namely point counting and area basis calculation under microscope. Effects of various concentration techniques used in mineral processing such as screening, heavy medium separation (HMS) and classification on the concentration of the cenospheres in the samples were also examined.

4.3.1 Determination of cenosphere content

In most of the literature, cenospheres are defined as hollow particles with density less than water. This definition is based on natural concentration of cenospheres as a result of fly ash disposal in water. However, depending on the wall thickness and the ratio of hollow part, hollow particles with density much higher than water are also present in fly ashes (Ramme *et al.*, 2008). The particles with density up to 3.2 g/cm^3 can be found in fly ashes. These particles are mostly iron oxides present in the silica matrix. For this reason, cenospheres present in fly ashes could have densities up to 2.2 g/cm^3, the lowest density oxide in fly ash, crystalline silica. These heavier cenospheres containing less hollow space could also have high-value applications in construction industry as fillers and reinforcements because their greater wall thicknesses contribute to the strength of the final product (Ghosal and Self, 1995; Gurupira *et al.*, 2001; Ramme *et al.*, 2008). In this study, the measurements used to estimate cenosphere contents of CFA and SFA as a result of different processing techniques were based on this new definition of cenosphere.

4.3.1.1 Point counting

This method involves observing thin-sections of the fly ash samples through a transmitted optical light microscope. Point counting method is relatively simple and provides reliable data for the estimation of a material's content. Swift automatic point counter was used to estimate cenosphere contents of the samples (Figure 4.23).

A fine cross-lined graticule is placed into the eyepiece of the microscope to determine the exact point of location. The instrument has a servo-operated traversing carriage can be fitted to any conventional microscope. It has also a counting unit under the control of the observer. The traverse of the specimen is broken into a series of equally-spaced steps which are moved electrically in the horizontal direction by switches in the counting unit. The counting unit includes a series of buttons. The operator uses the appropriate button when the particle of interest has been identified under the cross-wires (http://iopscience.iop.org; Hutchison, 1974).

As the method for estimation of the fly ashes' cenosphere contents, at least 500 particles were counted for each measurement by using point counting method under the microscope. According to this, the ratio of cenospheres over total particles gives percentage of cenospheres in the fly ash samples.

Figure 4. 23 Optical microscope equipped with a Swift point counter (right) (METU GeoE Lab.)

4.3.1.2 Area basis calculation

In this method, the fly ash samples were examined to estimate the cenosphere contents on the basis of area by using image analyzer. This method is based on area percentage of cenosphere over total area of particles. From the images taken during the experiments, besides various properties such as size and area, the instrument also gives information about the sphericity of the particles. Since cenospheres are spherical in shape, sphericity values of the samples were also measured for comparison of these values with the cenosphere contents calculated on the basis of the total area of cenospheres over total area of all particles investigated. In this method, thin sections of the samples were not prepared. Instead, particles were just put on a lamel, the images were taken and then the image analyzer gave areas and sphericity values of the all particles in the frame. Each images includes about 10-20 particles depending on the magnification. Approximately 20-30 images were analyzed for each measurement in order to characterize the sample precisely.

4.3.2 Processing methods for cenosphere enrichment

The effects of various concentration techniques commonly used in mineral processing such as screening, heavy medium separation (HMS) and classification on the concentration of the cenospheres in CFA and SFA were examined. The obtained results were evaluated on the basis of point counting and area calculation.

4.3.2.1 Heavy medium separation (HMS)

In these experiments, the float products of the fly ashes obtained from the float-sink tests performed were used in order to determine the relationship between density and yield and recovery of cenosphere in the float products. As explained before, the measurements were done using the thin sections prepared for the point counting experiments and the image analyzer for the experiments based on area percentage.

4.3.2.2 Screening

Similar to the method applied for the HMS process, the wet screening fractions were used to investigate the relationships between particle size and yield and recovery of cenosphere for the test samples. In

addition, density values of the size fractions were also determined to evaluate relationship between cenosphere content and density.

4.3.2.3 Dry classification

Cenosphere contents of the samples were also tried to be concentrated using an air classifier. In these experiments, air pressure and motor speeds are the main parameters affecting the cyclone efficiency. Four air pressure levels (30, 40, 46 and 52 psi) and four motor speeds (2400, 3000, 4000 and 5000 rpm) were used to determine the best processing conditions to obtain a product with high enough recovery. The air-cyclone used in the experiments is given in Figure 4.24.

Figure 4. 24 Alpine air-cyclone (HUME Lab.)

CHAPTER 5

RESULTS AND DISCUSSION

5.1 The results of sintering experiments

In this set of experiments, two different class F fly ashes obtained from Çatalağzı and Sugözü thermal power plants were compacted and then sintered to form ceramic materials without the addition of any materials. Optimum compaction pressure, preheating temperature and sintering conditions (temperature and time) were determined from the preliminary experiments. According to these experiments, optimum compaction pressure was chosen as 65 MPa, and 16 different temperature-time pairs were tested after the green pellets were preheated to $300^{o}C$ for 1 hour (h). Sintering experiments were conducted at the temperatures ranging from $1000^{o}C$ to $1150^{o}C$ with $50^{o}C$ interval for the residence times of 0.5 h, 1.0 h, 1.5 h and 2.0 h. The heating rate of $10^{o}C/min$ was used throughout the sintering experiments. Preheating is an important process in most sintering applications because it affects size and distribution of the pores in a sintered material. Preheating process assists slower release of moisture and adsorbed gases without forming considerable amount of pores. On the other hand, direct heating leads to larger pores in sintered materials, resulting in higher water absorption and porosity. Preheating treatment can also provide higher green and sintered body density (Aineto *et al.*, 2005; Benavidez *et al.*, 2003). According to the previous studies, sintering efficiency was evaluated by using many physical and mechanical tests and microstructural analyses. In this study, from these tests and analyses, better microstructure, the highest density and strength with the lowest porosity, shrinkage and water absorption values were accepted as the indications of the optimum sintering temperature-time pair (Erol *et al.*, 2008a; Biernacki *et al.*, 2008). Some codes were given to the as-received and sintered fly ashes throughout the experiments. These are CFA: Çatalağzı fly ash, SFA: Sugözü fly ash, SCFA: Sintered Çatalağzı fly ash and SSFA: Sintered Sugözü fly ash.

5.1.1 Physical and mechanical properties of the sintered samples

Figures 5.1-5.6 illustrate the physical and mechanical properties of sintered Çatalağzı (SCFA) and Sugözü (SSFA) fly ashes as a function of sintering temperature and sintering time.

5.1.1.1 Bulk density

Figure 5.1 shows effects of processing conditions on bulk densities of the fly ash samples. As seen from the figure, sintered density generally increased slightly with the increasing sintering time and significantly with the increasing sintering temperature for the majority of the samples. However, the maximum density of 2.12 g/cm^3 for SSFA was obtained for the processing condition of $1150^{o}C$ and 1 h followed by a small decrease for the higher residence times. Unlike SSFA, the highest density of 1.92 g/cm^3 for SCFA was achieved in the case of the maximum sintering temperature and time ($1150^{o}C$ and 2 h). It is clear from Figure 5.1 that sintering time has very low effect on density. For the constant temperature of $1000^{o}C$, bulk densities of SCFA and SSFA samples exhibited lower than 5% increase with the increasing times ranging from 0.5 h to 2.0 h. On the other hand, for the constant sintering time of 0.5 h, the sintered samples showed higher than 30% increase in density with the increasing temperatures varying from $1000^{o}C$ to $1150^{o}C$.

Figure 5. 1 Bulk densities as a function of sintering temperature and time

5.1.1.2 Splitting tensile strength (STS)

Figure 5.2 illustrates the splitting tensile strength (STS) values of SCFA and SSFA as a function of temperature and time. In the same manner as the density results, temperature had much more important effects on STS values of the sintered samples. For the majority of the samples except treated at 1000°C, strength generally increased with increasing sintering time up to 1.5 h. For the higher sintering time, 15% and 30% decrease in the STS values were observed for SSFA and SCFA, respectively for the highest temperature. Maximum strength values of 12.98 MPa and 8.22 MPa were obtained for SSFA and SCFA, respectively in the processing conditions of 1150°C and 1.5 h.
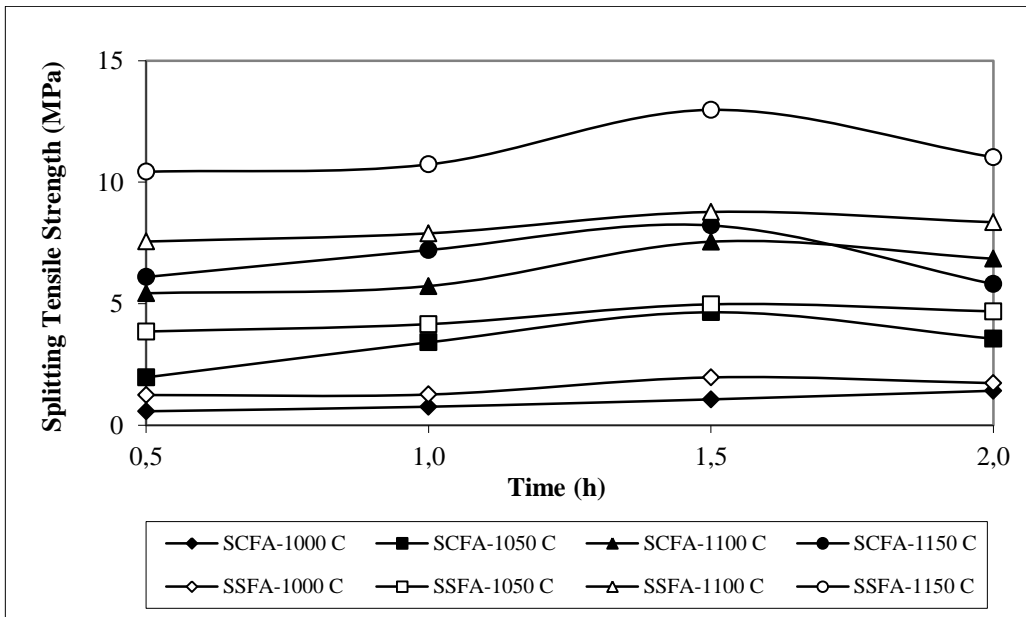
Figure 5. 2 STS results as a function of sintering temperature and time

66

5.1.1.3 Porosity

Porosity (sum of open and close porosity) is also accepted as another important measure of sintering efficiency. Porosity change of the sintered samples with temperature and time is shown in Figure 5.3. As seen from the figure, both SSFA and SCFA showed decreasing porosity values with increasing time and temperature. Minimum values were obtained for the highest sintering temperature and time. At this point, SSFA and SCFA exhibited the porosity values of 2.30% and 7.62%, respectively. For the constant temperature of 1150°C, SCFA and SSFA indicated respective 48% and 72% decrease in total porosity with the increasing times ranging from 0.5 h to 2.0 h. Conversely, for the constant sintering time of 2.0 h, SCFA and SSFA exhibited respective 78% and 93% decrease in total porosity with the increasing temperatures varying from 1000°C to 1150°C.
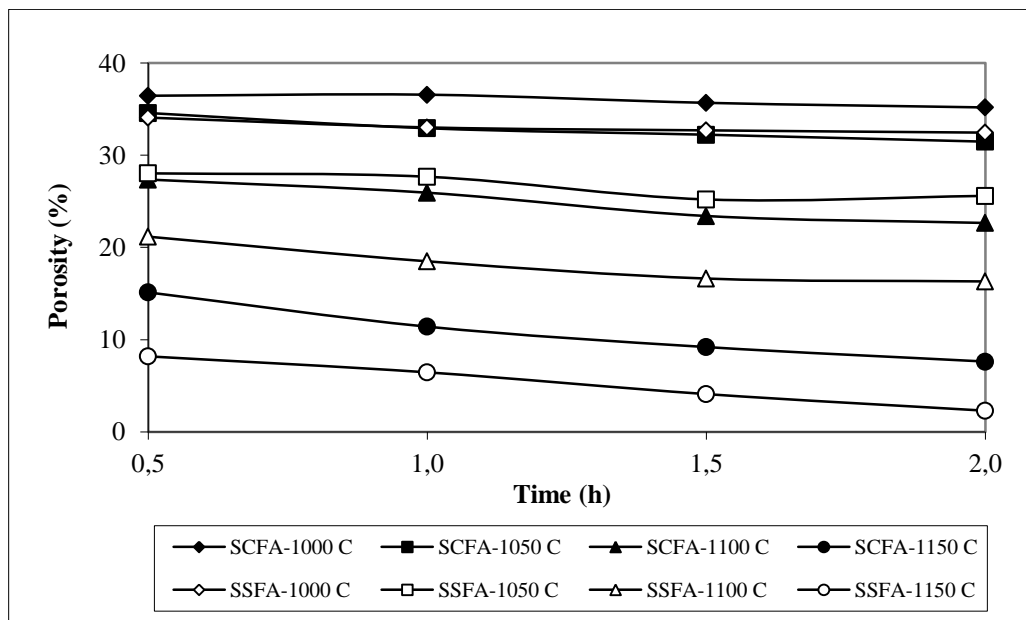
Figure 5. 3 Porosity values as a function of sintering temperature and time

5.1.1.4 Water absorption

Figure 5.4 illustrates the changes in water absorption (a measure of open porosity) values of the sintered samples with the increasing temperature and time. In a similar way to the obtained porosity values, both SCFA and SSFA showed decreasing water absorption values with increasing time and temperature, and the minimum values were achieved with the highest sintering temperature and time. At this point, SSFA and SCFA exhibited the porosity values of 1.09% and 3.99%, respectively. SSFA and SCFA indicated approximately same reduction ratios in water absorption values compared to the ones obtained in porosity values.
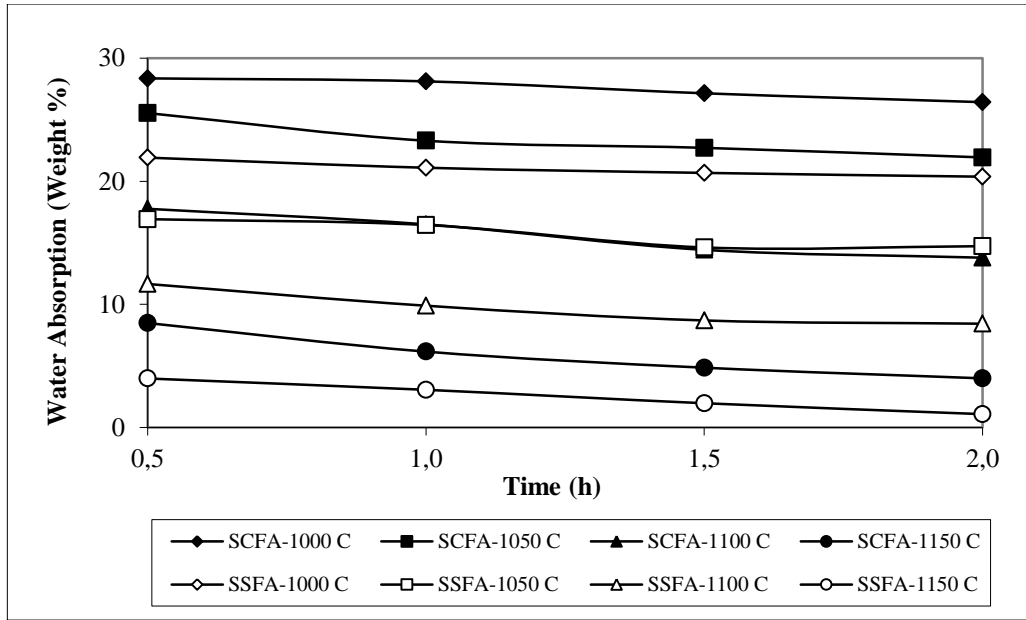
Figure 5. 4 Water absorption results as a function of sintering temperature and time

5.1.1.5 Axial and radial shrinkage

Shrinkage is another important measure of sintering efficiency. The effects of processing conditions on axial and radial shrinkages of the sintered samples are illustrated by Figures 5.5 and 5.6, respectively. According to these figures, both axial and radial shrinkage values exhibited nearly the same patterns, and shrinkage values slightly increased with the increasing time but SSFA treated at 1150°C. For the highest processing temperature, SSFA had maximum values of 10.86% and 10.60% for the respective axial and radial shrinkages for 1 h, and higher than 5% decrease was observed beyond this residence time. Unlike SSFA, shrinkage values of SCFA exhibited a gradual increase with the increasing time.
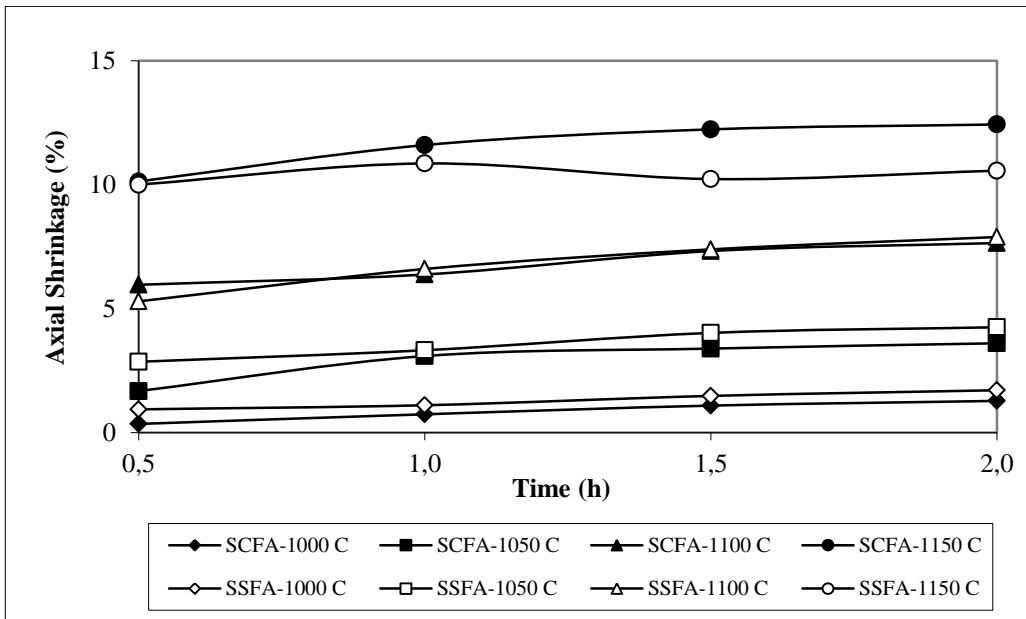
Figure 5. 5 Axial shrinkage values as a function of sintering temperature and time
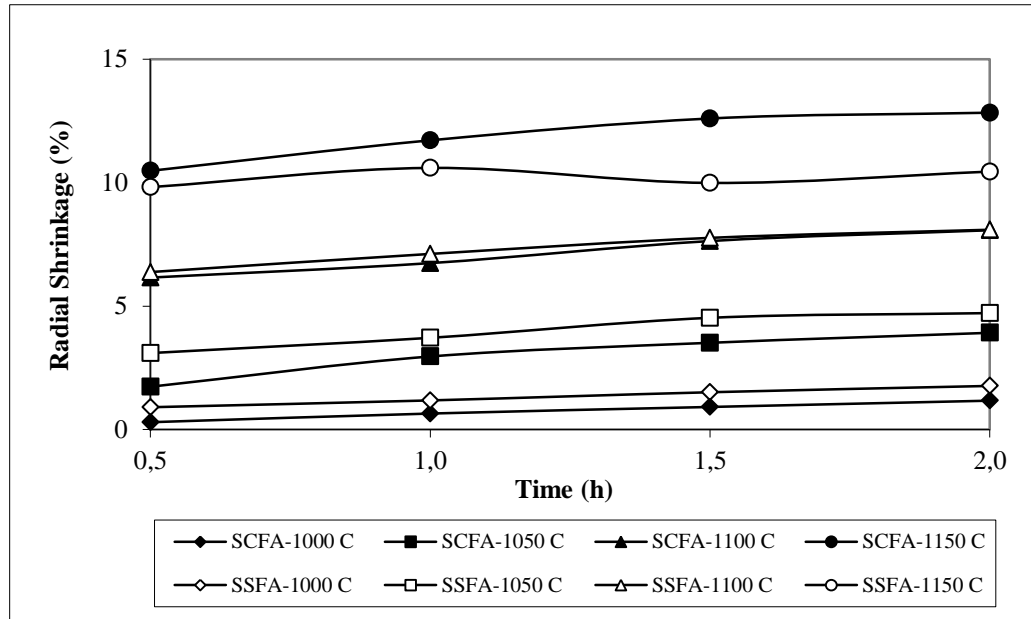
Figure 5. 6 Radial shrinkage values as a function of sintering temperature and time

Similar to the results obtained from the other physical and mechanical tests, temperature had also much more important effects on shrinkages compared to the residence time.

Overall Figures 5.1-5.6 illustrate a complex relationship between processing conditions and physical and mechanical properties of the sintered samples. From the literature data, strength of a sintered material would generally increase in direct proportion to the increase of density for all of the processing conditions. Although, STS values of SCFA and SSFA generally increased with increasing density for the majority of the samples except the sintering temperatures higher than 1100°C for the highest residence time (2 h). Possible mechanisms responsible from this situation were discussed in detail with the help of mineralogical and microstructural analyses of SCFA and SSFA.

Figures 5.7 and 5.8 also show the effects of processing conditions on the shrinkages of SCFA and SSFA pellets, respectively. These figures indicated that temperature had much more important effect on the shrinkages of the sintered samples compared to time. In addition, lower shrinkage values were observed for SSFA probably due to the lower porosity of as-received Sugözü fly ash. The results obtained from Figures 5.7 and 5.8 were in well agreement with the ones from the shrinkage tests.
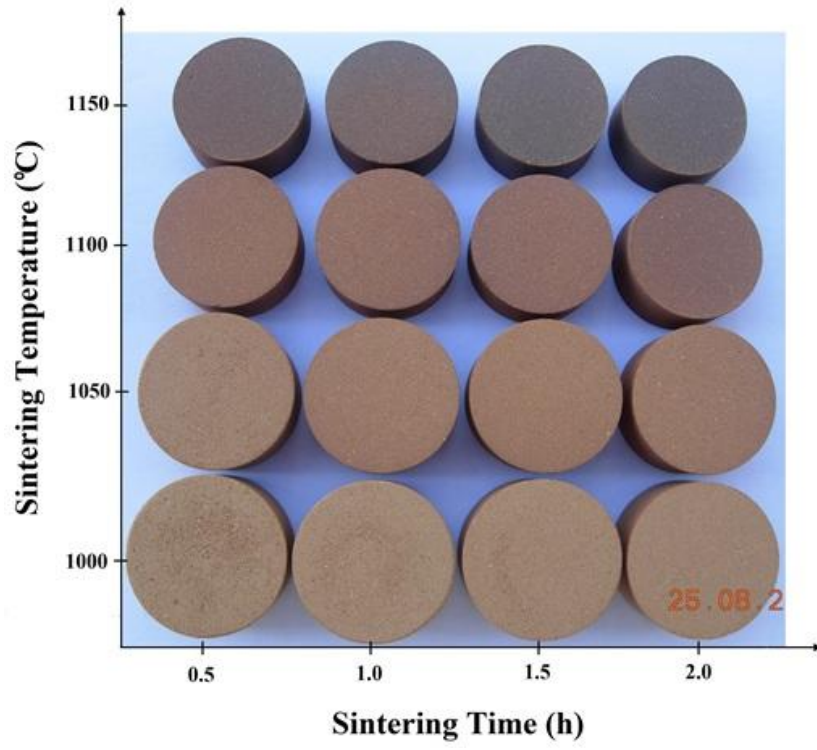
Figure 5. 7 Sintered CFA pellets as a function of temperature and time
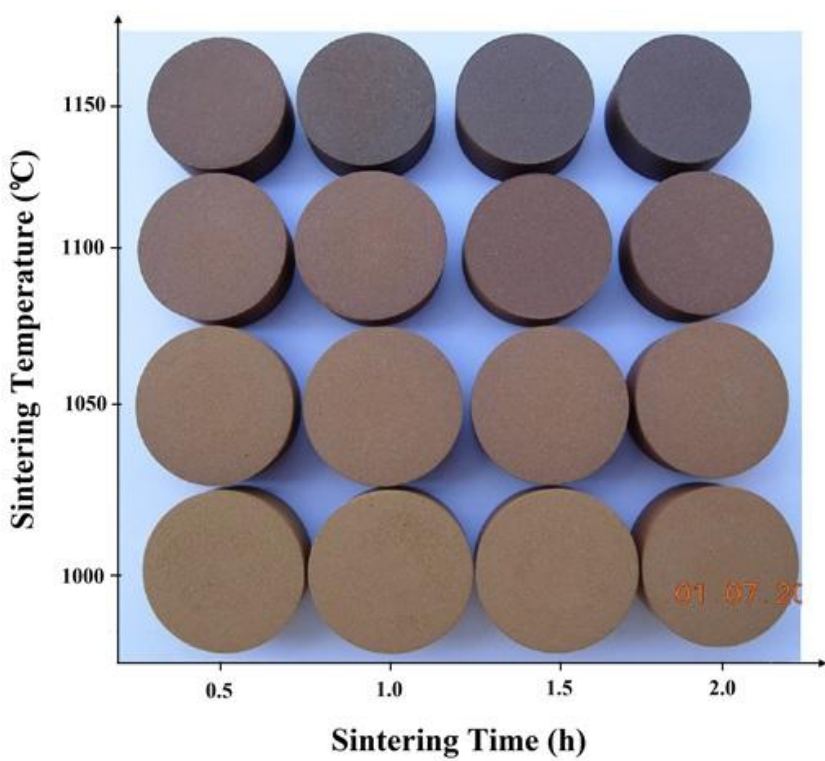
Figure 5. 8 Sintered SFA pellets as a function of temperature and time

5.1.2 Microstructural analyses of the sintered samples

In order to discuss the relationships between the sintered body properties and the processing conditions in detail, mineralogical and microstructural changes in Çatalağzı and Sugözü samples due to sintering were also examined with X-ray diffraction (XRD) and scanning electron microscopy (SEM) analyses.

5.1.2.1 X-ray diffraction (XRD) analyses

According to JCPDS data files, quartz (SiO_2, Card No: 46-1045) and mullite ($Al_6Si_2O_{13}$, Card No: 15-0776) were the major crystalline phases identified in the as-received fly ash samples. The XRD patterns also indicated small amount of hematite (Fe_2O_3, Card No: 33-0664) in addition to the major phases. Mineralogical changes in Çatalağzı and Sugözü fly ash pellets due to sintering are illustrated by Figures 5.9 and 5.10, respectively.

Figure 5.9 pointed out that mullite and hematite contents increased with increasing temperature and time. On the other hand, the amount of quartz decreased in that condition. Hercynite ($Fe+2Al_2O_4$, Card No: 34-0192) also formed as a result of sintering, and its amount increased with increasing temperature and time in a similar way to the changes in mullite and hematite.

Figure 5.10 illustrates the XRD patterns of as received and sintered Sugözü fly ash. As seen from this figure, in the same manner as SCFA samples, mullite and hematite contents in SSFA increased with increasing temperature and time whereas the quartz content decreased.

From the literature studies, increasing mullite content in both SCFA and SSFA points out the improvement of sintering since mullite has the properties of low thermal expansion, high hardness and low thermal conductivity. All of these advantageous properties make mullite a suitable raw material for ceramic industry (Erol *et al.*, 2008a). Figures 5.9 and 5.10 also indicate that both SCFA and SSFA had reduced background levels as a result of sintering compared to their respective as-received samples. In other words, SCFA and SSFA included less amorphous glassy phase than the as-received samples.
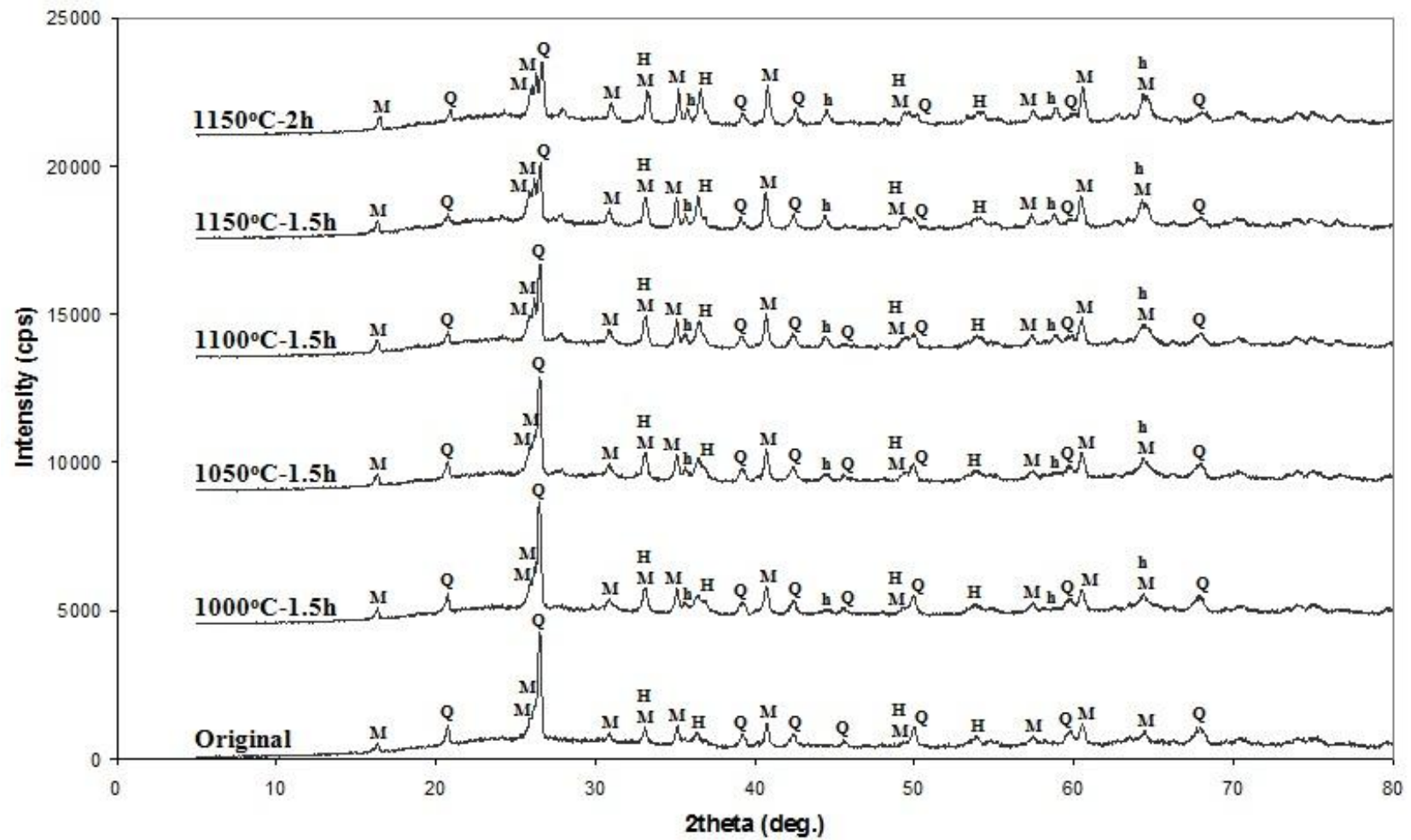
Figure 5. 9 XRD patterns of as-received and sintered CFA (M: Mullite, Q: Quartz, H: Hematite and h: Hercynite)
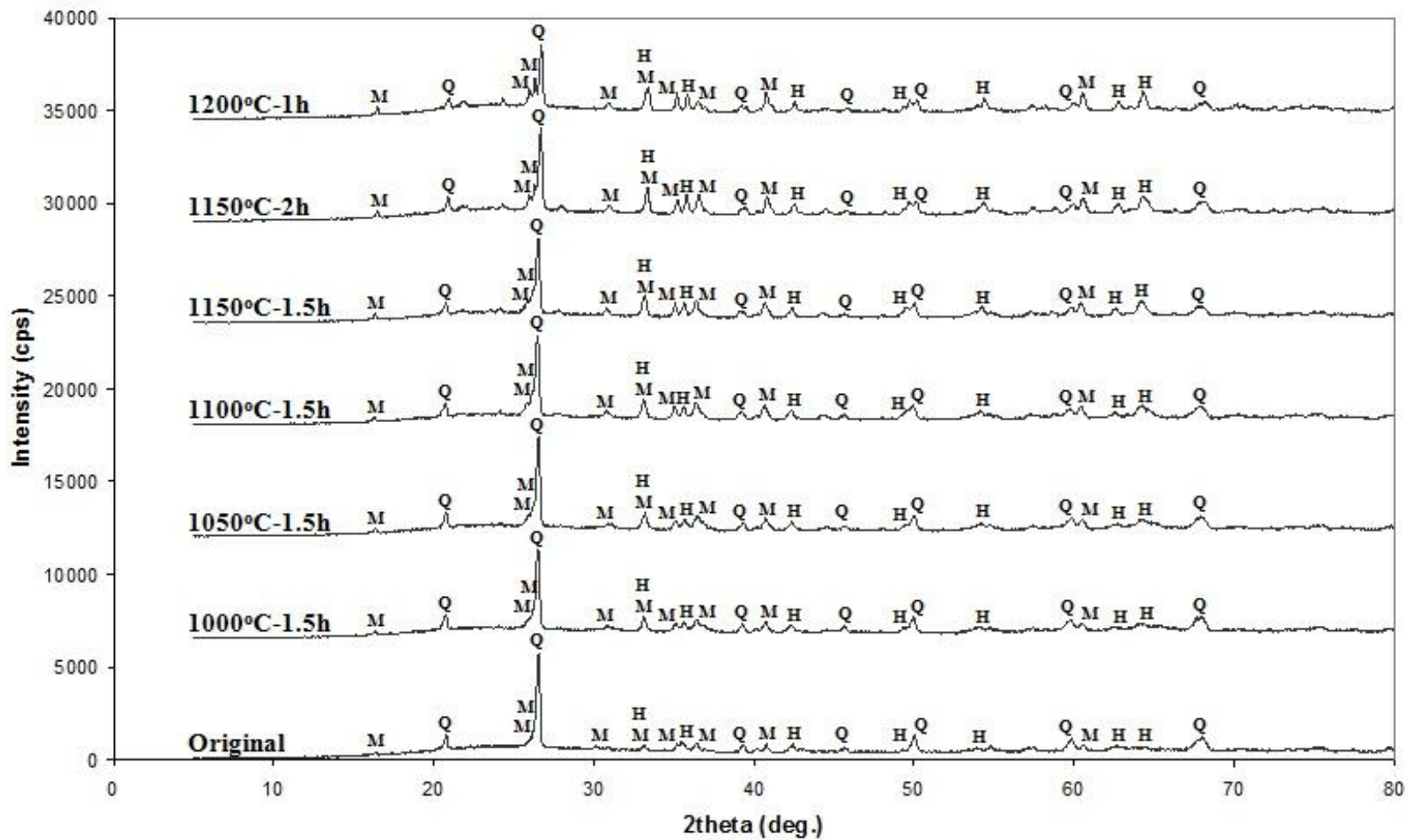
Figure 5. 10 XRD patterns of as-received and sintered SFA (M: Mullite, Q: Quartz and H: Hematite)

5.1.2.2 Scanning electron microscopy (SEM) analyses

SEM investigations were carried out with SCFA and SSFA treated at the same conditions used in the XRD analyses. Microstructural changes in the SCFA and SSFA were observed to have a better chance to explain the relationships between the sintered material properties obtained from the physical and mechanical tests and the processing conditions more clearly. SEM images and STS values of SCFA and SSFA samples can be seen from Figures 5.11 and 5.12, respectively.

According to these SEM images, both SCFA and SSFA samples exhibited relatively poor sintered materials with very few interactions among the particles for the sintering temperature of $1000^{o}C$, leading to weak materials with low density and high porosity and water absorption. Surfaces of both SCFA and SSFA were rough and granular for this case. Fly ash particles in both SCFA and SSFA coalesced more in direct proportion to the increasing temperature, providing more compact materials with much smoother surfaces. In this way, strong composites were formed from the as-received samples. These strong pellets had higher density, lower porosity and water absorption and better mechanical properties. Figures 5.11 and 5.12 pointed out that, for both SCFA and SSFA, the best microcrystalline structures (more compact surfaces with less pores) were achieved for the processing conditions of $1150^{o}C$ and 1.5 h. However, for the residence time of 2 h, a significant volume of approximately spherical pores were formed on the surfaces of the sintered samples, especially for SCFA.

Based on the results obtained from the physical and mechanical tests and the SEM images, for the sintering temperature of $1000^{o}C$, very low interactions among the large and irregularly shaped crystallites resulted in the minimum STS values with the lowest density and the highest porosity and water absorption for both SCFA and SSFA. With the increasing sintering temperature and time, more compact surfaces with better physical and mechanical properties were obtained. In this study, the best microcrystalline structures (denser, tiny crystalline and much smoother fracture surfaces), the highest density and strength and the lowest porosity, water absorption and shrinkage values were accepted as indication of the optimum sintering condition based on the literature studies (Erol *et al.*, 2008a; Biernacki *et al.*, 2008). Accordingly, the best overall properties for both SCFA and SSFA were achieved for the processing conditions of $1150^{o}C$ and 1.5 h. Also, both SCFA and SSFA exhibited the highest STS values at this point, indicating that the SEM observations were in well agreement with the STS values. However, for both SCFA and SSFA, the optimum physical properties were achieved for the processing condition of $1150^{o}C$ and 2 h. Possible mechanisms responsible from the strength losses and pore formations happened in the sintered samples for the highest sintering time were clearly explained in the following subsections.
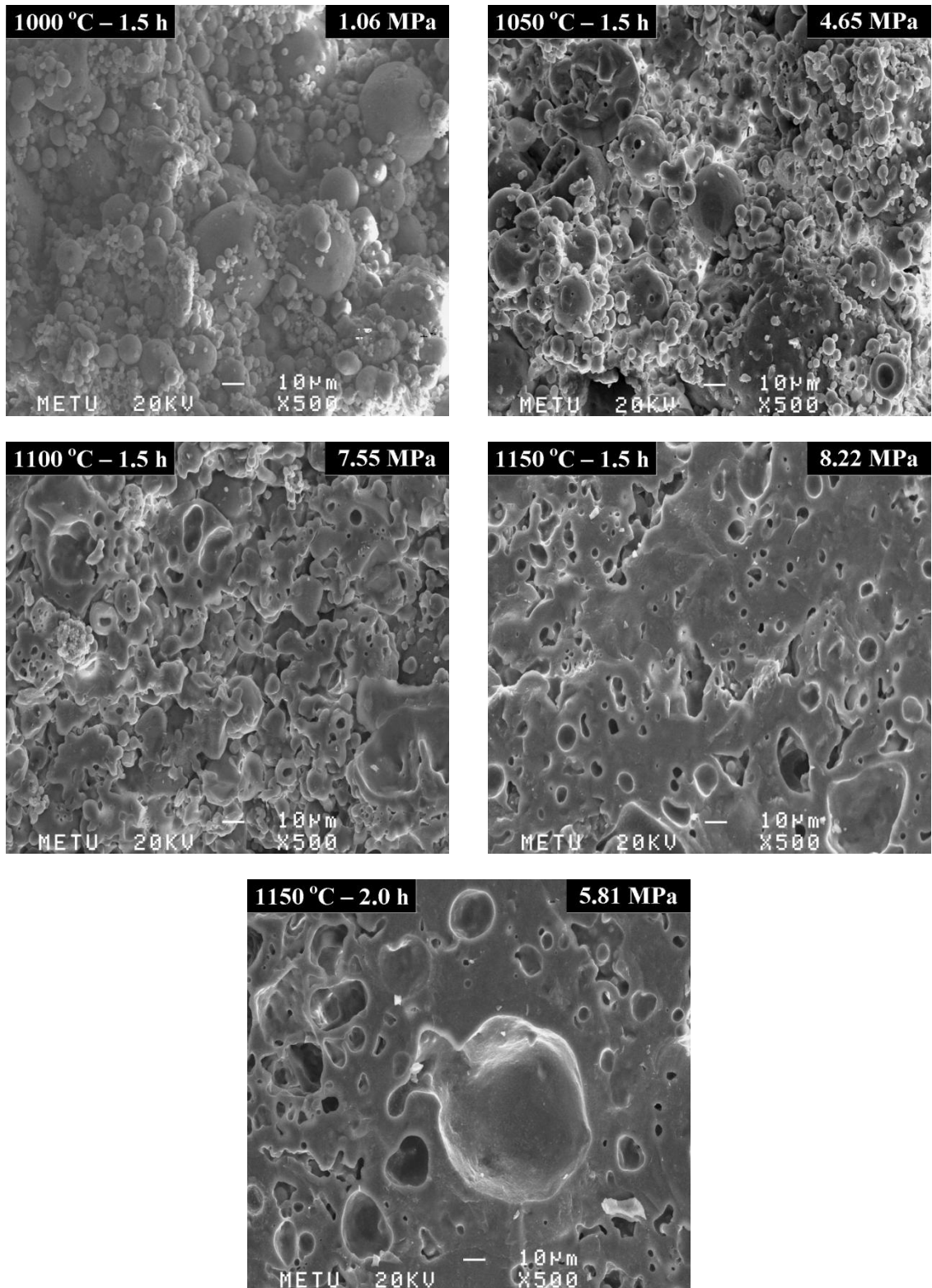
Figure 5. 11 SEM images and STS values of SCFA samples for different processing conditions
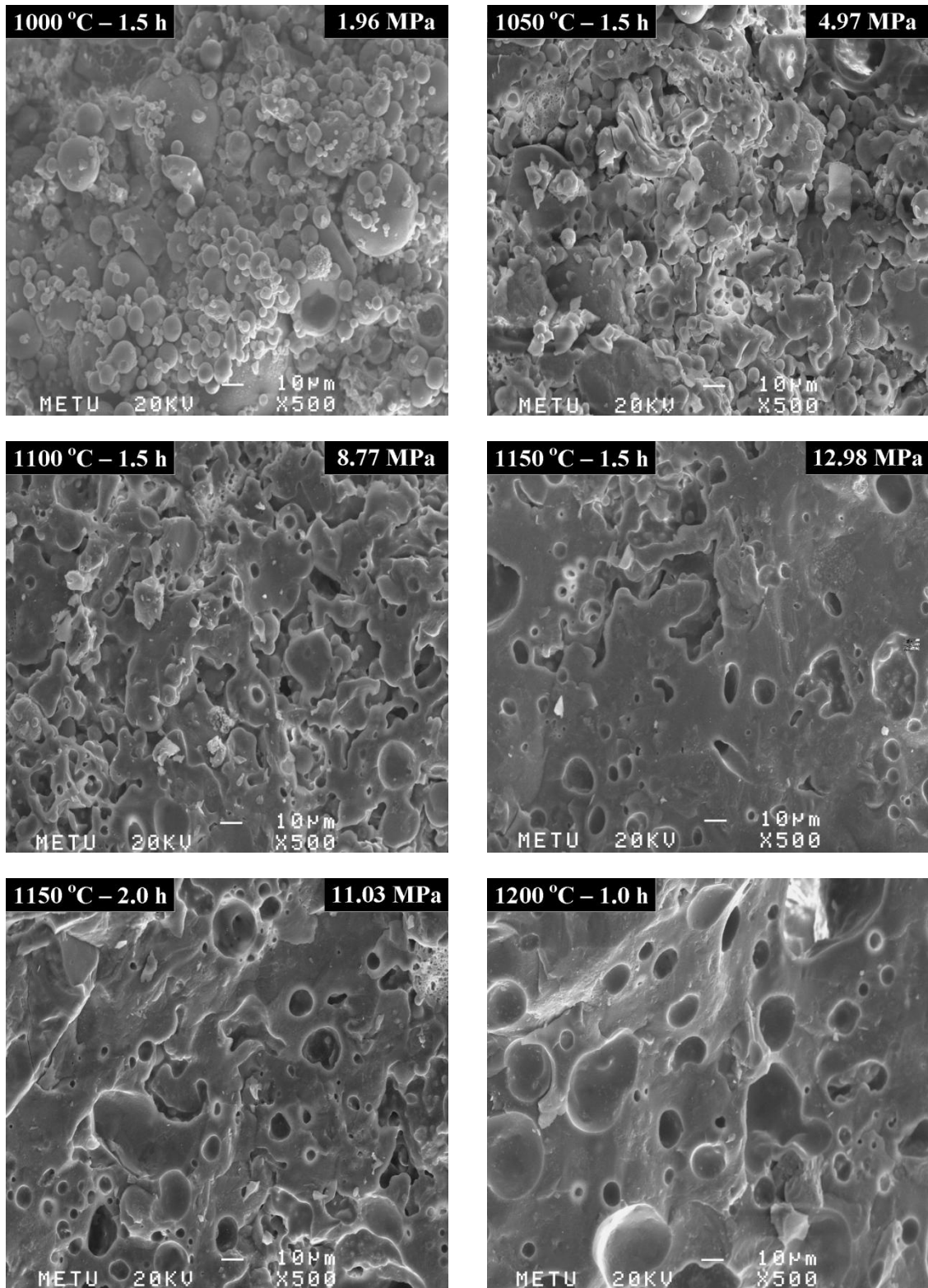
Figure 5. 12 SEM images and STS values of SSFA samples for different processing conditions

5.1.3 Effect of very high temperature on sintering

In order to test the effect of very high temperature on the sintering properties, only SFA sample was processed at 1200°C for 1 h. Contrary to the previous experiments, sample expansion occurred in this condition. Figure 5.13 illustrates the effect of temperatures varying from 1050°C to 1200°C for the constant sintering time of 1 h. As can be clearly seen from this figure, material shrinkages were observed as the sintering temperature increased up to 1150°C. However, sample expansion occurred for the sintering temperature of 1200°C. Sample expansion can also be called as "bloating" which means a decrease in bulk density (Biernacki *et al.*, 2008). The sample expansion occurred in SSFA for the temperature of 1200°C was considered to be resulted from the formation of large pores that can be seen from Figure 5.12. According to the related literature discussions, two possible mechanisms can be responsible from this situation. These are softening of the glassy phase in the ash and simultaneous gas release at this high temperature (Ilic *et al.*, 2003).
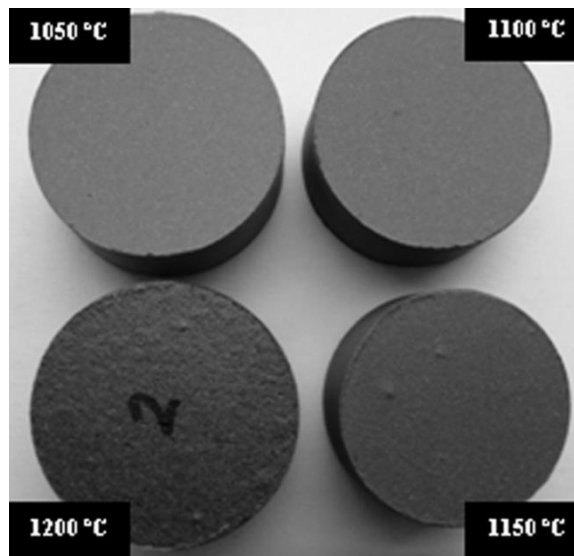
Figure 5. 13 SSFA pellets treated at different temperatures for the sintering time of 1 h

5.1.4 Density-strength relationship

According to the results obtained from physical and mechanical tests and microstructural analyses, the best overall properties for both SCFA and SSFA were achieved for the processing conditions of 1150°C and 1.5 h. For the higher sintering time, 15% and 30% decrease in the STS values were observed for SSFA and SCFA, respectively although the density increased in this condition. In other words, for both SSFA and SCFA, the highest density was not coincident with the highest STS in this study. Figures 5.1 and 5.2 point out that STS decreased with increasing density for the processing conditions of the temperatures higher than 1100°C and the highest residence time. However, this time bloating cannot be a possible mechanism because of the increasing density and shrinkage values as seen from Figures 5.1, 5.5 and 5.6. There must be other mechanisms responsible from this strength loss occurred for the highest residence time. Occurrence of crystalline inclusions from glassy phase can be a possible mechanism. As a result of this crystalline phase formation, the sintered samples can have increasing residual stress because of the significant volume changes. For example, glass, quartz and mullite have different specific gravities which are sequentially 2.30, 2.65 and 2.80. Relative amounts of major crystalline phases in the samples, namely mullite and quartz also changed with the increasing sintering temperature and time. As seen from Figures 5.9 and 5.10, peak intensities of these phases changed significantly after 1100°C, leading to occurrence of the weaker structures due to the phase redistributions during sintering for both SCFA and SSFA. In addition to these occurrences of crystalline phases from the amorphous glass phase and phase redistributions during sintering, glass, quartz and mullite have different thermal expansion coefficients.

This can also result in residual stress development in SCFA and SSFA samples. All of these factors could cause strength losses for the processing temperatures of 1100^oC and 1150^oC and the sintering time of 2 h though the density values increased in these conditions (Biernacki *et al.*, 2008).

5.1.5 Strength development during sintering

In this study, significant increases in STS values of SCFA and SSFA were obtained during sintering. Figure 5.2 indicates that STS values of SCFA and SSFA increased to 8.22 MPa and 12.98 MPa from the respective 1.06 MPa and 1.96 MPa with the increasing temperatures ranging from 1000^oC to 1150^oC for the constant residence time of 1.5 h. Strength development during sintering does not have a simple explanation but it changes with a number of variables like density, porosity, changes in crystalline phase, micro-crack formation, etc. From these variables, some of them increase strength while some cause a decrease for the same processing conditions. For the present fly ashes used in this study, the increasing density did not contribute to the strength after 1.5 h for the temperatures of 1100^oC and 1150^oC although strength increased with density for most of the temperature-time pairs. As clearly explained before, occurrence of the crystalline phases and redistributions of these phases and differences in thermal expansion coefficients of these phases can be possible mechanisms responsible from this situation. In other words, strength development during sintering depends on a number of materials' properties (Biernacki *et al.*, 2008). However, some of these properties played more important roles for the strength development in SCFA and SSFA samples. Figures 5.11 and 5.12 point out that strength development in the sintered samples was mainly resulted from the increasing amount of interactions among the particles with the increasing temperature and time, leading to more compact products with higher density and lower porosity, water absorption and shrinkages. If all of the results are taken into consideration, physical properties such as densification, porosity and surface condition had more important effects in strength development in comparison to the increasing mullite content during sintering.

5.1.6 Final discussion on the results of sintering experiments

Overall results indicate that Sugözü fly ash has better sintered properties than those of Çatalağzı fly ash due to its better microcrystalline structures, higher density and strength with the lower porosity, water absorption and shrinkage values. Since CFA and SFA samples have very similar chemical compositions, the differences in SCFA and SSFA were resulted from the differences in physical properties of as-received Çatalağzı and Sugözü fly ashes, such as particle size and porosity. As a conclusion, the optimum results were obtained for the temperature-time pair of 1150^oC and 1.5 h, and change in the processing temperatures has a more important effect than that in the residence times on the sintered material properties of both Çatalağzı and Sugözü fly ash samples.

5.2 The results of the experiments conducted in determination of pozzolanic reactivity

There are three main stages in this set of experiments. In the first stage, a new hydraulic classification technology was used to separate ultrafine particles from the fly ash samples. Secondly, the pozzolanic properties of these ultrafine fly ash products and as-received samples were examined for their utilization potentials as high quality cement replacement materials. In the last stage, paste experiments were designed to better understand the pozzolanic reactivity of the as-received samples and their ultrafine fractions during cement hydration. In these experiments, some codes were given to the as-received fly ashes (FA) and their ultrafine fractions (UFA). These codes are CFA (Çatalağzı fly ash), CUFA (Çatalağzı UFA), SFA (Sugözü fly ash) and SUFA (Sugözü UFA).

5.2.1 Classification experiments

5.2.1.1 The results of settling experiments

Two different types of superplasticizer polymers based on sulphonate (NSF, Disal) and carboxylate (Glenium 7500) were used in these experiments to determine their dispersive effects on CFA and SFA samples. Figures 5.14 and 5.15 illustrate the results of settling experiments for CFA and SFA, respectively. According to these figures, overflow weight percentages of the fly ash samples increased with increasing dispersant dosage. However, for both dispersants, very small increases in the overflow weight percentages were observed beyond the dispersant dosages of 2.0 mg/g for CFA and 1.5 mg/g for SFA.
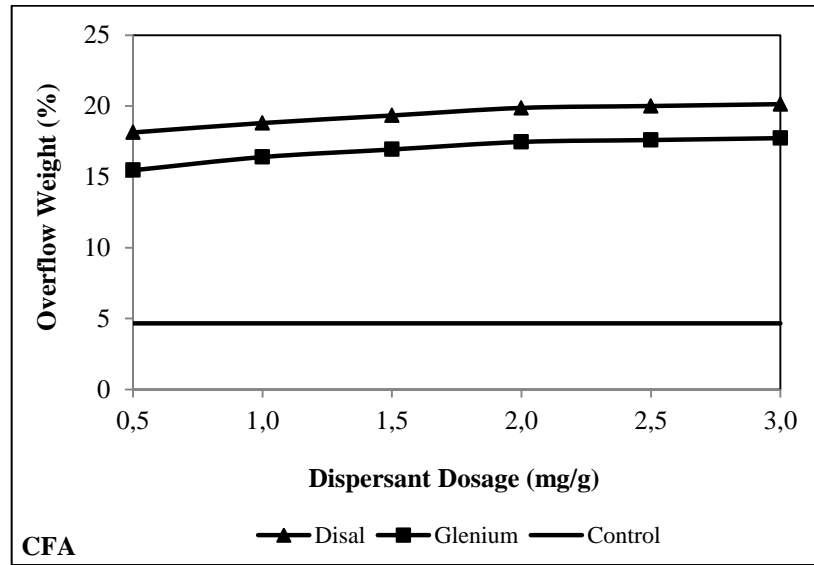
Figure 5. 14 The results of settling experiments for Çatalağzı fly ash
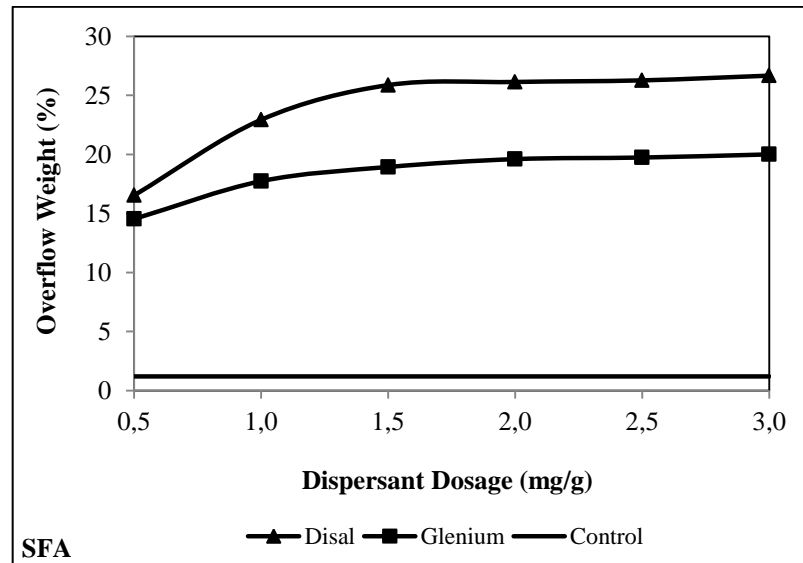
Figure 5. 15 The results of settling experiments for Sugözü fly ash

Although both dispersants showed the same patterns, better results were achieved with the use of Disal for both CFA and SFA. These figures also indicate that very low overflow weight percentages were obtained without the addition of dispersants.

According to Robl and Groppo, 2003, the long molecules of superplasticizers envelop individual ash particles and attached ionic groups, leading to an increase in the overall negative charge of the particles which provides electrostatic repulsion. Further reduction in the flocculation of the samples may be resulted from the steric hindrance caused by the large size and the geometries of these chemicals. Based on the test results, Disal provided better results in comparison to Glenium 7500, and the optimum Disal dosages were found as 1.5 mg/g and 2.0 mg/g for SFA and CFA, respectively.

5.2.1.2 Hydraulic classification experiments

In these experiments, it was aimed to separate the ultrafine fractions (-5 µm) from the as-received Çatalağzı (CFA) and Sugözü (SFA) fly ashes with high yield and recovery using a new hydraulic classification technology developed at CAER.

5.2.1.2.1 Çatalağzı fly ash

Classification conditions and the obtained results for Çatalağzı fly ash are shown in Tables 5.1 and 5.2, respectively. According to Table 5.2, from CFA with average particle size (d_{50}) of 39.29 µm, the ultrafine fraction (overflow product) with average particle size of 5.25 µm was separated with 10.75% yield and 53.28% recovery of -5 µm particles in the overflow (O/F) product. Table 5.3 shows chemical compositions of the classification products. As seen from Table 5.3, SiO_2 and Fe_2O_3 contents in the ultrafine fraction (CUFA) decreased in 3% and 9%, respectively while 7% increase was obtained in Al_2O_3 content. This result indicates that the hydraulic classification process provided not only size separation but also small amount of improvement in pozzolanic reactivity due to the decreasing SiO_2 and Fe_2O_3 and the increasing Al_2O_3 contents in CUFA.

Table 5. 1 Classification conditions for CFA

Operating conditions	
Feed pulp density	1.5% solids by wt. (0.015 kg/l)
Feed rate	11 l/min
Underflow discharge rates	U/F-1 = 300 cc/min, U/F-2 = 200 cc/min U/F-3 = 200 cc/min, U/F-4 = 200 cc/min
Dispersant	Disal
Dispersant dosage	2.0 mg Disal/g of fly ash

Table 5. 2 Classification results for CFA

Products	Weight (%)	Solid (%)	d_{50} (µm)	Vol. % of -5 µm	-5 µm recovery (%)
U/F-1	38.80	16.90	63.26	3.84	15.41
U/F-2	27.98	18.98	47.25	4.08	11.81
U/F-3	13.90	8.60	36.62	4.94	7.10
U/F-4	8.56	5.31	21.46	8.10	7.17
O/F (Ultrafine)	10.75	0.16	5.25	47.91	53.28
TOTAL (Feed)	100	1.49	39.29	9.67	

Table 5. 3 Chemical compositions of CFA classification products

Species (%)	Feed (CFA)	U/F-1	U/F-2	U/F-3	U/F-4	O/F (CUFA)
SiO_2	57.09	58.97	59.18	58.63	57.31	55.34
Al_2O_3	27.46	26.39	27.30	27.48	27.97	29.39
Fe_2O_3	6.56	6.91	6.72	6.80	6.49	5.97
CaO	1.97	1.86	1.79	1.81	1.63	1.20
MgO	2.38	2.36	2.40	2.41	2.37	2.22
Na_2O	0.31	0.28	0.27	0.27	0.27	0.26
K_2O	3.89	3.73	3.82	3.79	3.78	4.21
P_2O_5	0.11	0.10	0.11	0.11	0.12	0.14
TiO_2	1.13	1.10	1.13	1.15	1.18	1.23
SO_3	<0.01	<0.01	<0.01	<0.01	<0.01	<0.01
LOI	1.68	1.64	1.72	1.69	1.74	2.07

Figure 5.16 illustrates SEM images of CFA and CUFA samples for different magnifications. According to Table 5.2, approximately 7.5 times decrease in the average particle size was achieved in CUFA, which can also be seen visually from the SEM images. In addition to particle size, amount of amorphous glass inclusions is another important property affecting pozzolanic reactivity of fly ashes. In order to determine the amorphous glass contents, CFA and CUFA were examined under an optical microscope. These analyses indicate that the glass content was found as 100% for CUFA, while this value was 97.2% for CFA.

All of these results point out that a high value pozzolan with very fine particle size and enhanced chemical composition can be produced from CFA sample by using a relatively simple hydraulic classification technology.
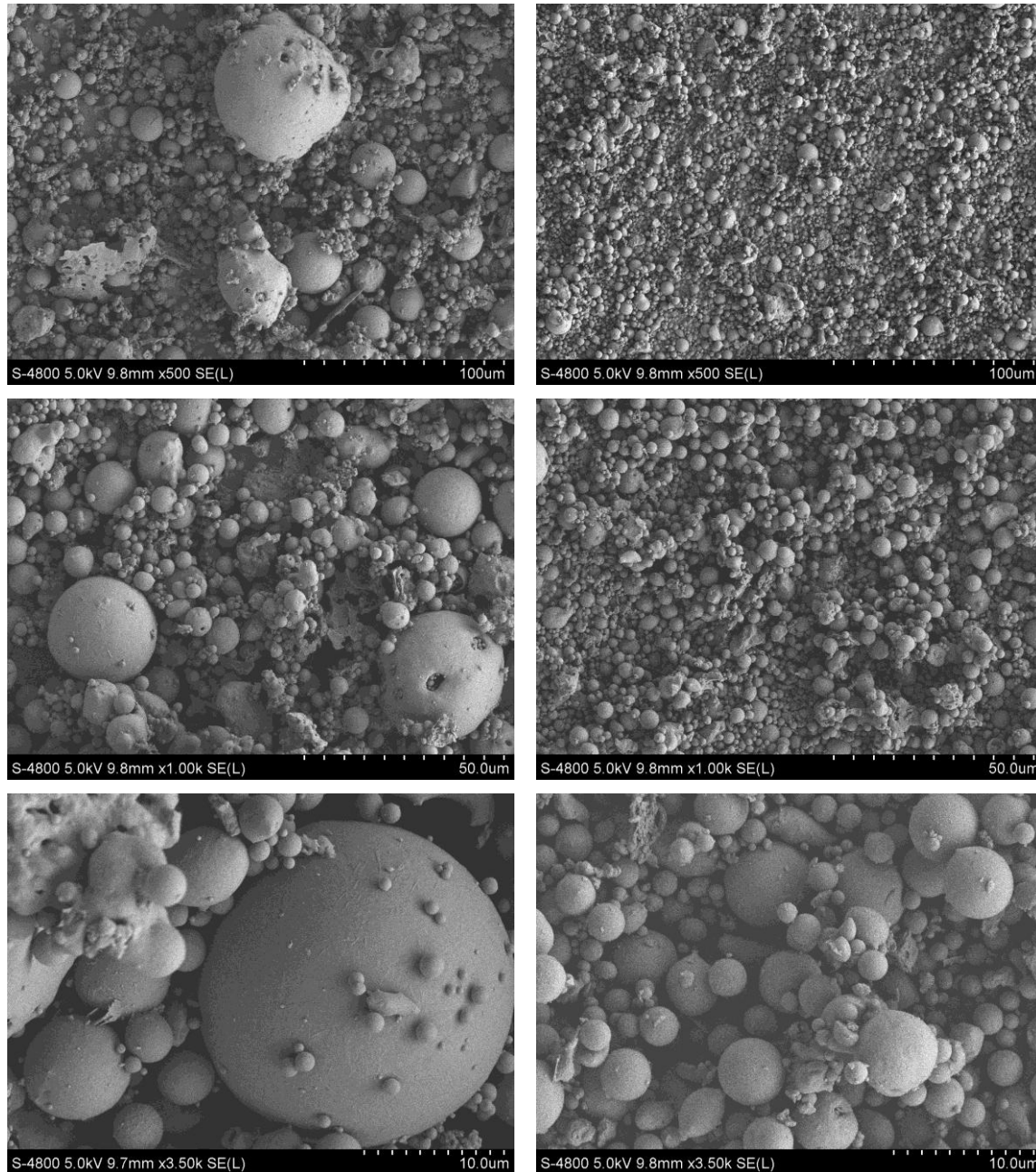
Figure 5. 16 SEM images of CFA (left) and CUFA (right) for different magnifications

5.2.1.2.2 Sugözü fly ash

Classification conditions and the obtained results for Sugözü fly ash (SFA) are shown in Tables 5.4 and 5.5, respectively. Smaller underflow rates were chosen this time because of the smaller particle size of SFA compared to that of CFA. According to Table 5.5, the average size of 4.41 µm particles was obtained with 17.51% yield and 63.13% recovery of -5 µm particles in the overflow product (SUFA). In other words, finer particle size with higher yield and recovery was obtained in this experiment compared to the hydraulic classification test of CFA. Table 5.6 shows chemical compositions of SFA classification products. As seen from Table 5.6, similar to the classification results of CFA, SiO_2 and Fe_2O_3 contents in SUFA decreased in 7.5% and 2.8%, respectively while 15% increase was obtained in Al_2O_3 content.

82

However, the lower SiO_2 and Fe_2O_3 contents and the higher Al_2O_3 content make CUFA a better pozzolan compared to SUFA in terms of chemical composition.

Table 5. 4 Classification conditions for SFA

Operating conditions	
Feed pulp density	1.5% solids by wt. (0.015 kg/l)
Feed rate	11 l/min
Underflow discharge rates	U/F-1 = 200 cc/min, U/F-2 = 150 cc/min U/F-3 = 150 cc/min, U/F-4 = 150 cc/min
Dispersant	Disal
Dispersant dosage	1.5 mg Disal/g of fly ash

Table 5. 5 Classification results for SFA

Products	Weight (%)	Solid (%)	d_{50} (µm)	Vol. % of -5 µm	-5 µm recovery (%)
U/F-1	32.18	21.45	34.13	5.43	11.27
U/F-2	25.69	23.08	32.63	5.52	9.15
U/F-3	13.63	12.35	26.90	6.40	5.63
U/F-4	11.00	9.96	16.31	9.76	6.93
O/F (Ultrafine)	*17.51*	*0.23*	*4.41*	*55.90*	*63.13*
TOTAL (Feed)	100.00	1.46	21.42	15.50	

Table 5. 6 Chemical compositions of SFA classification products

Species (%)	Feed (SFA)	U/F-1	U/F-2	U/F-3	U/F-4	O/F (SUFA)
SiO_2	63.35	63.62	63.83	63.5	62.11	58.62
Al_2O_3	22.01	19.68	20.33	21.67	23.25	25.49
Fe_2O_3	7.90	8.73	8.35	7.88	7.4	7.68
CaO	1.45	1.55	1.43	1.37	1.32	1.46
MgO	2.31	2.22	2.21	2.25	2.35	2.62
Na_2O	0.79	0.76	0.78	0.77	0.84	1.01
K_2O	1.95	1.77	1.79	1.88	2.03	2.34
P_2O_5	0.16	0.13	0.12	0.13	0.13	0.26
TiO_2	0.91	0.85	0.87	0.91	0.95	0.99
SO_3	<0.01	<0.01	<0.01	<0.01	<0.01	<0.01
LOI	2.15	1.85	2.24	2.63	2.4	1.94

Figure 5.17 illustrates SEM images of SFA and SUFA for different magnifications. This figure clearly indicates the very fine particle size of the overflow product compared to the as received Sugözü fly ash. According to the optical microscopy analyses of SFA and SUFA samples, the glass content of SFA was calculated as 88.8%, whereas this value was found as 98.8% for the overflow product.
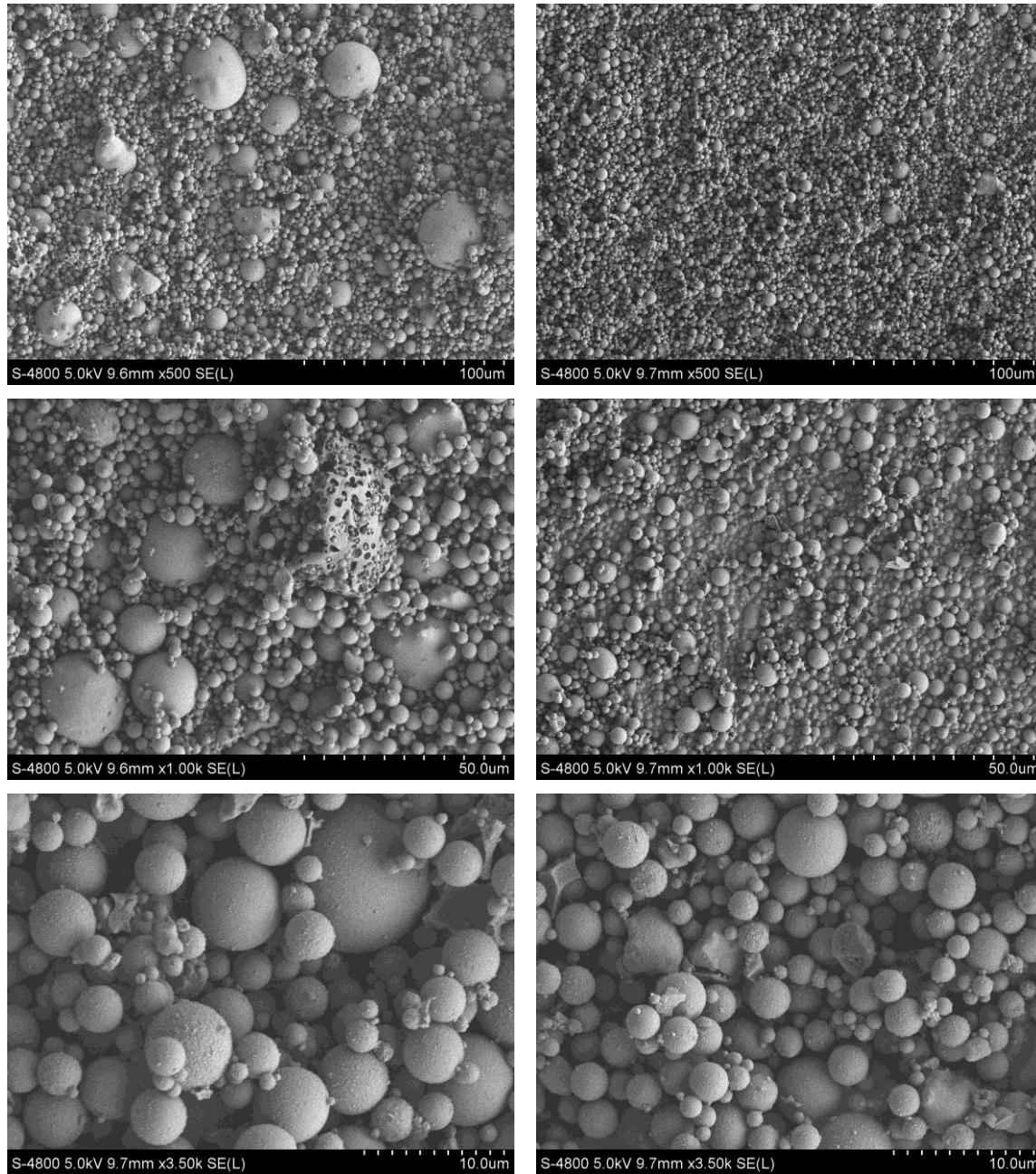
Figure 5. 17 SEM images of SFA (left) and SUFA (right) for different magnifications

Overall results obtained from the classification tests of Çatalağzı and Sugözü fly ashes indicate that the hydraulic classification technology developed at CAER gave good results for the recovery of very fine particles with enhanced chemical compositions. In other words, very fine particle sizes were obtained with high recoveries and acceptable yields for the fly ash samples, especially for Sugözü fly ash.

5.2.2 The results of mortar experiments

The fly ashes were tested on as-received and classified (UFA) bases in order to determine basic mortar properties in both fresh and hardened state. In these experiments, 10%, 20% and 30% of cement replacement ratios by the as-received fly ashes (FA) and their ultrafine fractions (UFA) were used for the mortar preparation.

5.2.2.1 Determination of water reductions

Water content is an important factor because it directly affects flowability and compressive strength of mortar and concrete. As water content increases, flowability also increases. However, in this case, compressive strengths of hardened mortar and concrete specimens decrease. Therefore, superplasticizers are used in construction industry to obtain a same flow with less water, leading to improvements in compressive strengths of mortar and concrete. In these experiments, according to ASTM C109, water contents of the mortars were adjusted to obtain a flow of 110 ± 5 in 25 drops of the flow table (ASTM, 2011). The percentages of water reductions provided by FA and UFA samples compared to the control sample are given in Tables 5.7 and 5.8. As seen from Table 5.7, the mortars containing CFA needed more water with increasing cement replacement ratios. For 30% cement replacement by CFA, the mortar demanded 6% more water to have the same flow with the mortar containing only PC. On the other hand, water reduction increased with increasing cement replacements by CUFA, and more than 10% water reduction was obtained for 30% cement replacement by CUFA. These results indicate that CUFA provided much better results compared to CFA in terms of water reductions.

Table 5. 7 Water reduction results of the mortars prepared with CFA and CUFA

Samples	Cement replacement ratio (%)	Cement (g)	Samples (g)	Sand (g)	Water (g)	Water reduction (%)
Cement control	-	500	0	1375	242.00	-
CFA	10	450	50	1375	245.00	-1.29
	20	400	100	1375	248.00	-2.63
	30	350	150	1375	257.00	-6.06
CUFA	10	450	50	1375	240.00	0.85
	20	400	100	1375	223.20	7.49
	30	350	150	1375	214.76	10.80

Table 5. 8 Water reduction results of the mortars prepared with SFA and SUFA

Samples	Cement replacement ratio (%)	Cement (g)	Samples (g)	Sand (g)	Water (g)	Water reduction (%)
Cement control	-	500	0	1375	242.00	-
SFA	10	450	50	1375	240.00	0.79
	20	400	100	1375	240.00	0.82
	30	350	150	1375	238.00	1.66
SUFA	10	450	50	1375	240.00	0.83
	20	400	100	1375	223.18	7.46
	30	350	150	1375	210.00	12.63

Table 5.8 shows water reductions provided by SFA and SUFA. According to Table 5.8, water reduction slightly increased with increasing cement replacements by SFA, and 1.66% reduction in water demand was obtained for 30% cement replacement. On the other hand, SUFA provided 12.63% water reduction for the same cement replacement which was the best result obtained in the mortar flow tests. Overall mortar flow tests indicate that both UFA samples enhanced flowability of the mortars especially for 30% cement replacement.

5.2.2.2 Compressive strength results of the mortar cubes

5.2.2.2.1 The mortar cubes prepared with CFA and CUFA

Figures 5.18-5.20 show the compressive strength test results of the mortar cubes prepared with different cement replacements by CFA and CUFA samples as a function of curing ages. As seen from the figures, in general, mortar cubes prepared with CFA and CUFA showed lower strength development rates than Portland cement (PC) control cubes up to 14 days. However, for the curing age of 28 days, CUFA cubes exceeded the compressive strength of the control for all the replacement ratios.
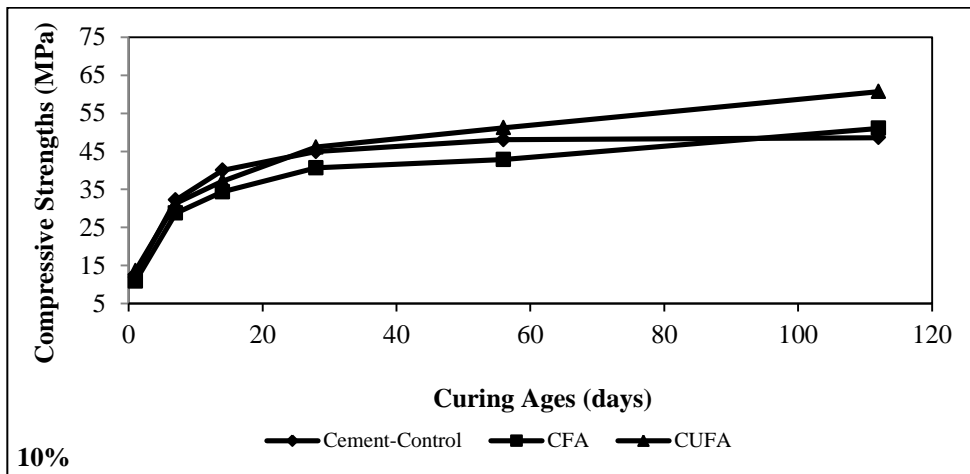
Figure 5. 18 Compressive strength results of CFA and CUFA for 10% cement replacement
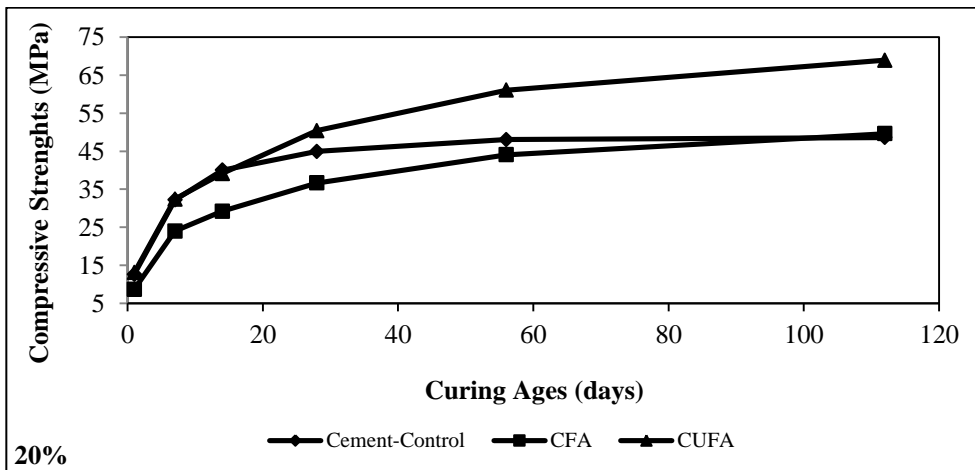
Figure 5. 19 Compressive strength results of CFA and CUFA for 20% cement replacement

86
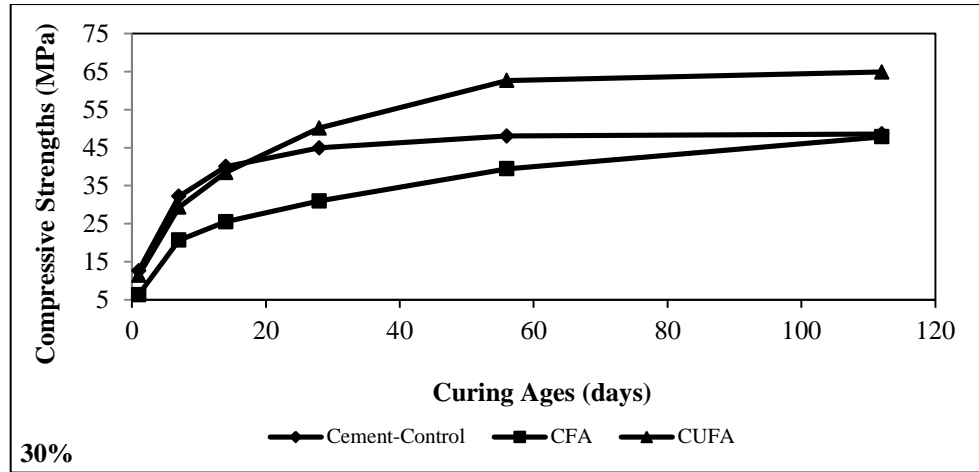
Figure 5. 20 Compressive strength results of CFA and CUFA for 30% cement replacement

Figures 5.18-5.20 also illustrate that strength development rates in CUFA cubes were much higher for 20% and 30% replacement ratios. After 56 days, the CUFA cubes prepared with 20% cement replacement show higher strength development rates compared to the ones made with 30% replacement. Overall, the CUFA cubes with 20% cement replacement gave the best results with competitive early strengths and much higher strength development rates compared to the cement control sample especially after 14 days of curing. On the other hand, the cubes prepared with CFA showed higher strength development rates only after 56 days of curing compared to the control cubes, and the best results for CFA were obtained with 10% cement replacement. At the end of the curing age of 112 days, CUFA provided about 42% increase in the compressive strength compared to the control sample for 20% replacement whereas only 1% increase was obtained with CFA for the same cement replacement.

5.2.2.2.2 Results of the mortar cubes prepared with SFA and SUFA

Figures 5.21-5.23 show the compressive strength test results of the mortar cubes prepared with different cement replacements by SFA and SUFA samples as a function of curing ages.
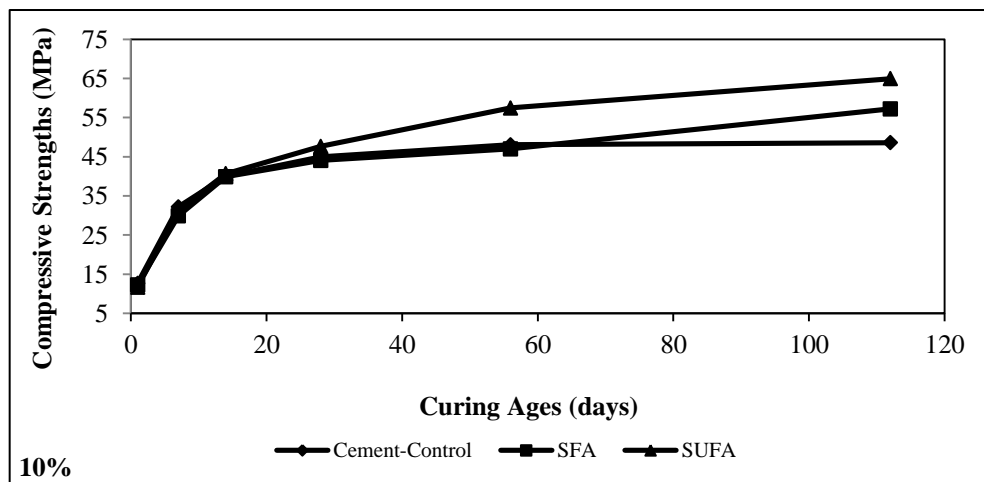

Figure 5. 21 Compressive strength results of SFA and SUFA for 10% cement replacement
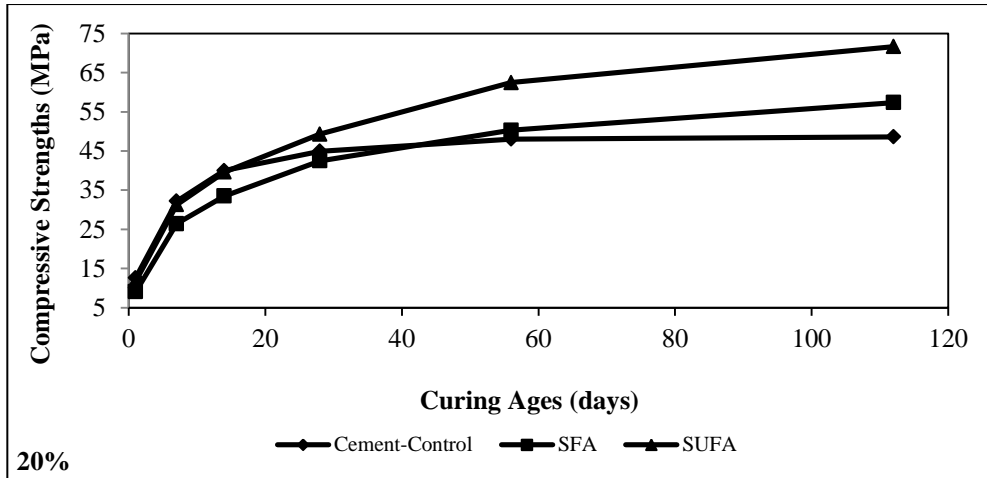
Figure 5. 22 Compressive strength results of SFA and SUFA for 20% cement replacement
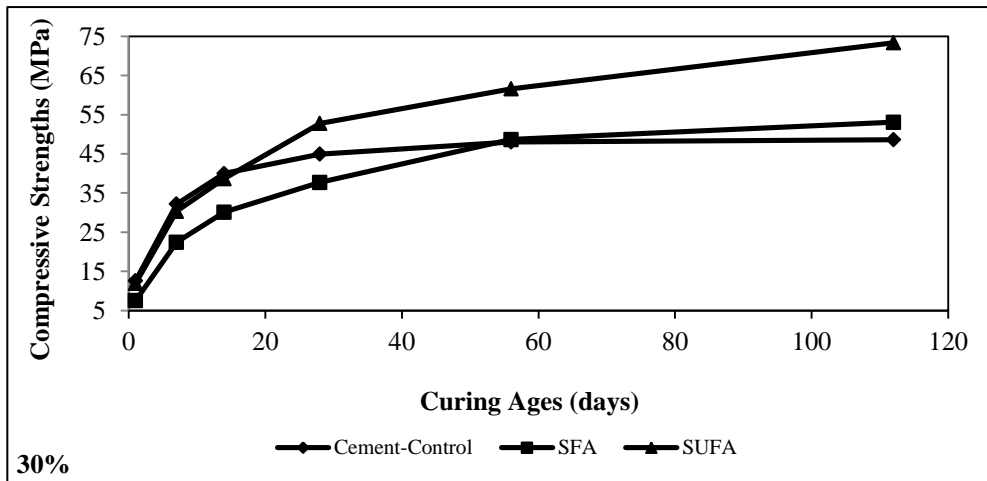

Figure 5. 23 Compressive strength results of SFA and SUFA for 30% cement replacement

According to Figures 5.21-5.23, the mortar cubes prepared with SFA and SUFA gave similar strength development patterns with the ones containing CFA and CUFA samples. However, both SFA and SUFA provided better results than the respective CFA and CUFA samples for all the PC replacements. Best results were obtained with SUFA for the highest PC replacement. These cubes showed better strength development rates compared to the mortar cubes prepared with 20% replacement especially after 56 days. At the end of 112 days, SUFA provided 50% increase in compressive strength compared to the control sample for 30% PC replacement while 9% increase was obtained with SFA for the same PC replacement.

5.2.2.3 The results of dimensional stability experiments

Dimensional stability of the mortar bars were examined with drying shrinkage and water expansion tests.

5.2.2.3.1. The shrinkage test results of CFA and CUFA

Figures 5.24-5.26 show drying shrinkage test results of the mortar bars prepared with different PC replacements by CFA and CUFA samples as a function of curing ages.
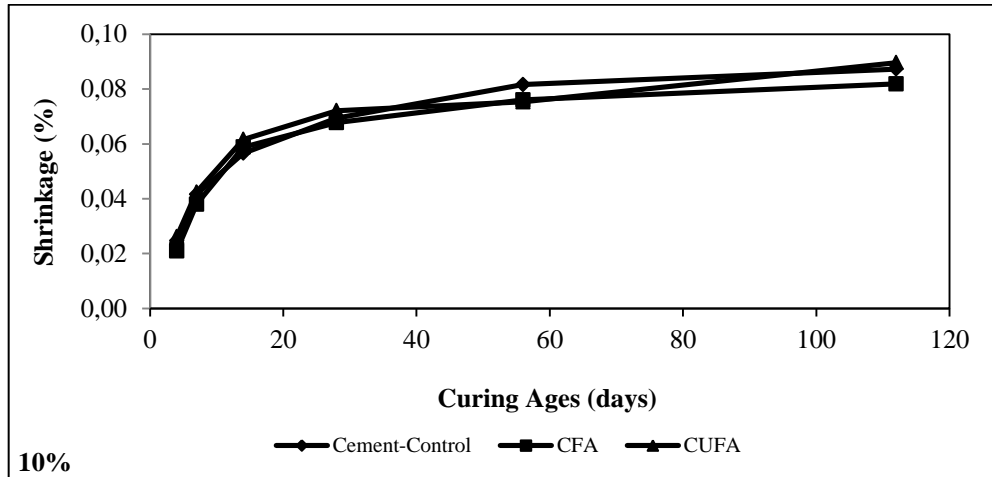
Figure 5. 24 Shrinkage results of CFA and CUFA for 10% cement replacement
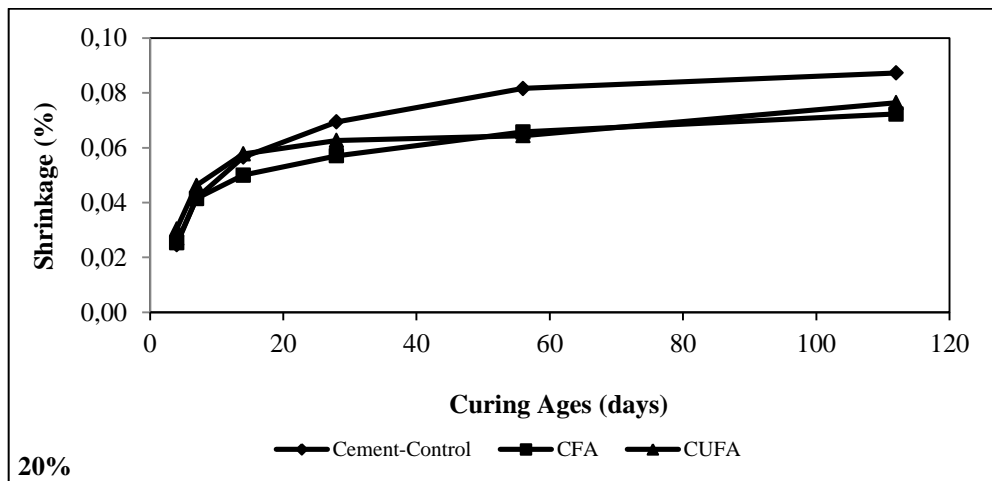
Figure 5. 25 Shrinkage results of CFA and CUFA for 20% cement replacement
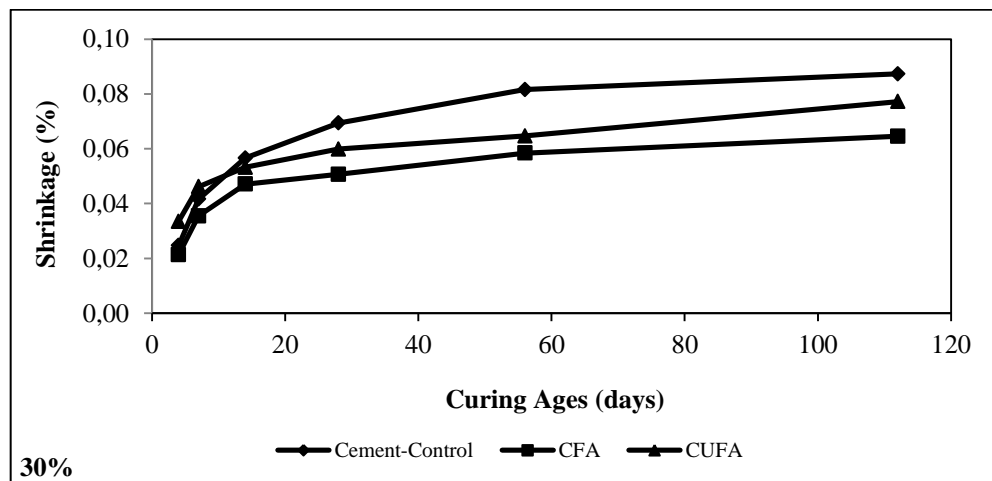
Figure 5. 26 Shrinkage results of CFA and CUFA for 30% cement replacement

As seen from Figures 5.24-5.26, in the early ages, mortar bars prepared with CUFA showed higher shrinkages compared to those containing PC only and CFA. However, except 10% cement replacement, both CFA and CUFA added bars exhibited lower shrinkages after 14 days. The optimum shrinkage result of CUFA was achieved with 20% cement replacement while 30% PC replacement by CFA provided the lowest shrinkage among all the measurements. Figures 5.24-5.26 also indicate that an increase in cement replacement by both CFA and CUFA resulted in a decrease in the shrinkages of the mortar bars especially after 14 days. The overall shrinkage test results showed that all the bars exhibited less than 0.09% shrinkages at the end of 112 days. At this point, CUFA added bars provided 11% decrease in shrinkage compared to the control bars whereas 26% decrease was obtained with the mortar bars containing CFA for 30% PC replacement.

5.2.2.3.2 The shrinkage test results of SFA and SUFA

Figures 5.27-5.29 show drying shrinkage test results of the mortar bars prepared with different cement replacements by SFA and SUFA samples as a function of curing ages.
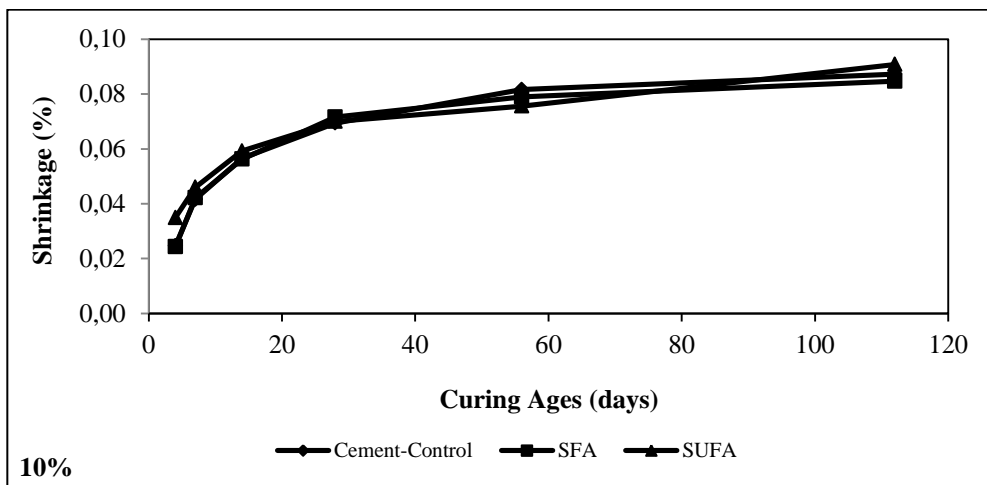
Figure 5. 27 Shrinkage results of SFA and SUFA for 10% cement replacement
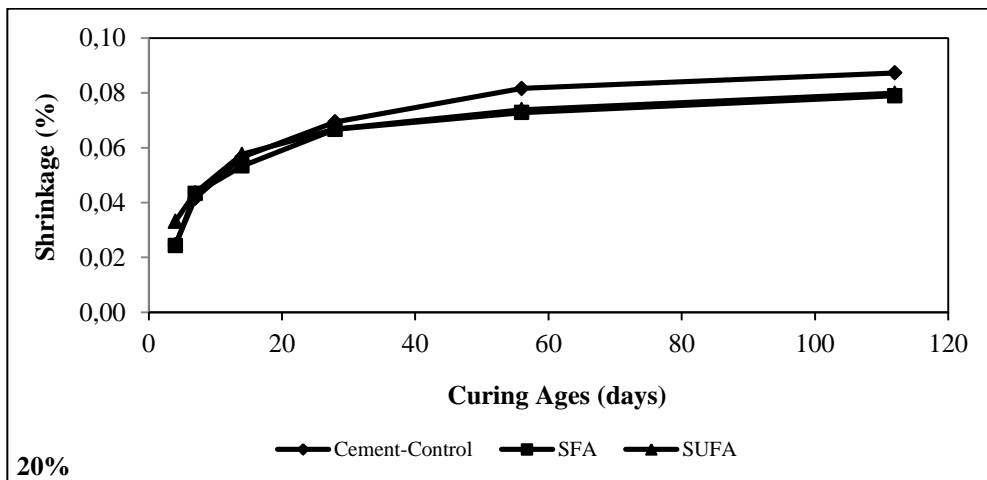
Figure 5. 28 Shrinkage results of SFA and SUFA for 20% cement replacement
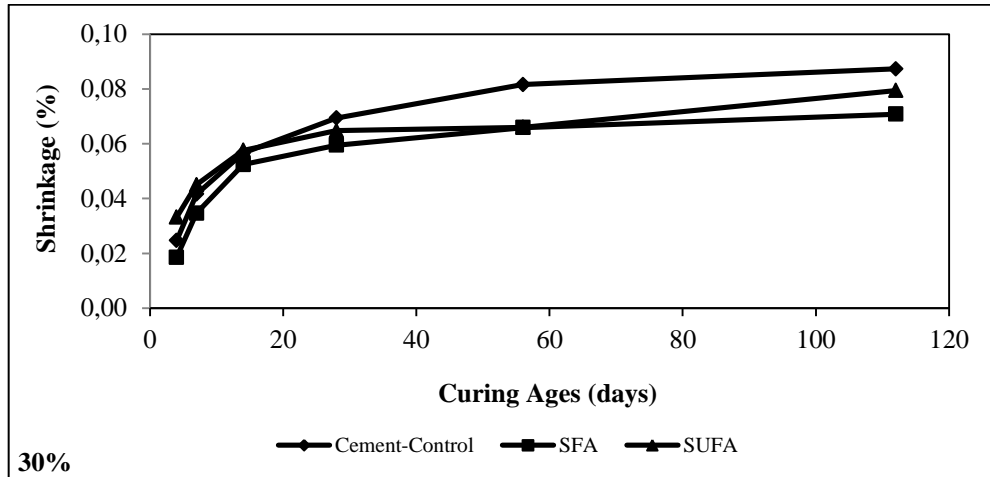
Figure 5. 29 Shrinkage results of SFA and SUFA for 30% cement replacement

In a similar way to the CFA and CUFA added bars, similar shrinkage patterns were observed for the bars prepared with SFA and SUFA. According to Figures 5.27-5.29, increasing cement replacement by both SFA and SUFA provided lower shrinkage values after the curing age of 28 days. These figures also indicate that the SUFA added bars did not exhibit lower shrinkages compared to those prepared with SFA. However, similar to the shrinkage results obtained with CFA and CUFA, the SFA and SUFA added bars also showed very low shrinkage values. The mortar bars prepared with 30% PC replacements by SFA and SUFA provided 19% and 9% decreases in shrinkage compared to those with PC only for the curing age of 112 days.

In the early ages of curing, mortar products have a tendency to shrink slightly because of the hydration reactions which consume the free water from the mix. Especially after the curing age of 28 days, the tested fly ashes and UFA's enhanced shrinkage of the bars due to the pozzolanic reactions between fly ashes and calcium hydroxide resulted from cement hydration. As a conclusion, drying shrinkage will not be a barrier for the utilization of the tested as received and classified fly ash samples as pozzolans.

5.2.2.3.3 Water expansion test results of CFA and CUFA

Lime saturated water was used for storage of the bars for the purpose of supplying unlimited source for the hydration reactions, resulting in the maximum possible amount of expansion in mortar bars. Figures 5.30-5.32 show water expansion test results of the mortar bars prepared with different cement replacements by CFA and CUFA samples as a function of curing ages. According to these figures, lower expansions in the bars prepared with CFA and CUFA were observed compared to the control sample as the cement replacement ratio increased from 10% to 30%. Also, further reductions in the expansion values were obtained with the CUFA added bars in comparison to those containing CFA especially after the curing age of 56 days. In the same manner as the shrinkage results, the mortar bars prepared with CFA and CUFA exhibited very low amounts of expansion. At the end of 112 days, CUFA added bars provided 17.5% reduction in water expansion compared to the control bars for 30% PC replacement while CFA added bars exhibited only 3% reduction for the same cement replacement. The maximum expansion value was measured as less than 0.02% after 112 days, indicating that water expansion is not a limiting factor for the utilization of CFA and CUFA as pozzolans.
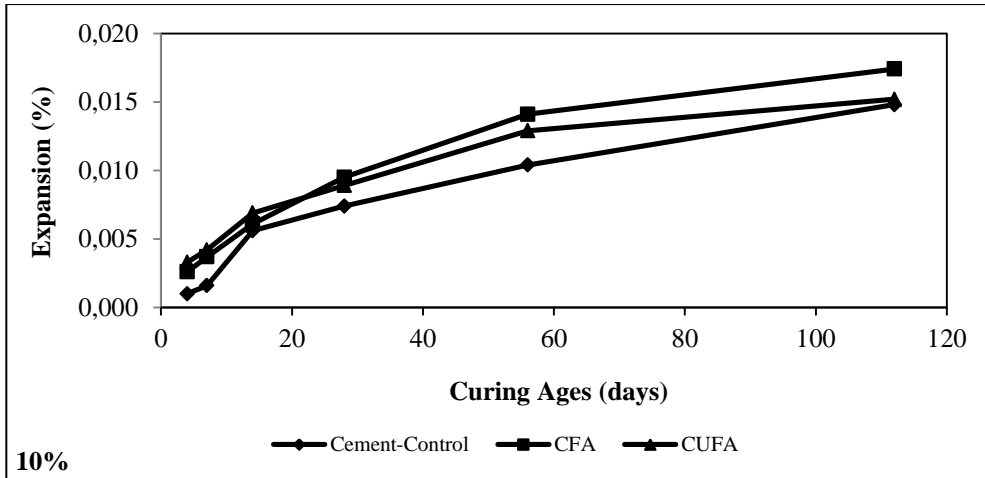
Figure 5. 30 Expansion results of CFA and CUFA for 10% cement replacement
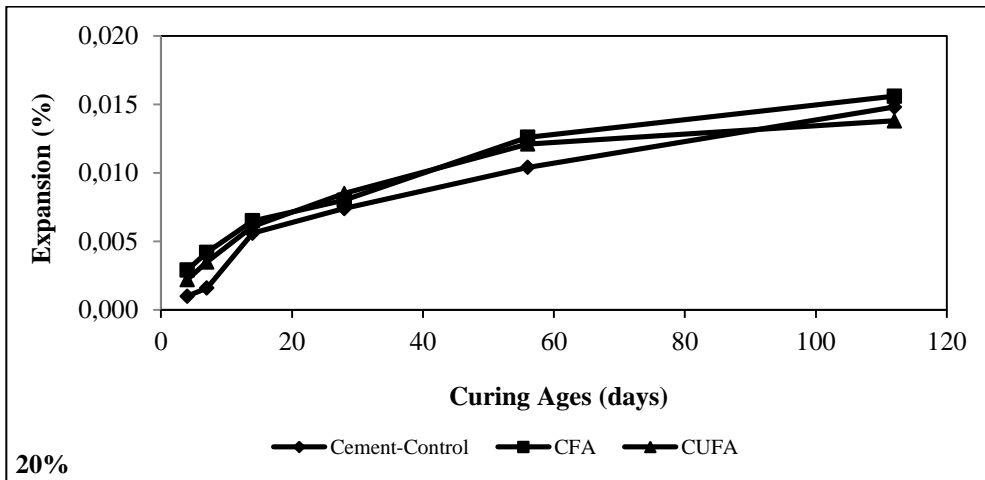
Figure 5. 31 Expansion results of CFA and CUFA for 20% cement replacement
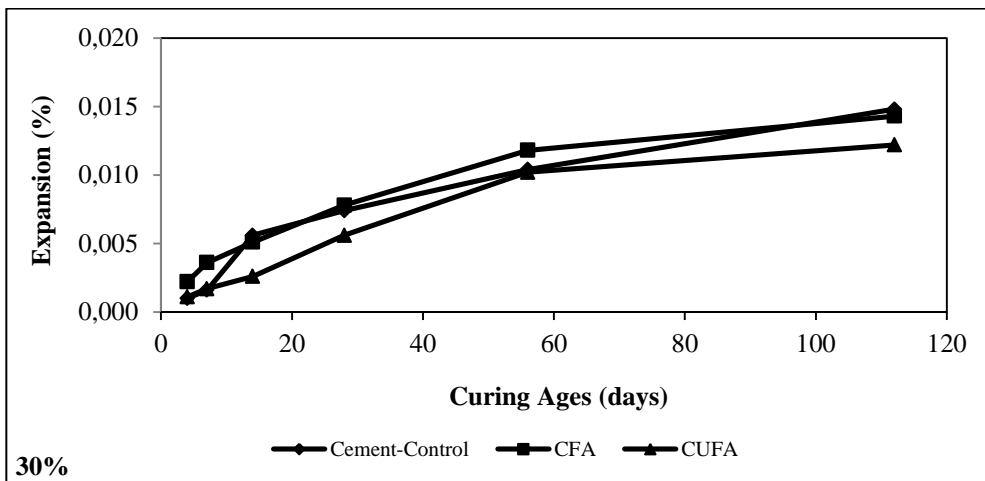
Figure 5. 32 Expansion results of CFA and CUFA for 30% cement replacement

5.2.2.3.4 Water expansion test results of SFA and SUFA

Figures 5.33-5.35 illustrate water expansion test results of the mortar bars prepared with different cement replacements by SFA and SUFA samples as a function of curing ages. According to Figures 5.33-5.35, in a similar way to the expansion results obtained with CFA and CUFA samples, the expansion values of the bars prepared with both SFA and SUFA decreased with the increasing cement replacement especially after 56 days. For the curing age of 112 days, the mortar bars containing SFA and SUFA provided respective 17% and 21% reductions in water expansion compared to the control bars for 30% PC replacement, indicating that SFA and SUFA gave better results than CFA and CUFA, respectively.

Overall water expansion test results showed that all of the as received and classified fly ashes added bars exhibited lower water expansions compared to the control bars at the end of 112 days. As a comparison, the ultrafine fly ashes added bars showed better results than the ones prepared with the as received samples for the PC replacement ratios of 20% and higher.
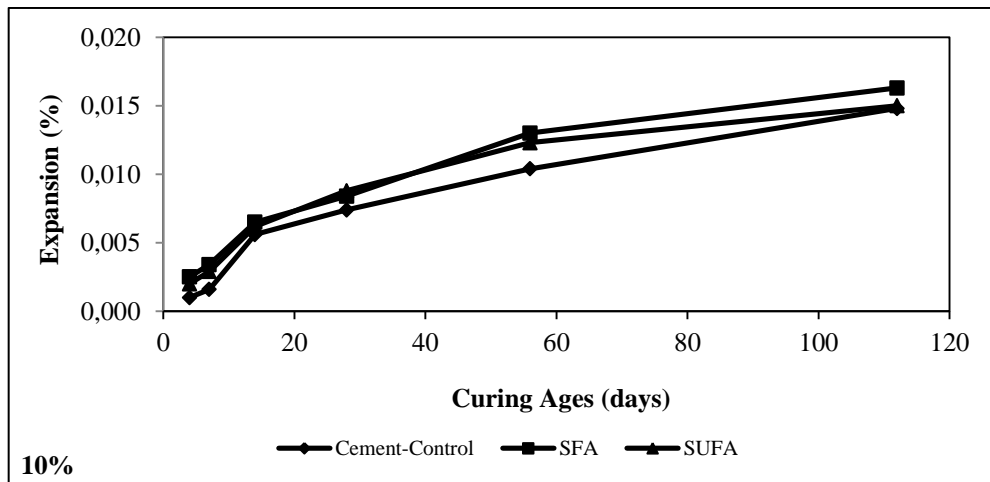

Figure 5. 33 Expansion results of SFA and SUFA for 10% cement replacement
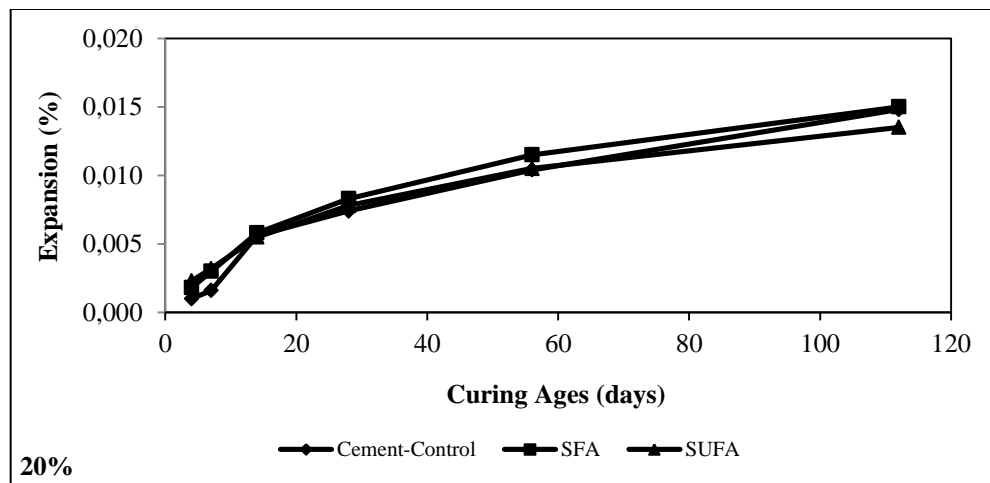
Figure 5. 34 Expansion results of SFA and SUFA for 20% cement replacement
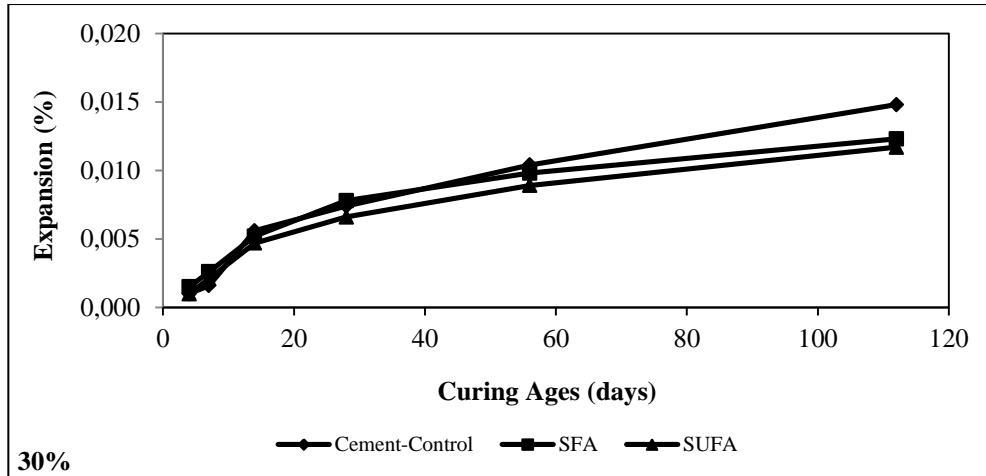
Figure 5. 35 Expansion results of SFA and SUFA for 30% cement replacement

5.2.3 The results of paste experiments

5.2.3.1 Microstructural evolution of the PC/FA and PC/UFA pastes

X-ray diffraction (XRD) analysis was used to evaluate mineralogical changes in the PC/FA and PC/UFA paste specimens. Analyses of the patterns were done by comparing the peak positions and intensities of the samples with those in the Joint Committee on Powder Diffraction Standards (JCPDS) data files. According to JCPDS data files, the main crystalline components in paste specimens are portlandite ($Ca(OH)_2$), hatrurite (alite, Ca_3SiO_5), ettringite ($Ca_6(Al(OH)_6)_2(SO4)_3(H_2O)_{26}$), belite ($Ca_2SiO_4$) and brownmillerite ($Ca_2FeAlO_5$). The other crystalline phases are mostly found in very low amounts, namely tricalcium aluminate ($Ca_3Al_2O_6$), quartz (SiO_2), calcite ($CaCO_3$), clinotobermorite ($Ca_5(Si_6O_{17})(H_2O)_5$), periclase (MgO), hydrocalumite ($Ca_8Al_4(OH)_{24}(CO_3)Cl_2(H_2O)_{9.6}$) and $Ca_4Al_2O_6CO_3.11$ H_2O. These crystalline phases were represented as a letter or letters in the figures; portlandite (P), hatrurite (H), ettringite (E), belite (B), brownmillerite (Br), tricalcium aluminate (T), quartz (Q), calcite (C), clinotobermorite (Cl), periclase (Pe), hydrocalumite (Hy) and $Ca_4Al_2O_6CO_3.11$ H_2O (Ca).

5.2.3.1.1 XRD analyses of blended PC/CFA and PC/CUFA pastes

Figures 5.36-5.41 illustrate the mineralogical changes occurred in the PC/CFA and PC/CUFA pastes for the curing ages of 1, 7, 14, 28, 56 and 112 days. These figures also provide the changes in the XRD patterns of PC only paste, providing an opportunity for comparison of the samples. According to Figure 5.36, after 1 day, portlandite, hatrurite and ettringite were the main crystalline phases in the paste specimens. In fact, the main cement hydration product is calcium silicate hydrate (C-S-H) gel phase in the early age. However, it cannot be detected by XRD analysis because it does not have a crystal structure. After 7 days (Figure 5.37), portlandite became the main crystalline phase as a result of cement hydration for all of the paste specimens. Almost no hatrurite phase was found in the PC/CUFA paste specimen after 14 days of curing. According to the main portlandite peaks illustrated in Figures 5.38-5.40, potlandite contents in the PC/CUFA paste decreased significantly between the curing ages of 14 and 56 days compared to those in PC/CFA and PC only paste specimens due to the higher pozzolanic reactivity of CUFA than that of CFA between the same curing ages. Figure 5.41 indicates that the differences in the main portlandite peaks between the PC/CUFA and PC/CFA pastes became smaller at the end of 112 days since CFA had a higher pozzolanic reactivity compared to CUFA after 56 days.
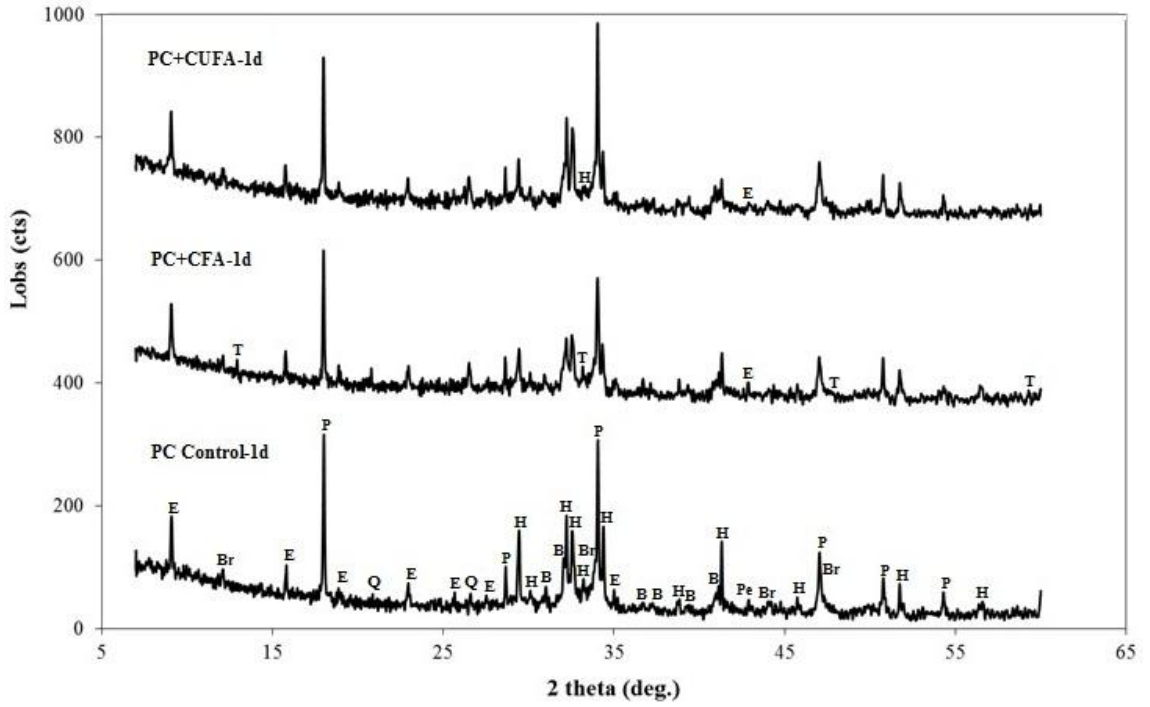
Figure 5. 36 Mineralogical compositions of PC/CFA and PC/CUFA pastes after 1 day
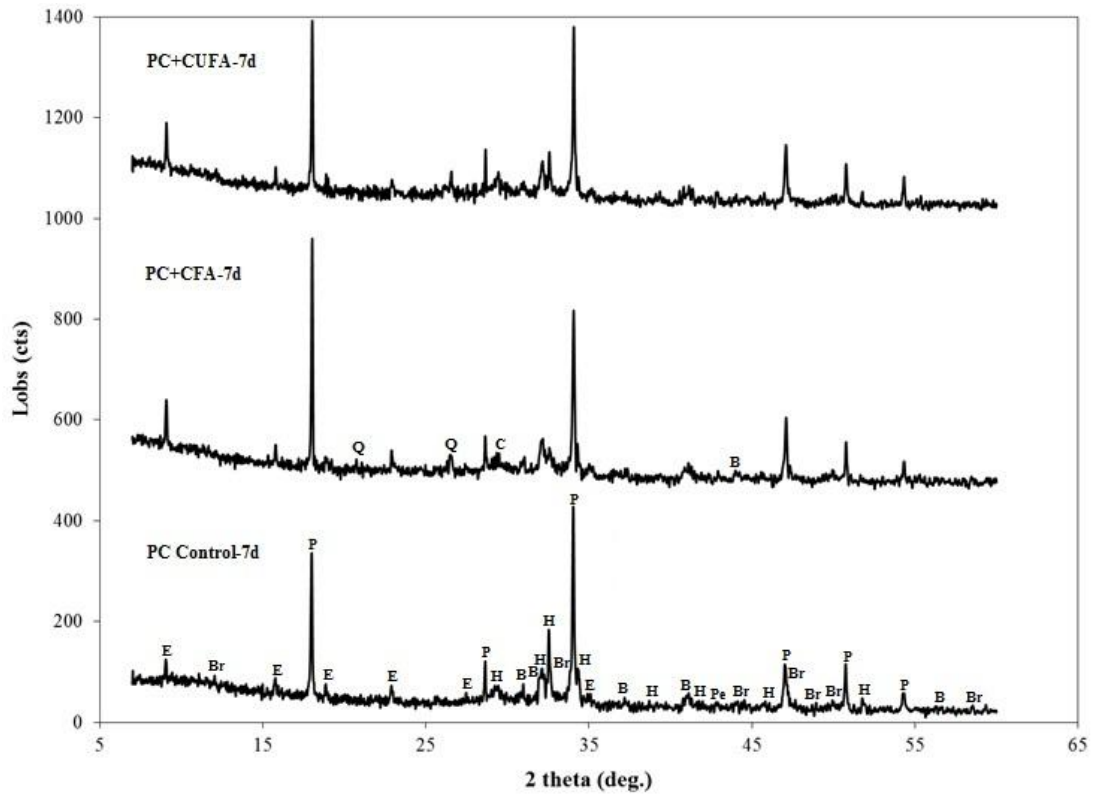
Figure 5. 37 Mineralogical compositions of PC/CFA and PC/CUFA pastes after 7 days
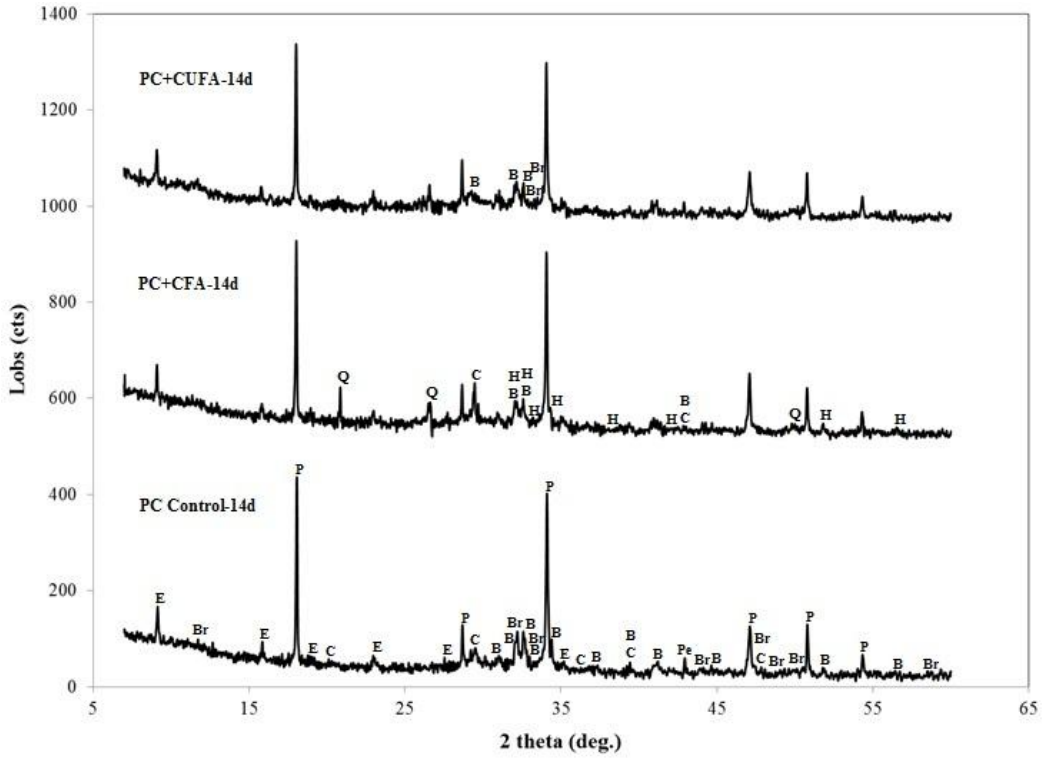
Figure 5. 38 Mineralogical compositions of PC/CFA and PC/CUFA pastes after 14 days
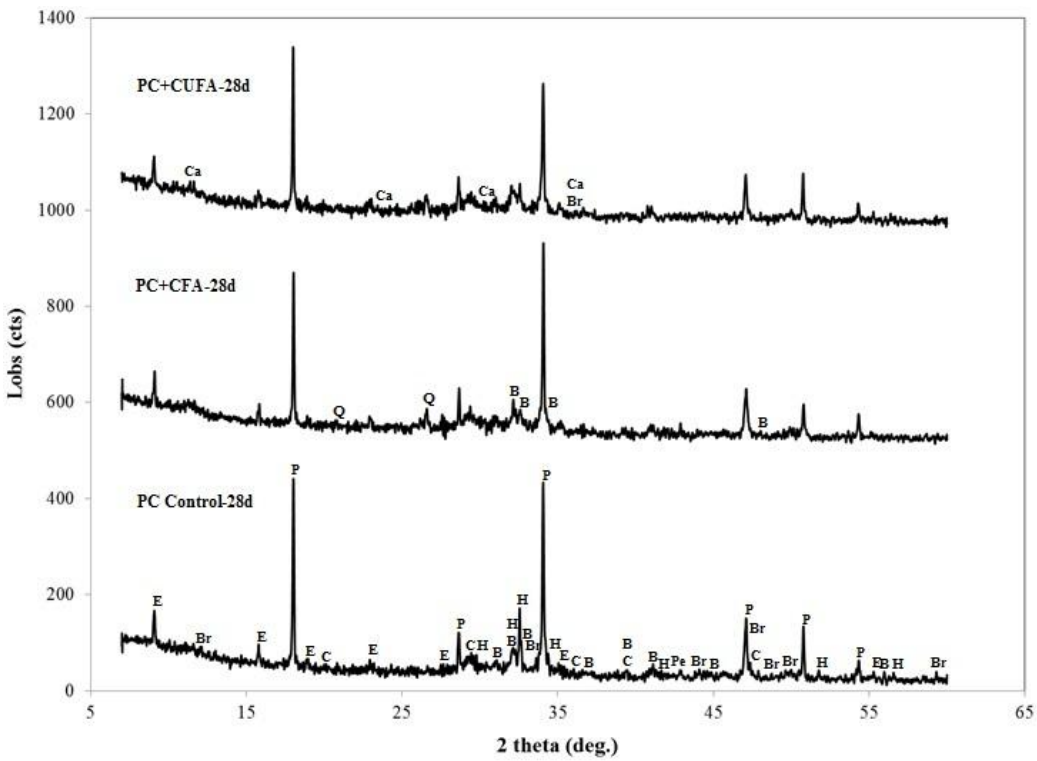
Figure 5. 39 Mineralogical compositions of PC/CFA and PC/CUFA pastes after 28 days
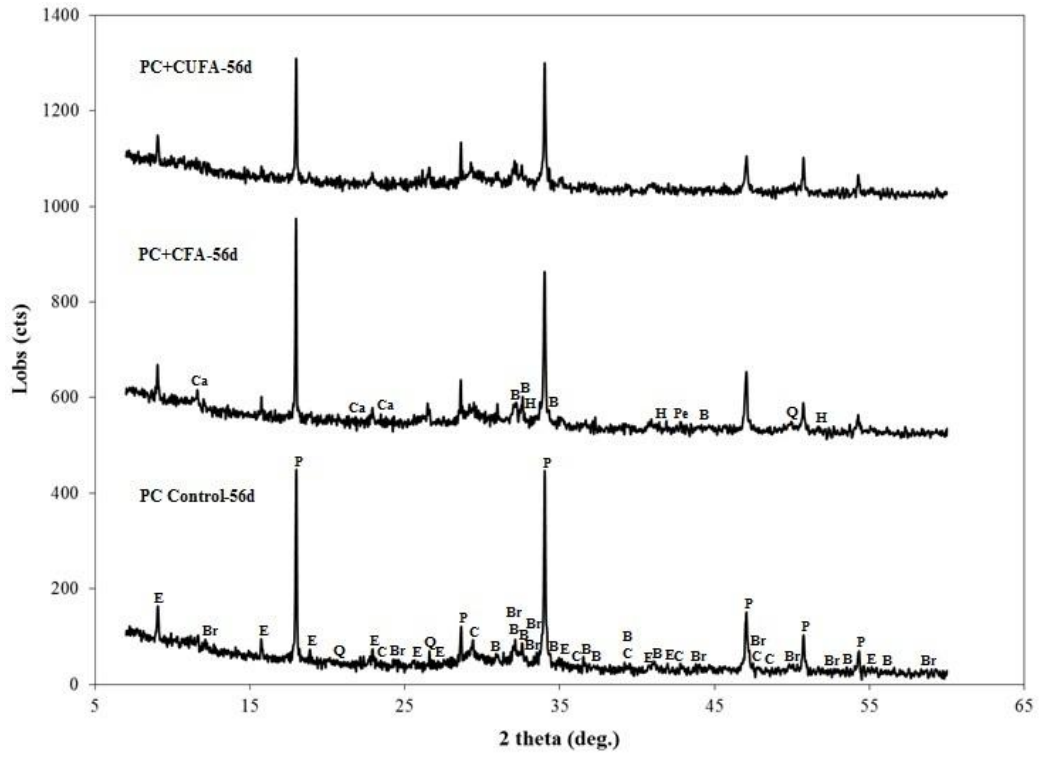
Figure 5. 40 Mineralogical compositions of PC/CFA and PC/CUFA pastes after 56 days
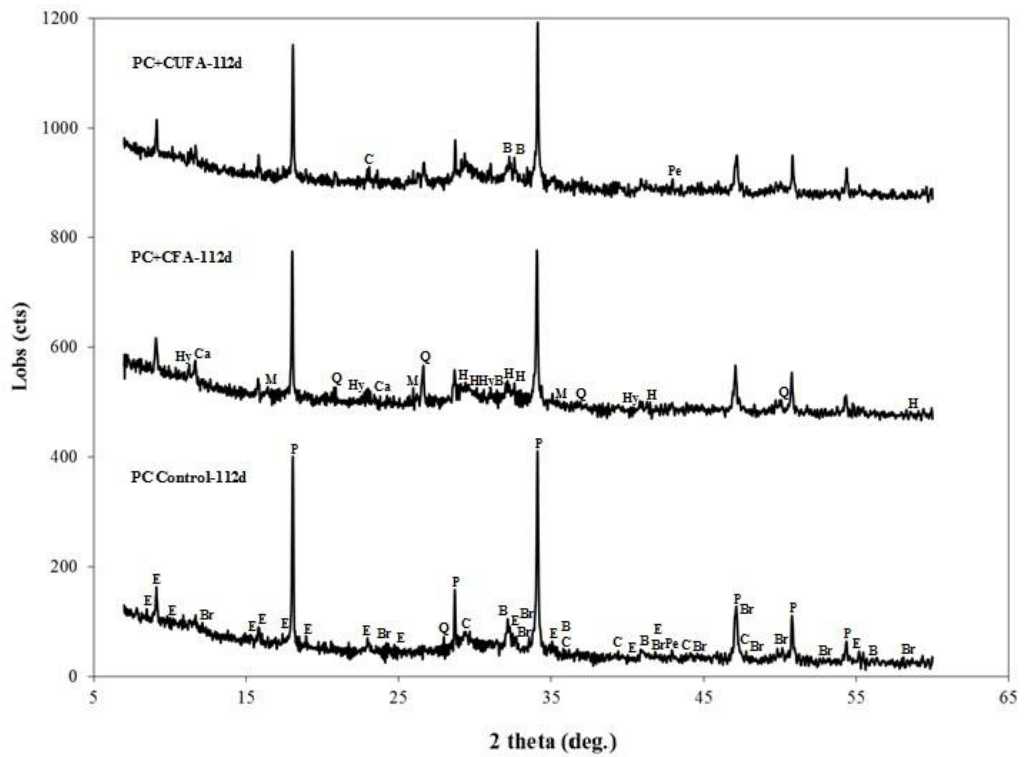
Figure 5. 41 Mineralogical compositions of PC/CFA and PC/CUFA pastes after 112 days

97

5.2.3.1.2 XRD analyses of blended PC/SFA and PC/SUFA pastes

Figures 5.42-5.47 illustrate the mineralogical evolution of the PC/SFA and PC/SUFA paste specimens with the curing ages of 1, 7, 14, 28, 56 and 112 days. These figures also provide the changes in the XRD patterns of the PC only paste for comparison. In the same manner as the paste specimens prepared with CFA and CUFA, according to Figure 5.42, after 1 day, portlandite, hatrurite and ettringite were the main crystalline phases in the paste specimens except the PC/SFA paste. After 7 days, portlandite became the main crystalline phase as a result of cement hydration for all the paste specimens shown in Figure 5.43. As seen from Figures 5.44 and 5.45, potlandite contents in the PC/SUFA paste decreased significantly between the curing ages of 14 and 28 days compared to those in PC/SFA and PC only paste specimens because of the higher pozzolanic reactivity of SUFA than that of SFA between the same curing ages. According to Figures 5.46 and 5.47, the differences in the main portlandite peaks between the PC/SUFA and PC/SFA pastes became smaller with the increasing curing ages after 28 days due to the increasing pozzolanic reactivity of SFA.

If all the XRD patterns are taken into account, the reactivity difference between CUFA and CFA seems to be more prominent than that of SUFA and SFA because of the large difference in particle sizes of CUFA and CFA.
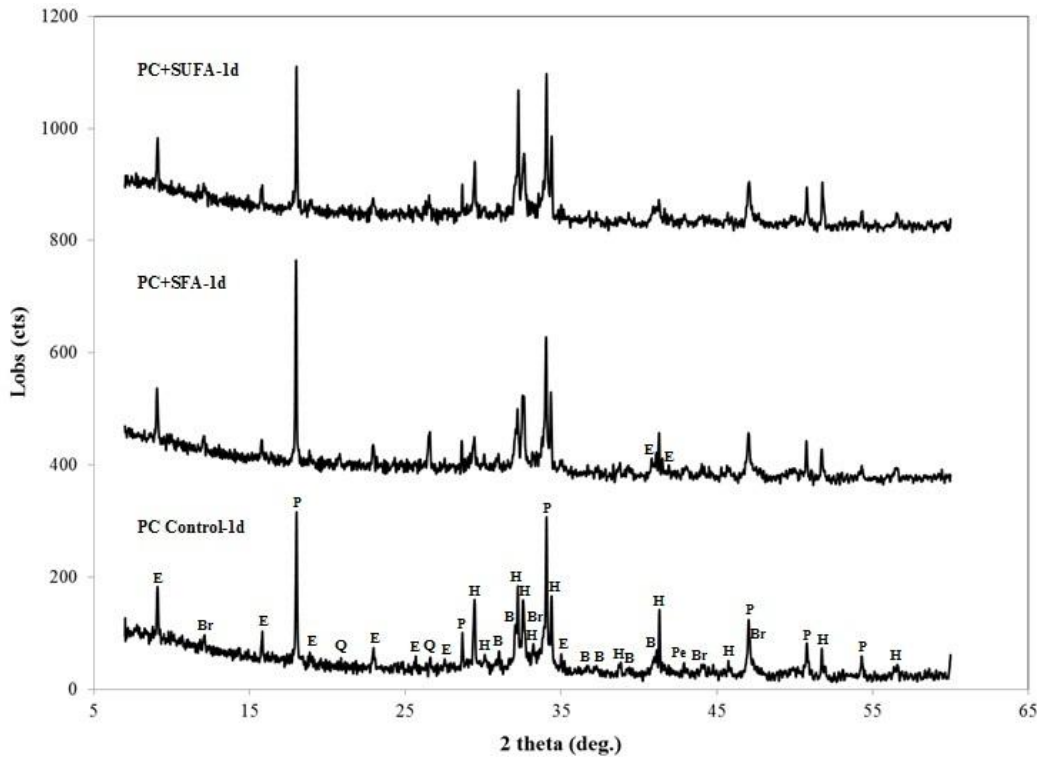
Figure 5. 42 Mineralogical compositions of PC/SFA and PC/SUFA pastes after 1 day
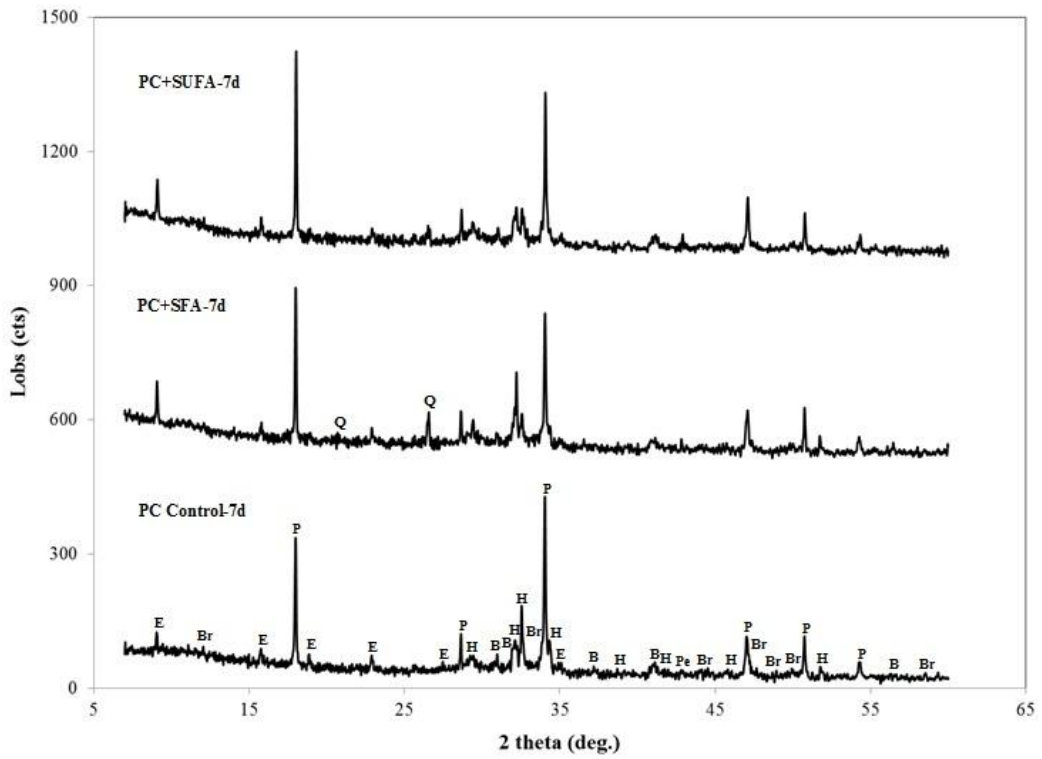
Figure 5. 43 Mineralogical compositions of PC/SFA and PC/SUFA pastes after 7 days
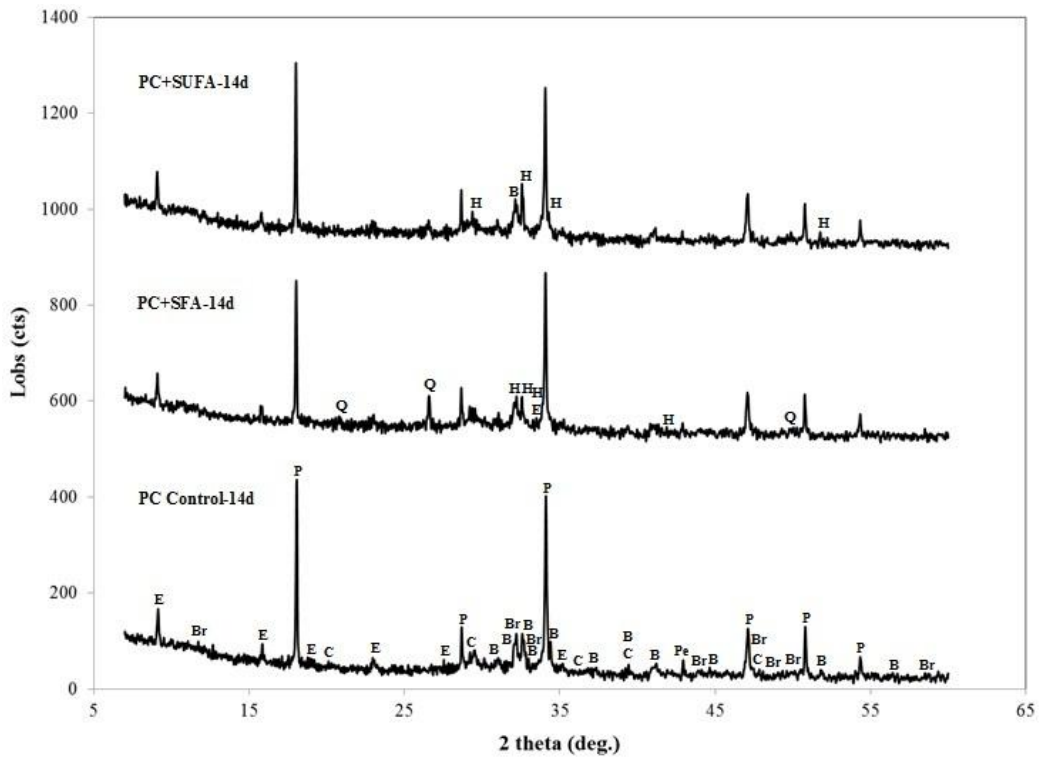
Figure 5. 44 Mineralogical compositions of PC/SFA and PC/SUFA pastes after 14 days
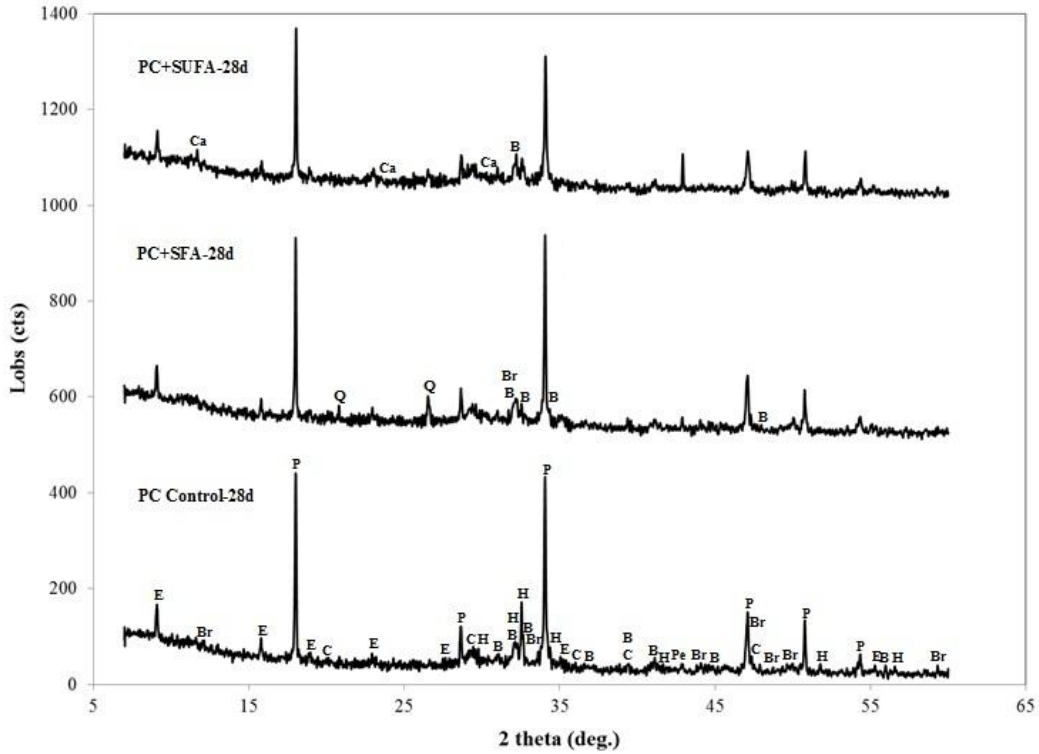
Figure 5. 45 Mineralogical compositions of PC/SFA and PC/SUFA pastes after 28 days
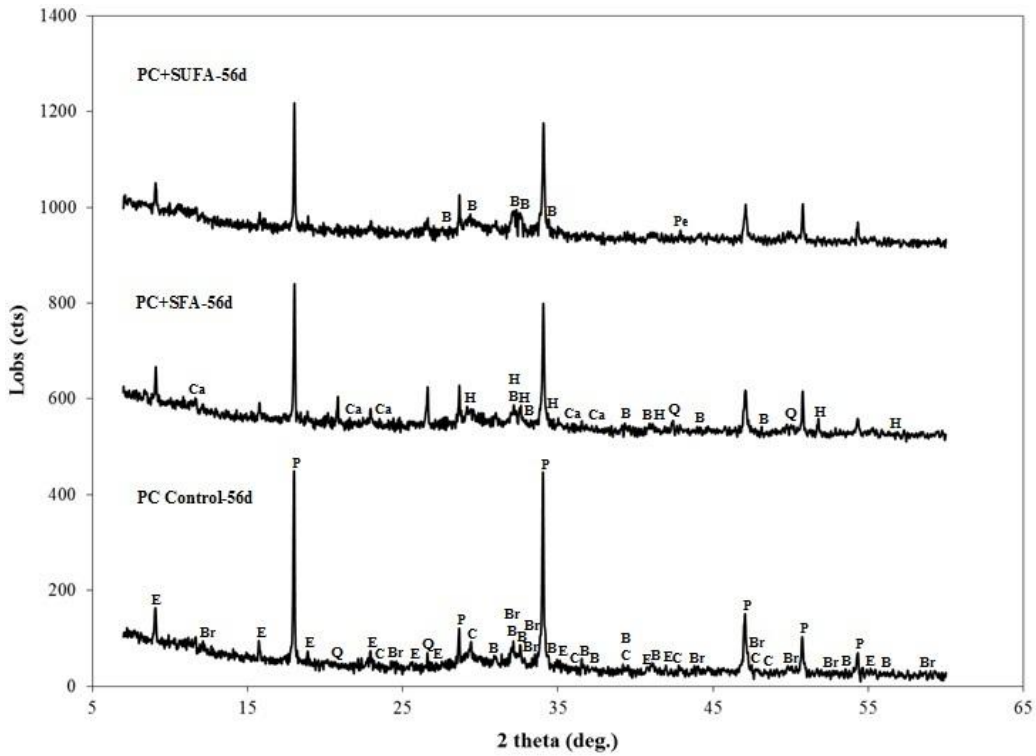
Figure 5. 46 Mineralogical compositions of PC/SFA and PC/SUFA pastes after 56 days
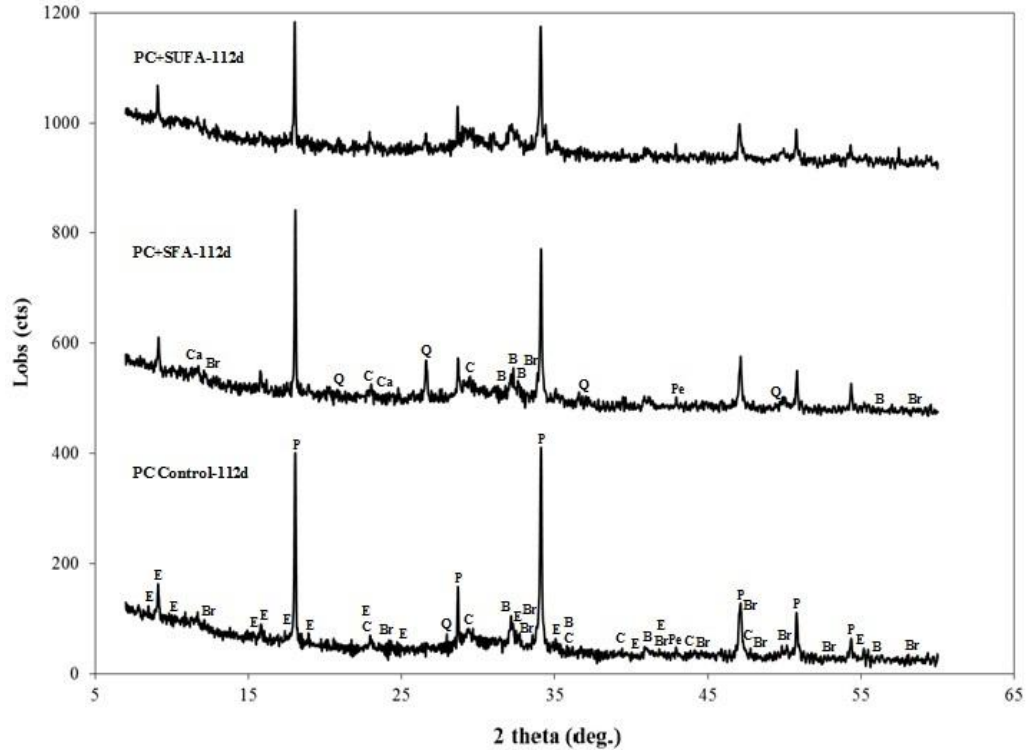
Figure 5. 47 Mineralogical compositions of PC/SFA and PC/SUFA pastes after 112 days

5.2.3.2 Measurement of pozzolanic reactivity by using TGA

In these experiments, the reactivity of the fly ashes (FA) and their ultrafine fractions (UFA) was evaluated by thermogravimetric (TG) analyses of the PC/FA and PC/UFA paste specimens. The main purpose of these TG analyses was to measure the pozzolanic reactivity of the samples without the packing effect of sand, which might occur in mortar tests.

5.2.3.2.1 The results of CFA and CUFA samples

Figure 5.48 gives the change in $Ca(OH)_2$ content in PC/CFA and PC/CUFA pastes as a function of curing ages. These results were given as percentages of the $Ca(OH)_2$ content in the PC only paste. As seen from the figure, significant $Ca(OH)_2$ consumption compared to the control sample was obtained with both CFA and CUFA between the curing ages of 7 and 28 days. However, after 28 days, pozzolanic reactivity of CUFA was higher than that of CFA. At the end of 112 days, 77.02% and 68.56% $Ca(OH)_2$ content of the PC only paste were obtained with CFA and CUFA, respectively. For all the curing ages except 1 day, CUFA exhibited better results compared to CFA due to its finer particle size.
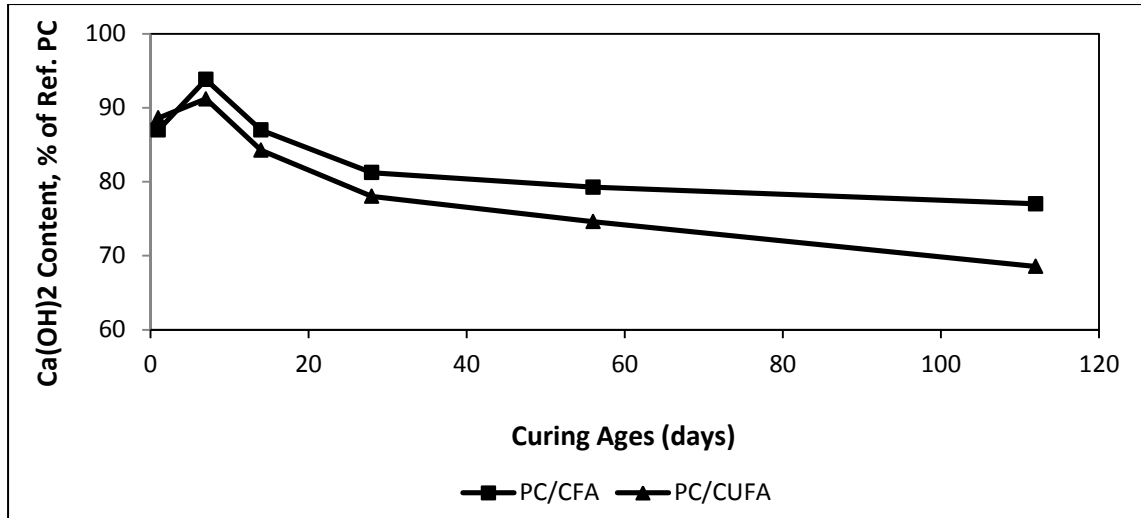
Figure 5. 48 Ca(OH)$_2$ content variation in PC/CFA and PC/CUFA pastes

5.2.3.2.2 The results of SFA and SUFA samples

Figure 5.49 illustrates the changes in Ca(OH)$_2$ content of the PC/CFA and PC/CUFA pastes as a function of curing ages. These changes were given as percentages of the Ca(OH)$_2$ content in the control paste. According to this figure, in the same manner as CFA and CUFA samples, similar Ca(OH)$_2$ consumption patterns were also obtained with SFA and SUFA samples. Figure 5.49 also points out that SUFA was very reactive compared to SFA in the range of 28-56 days. At the end of 112 days, 72.55% and 62.68% Ca(OH)$_2$ content of the PC only paste were achieved with SFA and SUFA, respectively.
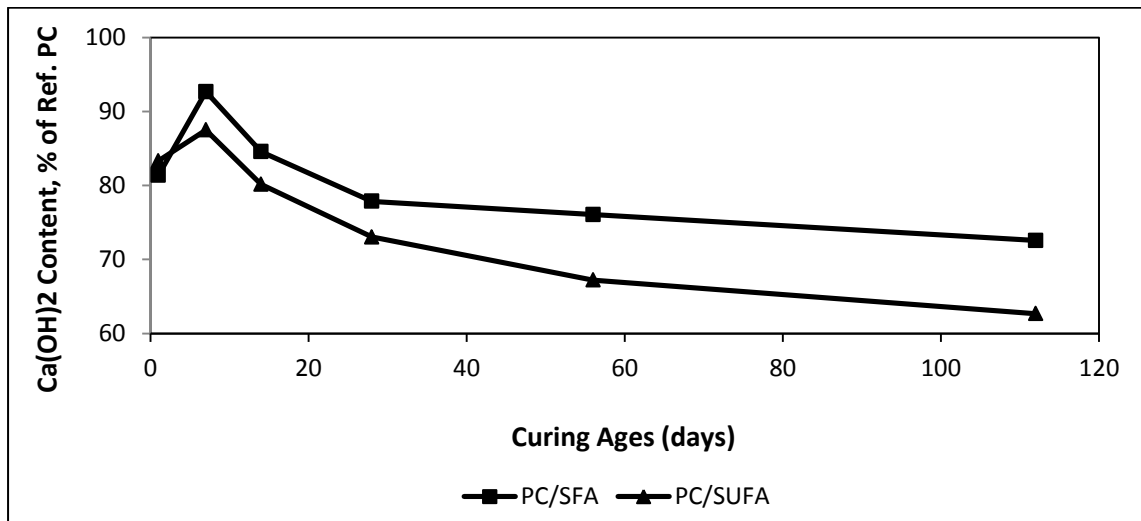
Figure 5. 49 Ca(OH)$_2$ content variation in PC/SFA and PC/SUFA pastes

Overall Figures 5.48 and 5.49 indicate that the highest Ca(OH)$_2$ consumption in reference to the PC only paste was obtained with SUFA sample most probably because of its finer particle size and higher surface area compared to the other samples.

5.3 The results of the experiments conducted in determination of cenosphere recovery potential

5.3.1 The results of float-sink experiments

Float-sink experiments were conducted to observe the relationship between particle density and yield of the float products. These float products were further analyzed under optical microscope for their cenosphere contents on the basis of point and area calculation.

5.3.1.1 The float-sink experiments conducted with CFA

Figure 5.50 illustrates yield, grade and recovery of cenosphere in CFA float products as a function of specific gravity ranging from 1.00 to 1.80. Cenosphere contents of the float products were determined on the basis of point counting. According to this figure, yield and recovery of cenospheres in the float products increased with increasing specific gravity whereas the cenosphere contents in these fractions decreased with increasing specific gravity as expected. Based on the point-counting measurements, CFA sample contains 11.30% cenosphere content. However, for the highest specific gravity tested, a float product with 25.60% cenosphere content was obtained with a yield of about 25% of feed and a recovery of 56%. This result points out that a considerable amount of cenosphere was found in CFA even at the specific gravity of 1.80.
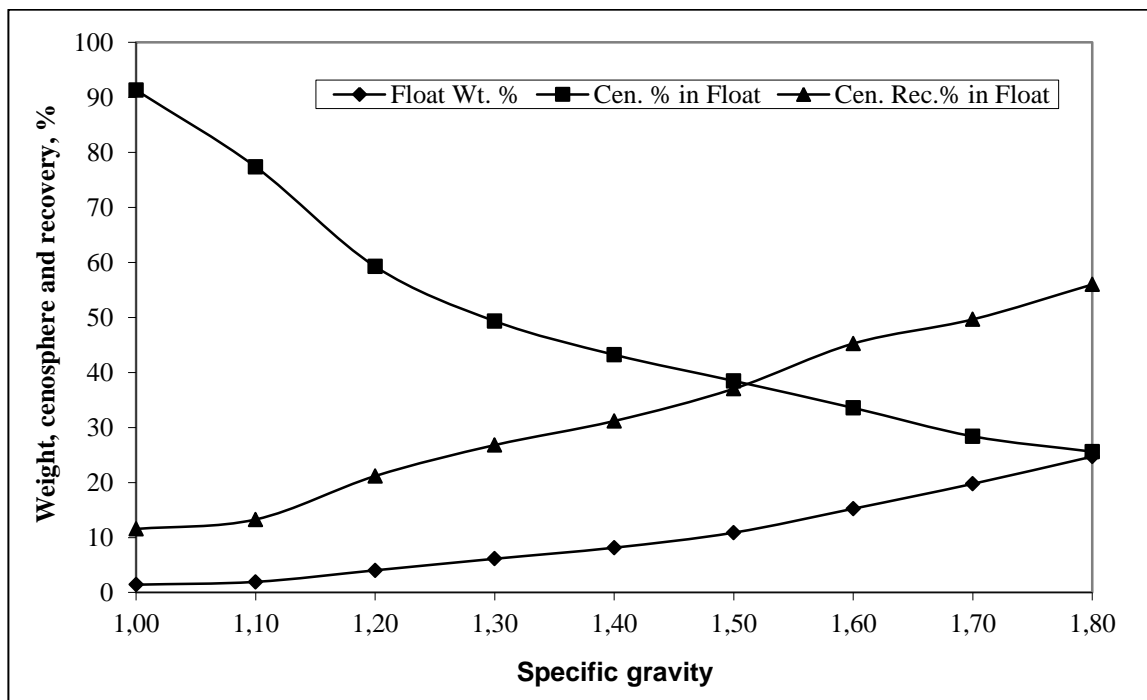
Figure 5. 50 The experimental results of float-sink tests performed with CFA

Figure 5.51 shows the images taken from the thin sections of the as-received and different float products of CFA. In this figure, the as-received CFA and its fractions floating for the specific gravities of 1.0, 1.4 and 1.8 were sequentially indicated by (a), (b), (c) and (d). Decreasing cenosphere contents of CFA with increasing specific gravities given by Figure 5.50 can also be visually seen from Figure 5.51 for the as-received CFA and its float products for the specific gravities of 1.0, 1.4 and 1.8.
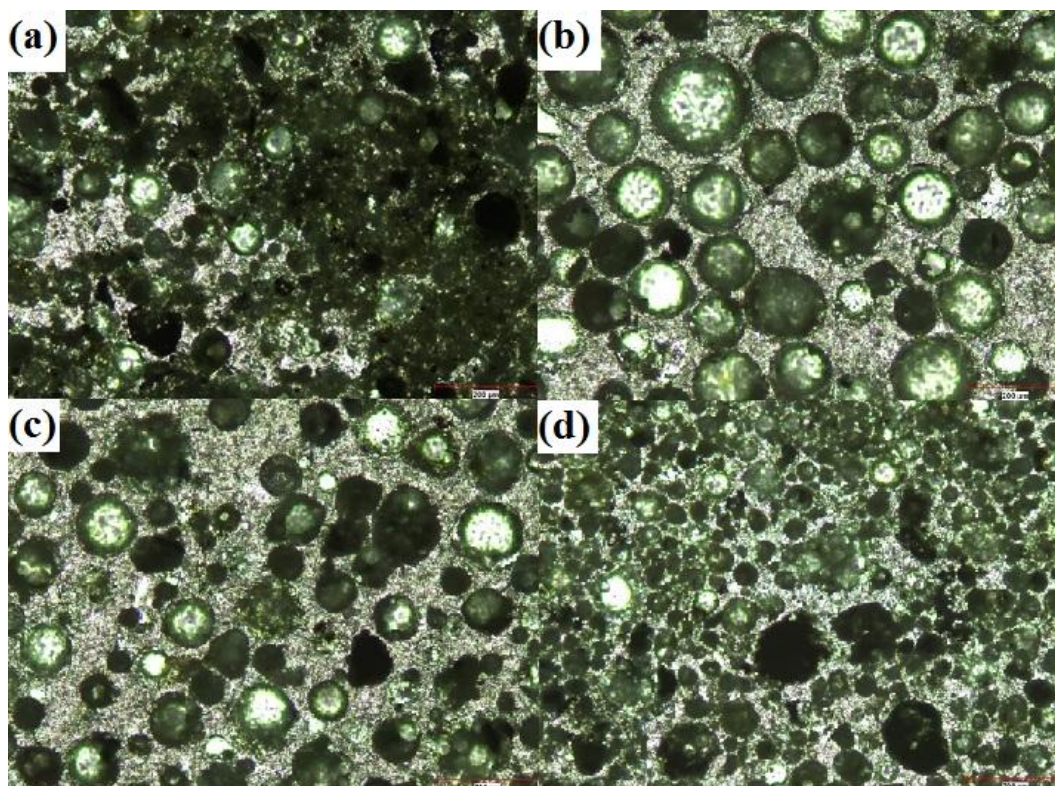
Figure 5. 51 As-received and different float products of CFA sample (HUME Lab.)
(a), (b), (c) and (d) indicate sequentially as-received CFA and its floating fractions for the specific gravities of 1.0, 1.4 and 1.8

Table 5.9 shows the cenosphere contents in the as received and the floating products of CFA based on point and area calculation.

Table 5. 9 Cenosphere contents of CFA as a function of specific gravity

Specific gravity	Cenosphere contents in feed and floating products	
	Point-counting (%)	Area calculation (%)
1.00	91.30	87.30
1.10	77.35	74.92
1.20	59.25	55.85
1.30	49.33	47.37
1.40	43.21	42.16
1.50	38.46	36.93
1.60	33.56	31.86
1.70	28.39	ND*
1.80	25.60	ND*
Feed	**11.30**	**ND***

* Cannot be determined by means of the image analyzer.

As can be seen from Table 5.9, similar cenosphere contents were found by using point-counting and area calculation. However, the cenosphere contents of feed and floating products of 1.70 and 1.80 cannot be

determined with area calculation due to high amount of fine particles. The image analyzer needs separated particles and it was very difficult to separate fine particles from each other due to the electrostatic attraction forces between the fly ash particles. Also, the image analyzer was generally not suitable for the particle size finer than 150 μm.

5.3.1.2 The float-sink experiments conducted with SFA

Figure 5.52 shows yield, grade and recovery of cenosphere in SFA float products as a function of specific gravity ranging from 1.00 to 1.80. Cenosphere contents of the float products were again determined on the basis of point counting. In the same manner as CFA, similar cenosphere contents were obtained by using SFA. However, in this case, especially much lower yields were obtained in comparison to CFA for the respective specific gravity.
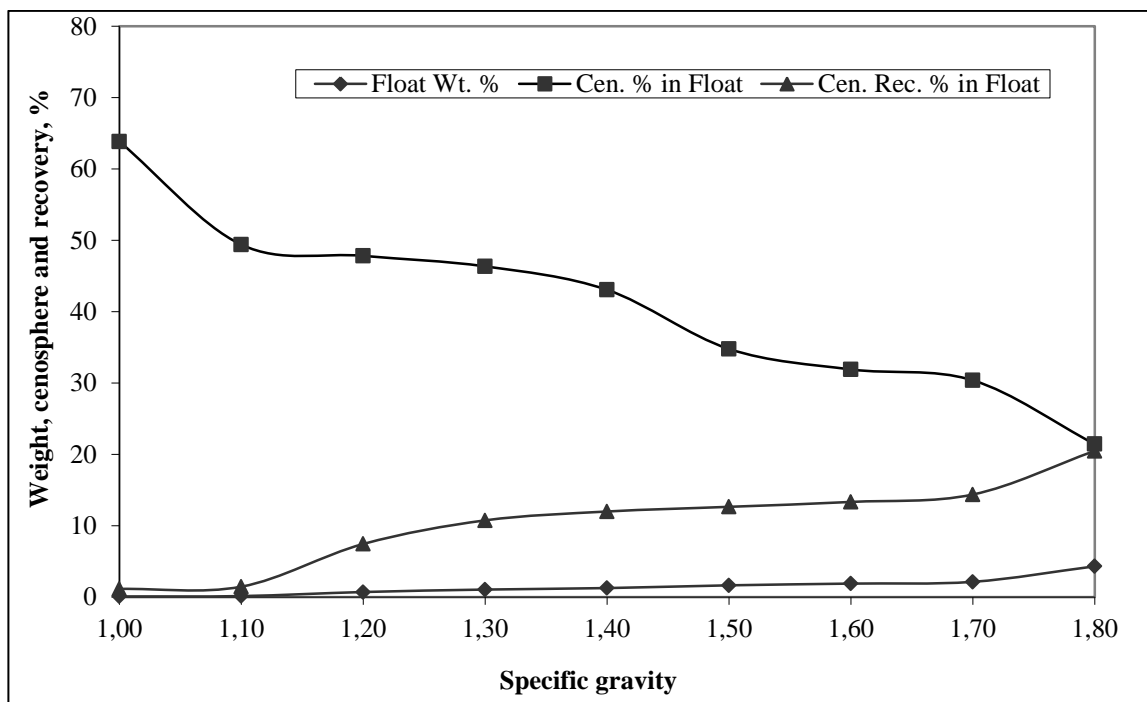

Figure 5. 52 The experimental results of float-sink tests performed with SFA

Figure 5.53 illustrates the images taken from the thin sections of the as-received and different float products of SFA. In this figure, the as-received SFA and its fractions floating for the specific gravities of 1.0, 1.4 and 1.8 were sequentially indicated by (a), (b), (c) and (d). In a similar way to Figure 5.51, decreasing cenosphere contents of SFA with increasing specific gravities given by Figure 5.52 can also be visually seen from Figure 5.53 for the as-received SFA and its floating products for the specific gravities of 1.0, 1.4 and 1.8.

As seen from Figures 5.51 and 5.53, similar variations in cenosphere contents were observed for CFA and SFA samples as a measure of specific gravity. On the other hand, higher particle size of CFA cenospheres compared to SFA can easily be seen from the figures. All of these results are well suited with the ones obtained from the particle size and density measurements of the as received samples. Based on the point-counting calculation, SFA sample originally contains 4.50% cenospheres, which is very low in comparison to CFA cenosphere content. Although similar cenosphere contents were obtained in the float products, SFA sample exhibited very low yields compared to CFA for the respective specific gravity.
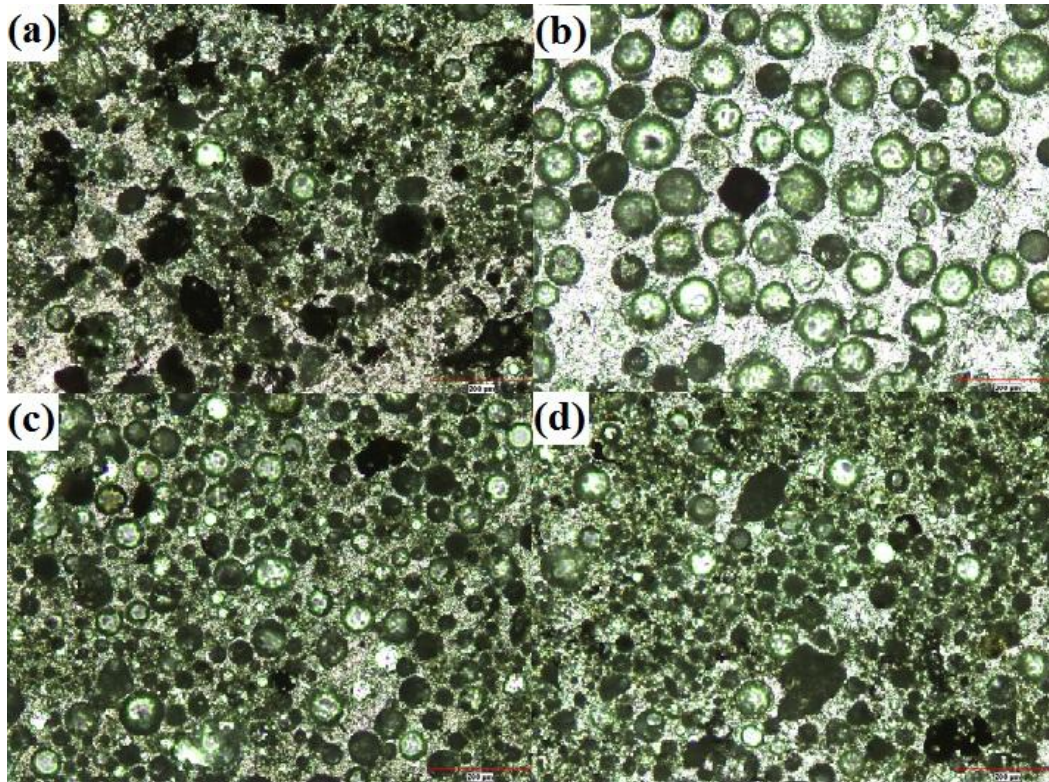
Figure 5. 53 As received and different float products of SFA sample (HUME Lab.)
(a), (b), (c) and (d) indicate sequentially as-received SFA and its floating fractions for the specific gravities of 1.0, 1.4 and 1.8

Table 5.10 shows the cenosphere contents in the as received and the floating products of SFA based on point-counting and area calculation.

Table 5. 10 Cenosphere contents of SFA as a function of specific gravity

Specific gravity	Cenosphere contents in feed and floating products	
	Point-counting (%)	Area calculation (%)
1.00	63.84	66.73
1.10	49.39	53.42
1.20	47.81	47.68
1.30	46.34	44.59
1.40	43.05	41.05
1.50	34.77	35.26
1.60	31.89	ND*
1.70	30.37	ND*
1.80	21.43	ND*
Feed	**4.50**	**ND***

* Cannot be determined by means of the image analyzer.

In a similar way to the results obtained with CFA, Table 5.10 indicates that similar cenosphere contents of SFA were found by using point-counting and area calculation. However, because of the same problem happened in the area base counting of CFA, the cenosphere contents of as-received SFA and its floating products for the specific gravities higher than 1.50 cannot be determined with the image analyzer.

5.3.2 The results of screening tests

5.3.2.1 Wet screening tests conducted with CFA

Figure 5.54 shows the relationship between density and cenosphere contents in CFA as a function of particle size. Recovery values of cenospheres in different size intervals were determined on the basis of point counting. Also, cenosphere contents in cumulative retain products were calculated from the point-counting data. Density measurements were done using helium pycnometer. As seen from the figure, density increased with decreasing particle size whereas more amounts of cenospheres were present in coarse size fractions.
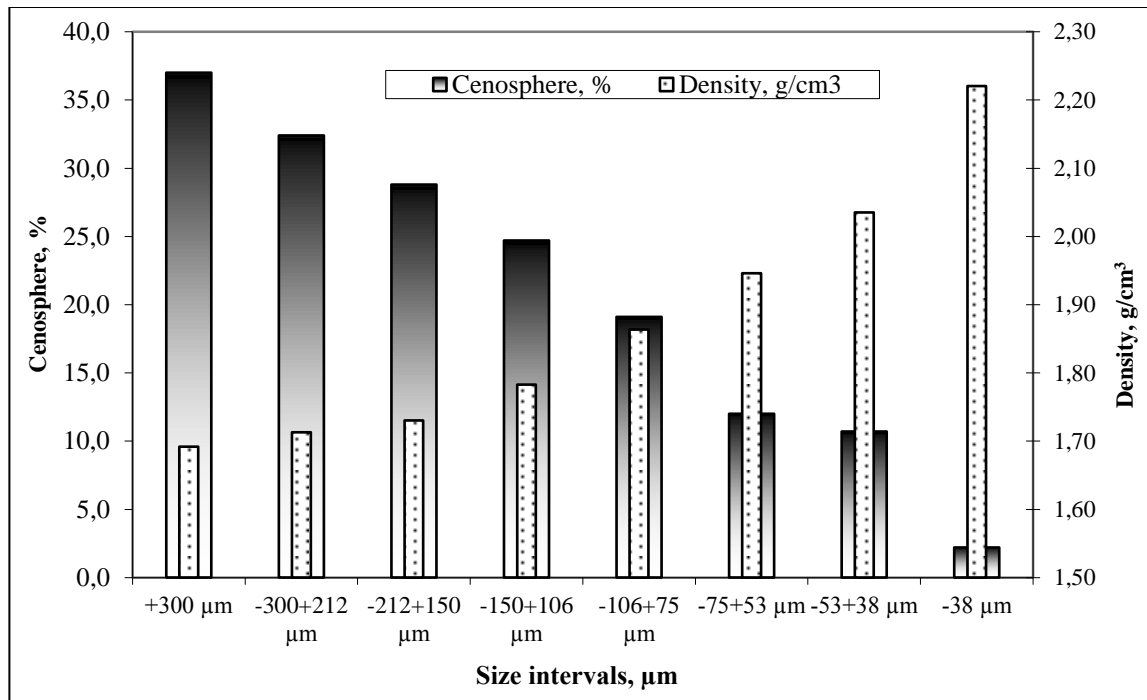
Figure 5. 54 The variations of density and cenosphere contents in CFA as a function of particle size

Figure 5.54 also points out that very low amounts of cenospheres were present in -38 μm size fraction. Yield, cenosphere content and recovery values in CFA based on point-counting for different size intervals are given in Table 5.11. According to this table, cenosphere content of CFA can be concentrated from 11.3% to 21.65% by only using simple screening through 38 μm. As a result of this screening process, only about 10% of the total cenosphere contents would be lost in screen undersize product.

Table 5.11 also shows the cenosphere contents in different size fractions of CFA coarser than 150 μm based on the area calculation. The cenosphere contents in finer fractions cannot be determined by means of the image analyzer due to the same problem occurred in the float-sink tests.

Table 5. 11 Wet screening results of CFA

| Size intervals (μm) | Weight (%) | Cenosphere contents | | Density (g/cm³) | Recovery of cenosphere (%) | Cumulative cenosphere (%) in retain |
		Point (%)	Area (%)			
+300	4.60	37.0	37.79	1.6918	15.06	37.00
-300+212	3.41	32.4	34.92	1.7128	9.78	35.04
-212+150	7.28	28.8	31.27	1.7300	18.55	32.07
-150+106	7.59	24.7	ND*	1.7826	16.59	29.63
-106+75	8.64	19.1	ND*	1.8633	14.60	26.74
-75+53	8.44	12.0	ND*	1.9462	8.96	23.63
-53+38	*7.23*	*10.7*	ND*	*2.0353*	*6.85*	*21.65*
-38	52.81	2.20	ND*	2.2205	10.28	
Original	**100.00**	**11.3**	**ND***	**2.0765**		

* Cannot be determined by means of the image analyzer.

5.3.2.2 Wet screening test results for SFA

Figure 5.55 shows the relationship between density and cenosphere contents in SFA as a measure of different size intervals. In a similar way to CFA, recovery values of cenospheres in different size intervals were again determined on the basis of point counting. In addition, cenosphere contents in cumulative retain products were calculated from the point-counting data. Density measurements were also carried out using helium pycnometer. As seen from Figure 5.55, in the same manner as the screening tests carried out with CFA, density increased with decreasing particle size for SFA, and more amounts of cenospheres were present in the coarse size fractions. However, lower cenosphere contents and higher density values of SFA were obtained compared to CFA for the respective size interval.
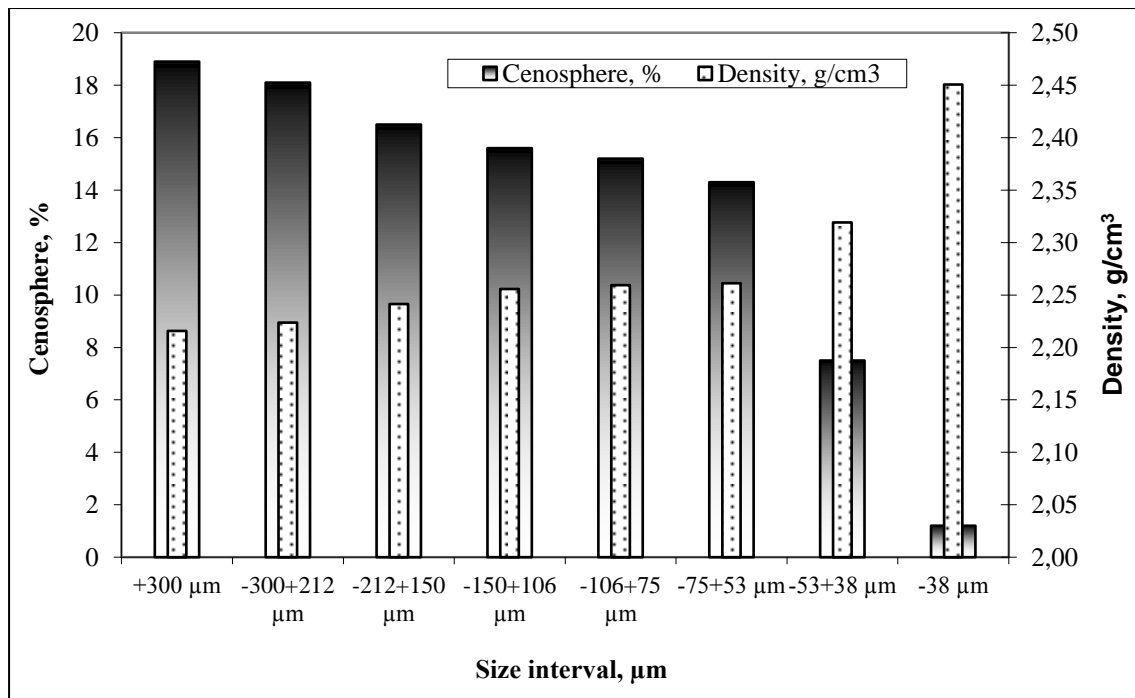

Figure 5. 55 The variations of density and cenosphere contents in SFA as a function of particle size

Figure 5.55 also indicates that very low amounts of cenospheres were present in -38 µm size fraction. Yield, cenosphere content and recovery values in SFA sample based on point-counting for different size intervals are given in Table 5.12. According to this table, cenosphere contents of SFA can be concentrated from 4.5% to 11.83% by using only screening through 38 µm.

Table 5.12 also shows the cenosphere contents in different size fractions of SFA coarser than 150 µm based on the area calculation. Similarly, the cenosphere grades in finer fractions cannot be determined with the use of area method.

Table 5. 12 Wet screening results of SFA

Size intervals (µm)	Weight (%)	Cenosphere contents		Density (g/cm³)	Recovery of cenosphere (%)	Cumulative cenosphere (%) in retain
		Point (%)	Area (%)			
+300	0.59	18.9	16.5	2.2158	2.48	18.90
-300+212	0.16	18.1	16.2	2.2236	0.65	18.73
-212+150	0.36	16.5	15.9	2.2415	1.31	18.01
-150+106	2.77	15.6	ND*	2.2557	9.59	16.29
-106+75	6.97	15.2	ND*	2.2593	23.54	15.59
-75+53	6.65	14.3	ND*	2.2612	21.14	15.10
-53+38	*13.24*	*7.5*	ND*	*2.3192*	*22.07*	*11.83*
-38	69.26	1.2	ND*	2.4508	18.47	
Original	**100.00**	**4.5**	**ND***	**2.3648**	**99.24**	

* Cannot be determined by means of the image analyzer.

5.3.3 The results of air cyclone tests

5.3.3.1 Air cyclone test results of CFA

Figure 5.56 shows the results of air cyclone tests carried out with CFA. In air classification, cenospheres were concentrated in the underflow as expected because this process is mainly based on size rather than density. Cenosphere contents were determined by point-counting and recovery values were calculated on the bases of these measurements. Yields, cenosphere contents and recovery of cenospheres in the CFA underflow products as a function of motor speed and air pressure can be seen from Figure 5.56. As seen from the figure, cenosphere contents in the underflow products increased with increasing air pressure and decreasing motor speed. The highest cenosphere content was obtained for 52 psi of the air pressure and 2400 rpm of the motor speed. At this point, an underflow product containing 25.6% cenospheres was obtained with 62% recovery and 27.4% yield.
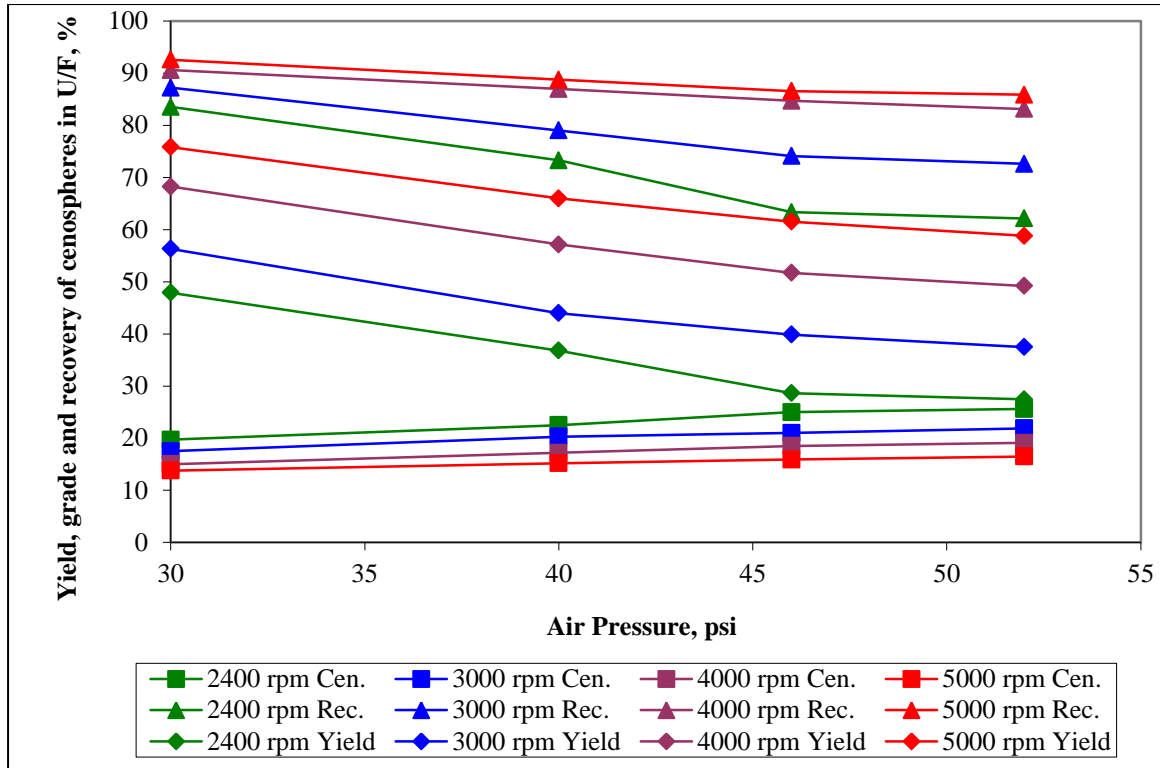
Figure 5. 56 The results of air cyclone tests conducted with CFA

5.3.3.2 Air cyclone test results of SFA

Figure 5.57 shows the results of air cyclone tests conducted with SFA. In the same manner as the air cyclone tests with CFA, cenosphere rich fractions were also concentrated in the underflow products of SFA, and the cenosphere contents were determined using point-counting method. Yields, cenosphere contents and recovery values of the SFA underflow products as a function of motor speed and air pressure can be seen from Figure 5.57. Similar to the air classification tests conducted with CFA, cenosphere contents in the underflow products of SFA increased with increasing air pressure and decreasing motor speed. For the highest air pressure and the lowest motor speed, an underflow product with 13.3% cenospheres was obtained with 22% recovery and 7.5% yield. As a comparison, SFA exhibited much lower yield and recovery in the richest cenosphere product compared to CFA.

110
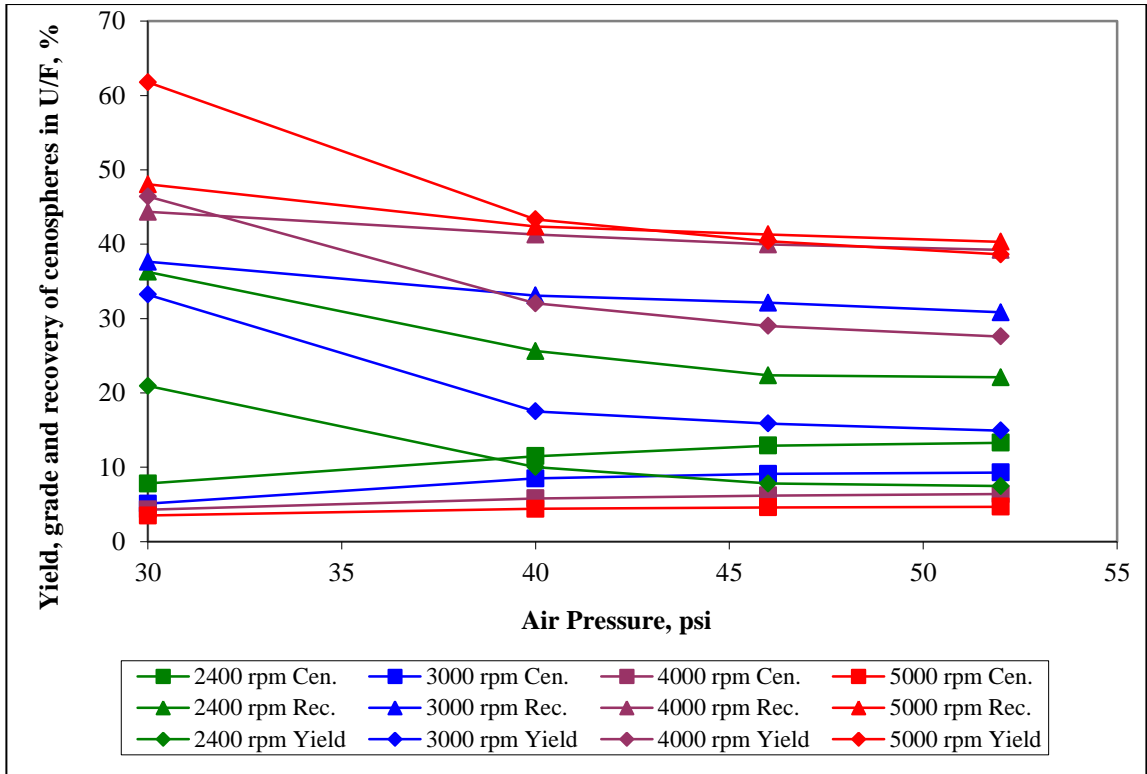
Figure 5. 57 The results of air cyclone tests conducted with SFA

CHAPTER 6

CONCLUSION

In this thesis, two class F fly ashes from Çatalağzı and Sugözü thermal power plants in Turkey were characterized in many ways by using various physical, chemical, microstructural and mechanical tests and analysis, and investigated for their utilization potentials as raw materials in three different fields, namely ceramic industry, construction industry and cenosphere production. In this respect, the fly ash samples were examined for their sintering characteristics, pozzolanic properties and cenosphere contents. The main conclusions obtained from all the experimental studies conducted are summarized as follows:

1. Sintering experiments have shown that Sugözü fly ash gave better results than Çatalağzı fly ash because it provided better microcrystalline structure, higher density and strength with the lower porosity, water absorption and shrinkage values compared to Çatalağzı fly ash. Since CFA and SFA samples have very similar chemical compositions, the differences in SCFA and SSFA were resulted from the differences in physical properties of as-received Çatalağzı and Sugözü fly ashes, such as particle size and porosity. The optimum processing conditions were achieved for 1150°C and 1.5 hours for both samples. For the higher residence time, 15% and 30% decrease in the STS values were observed for SSFA and SCFA, respectively. These strength losses were considered to be resulted from the residual stress development due to the three possible reasons, namely occurrences of crystalline phases from the amorphous glass phase, phase redistributions and the different thermal expansion coefficients of glass, quartz and mullite during sintering. It was understood that physical properties such as densification, porosity and surface condition had more important effects in the strength development in comparison to the increasing mullite content during sintering. Changes in the processing temperatures had a more important effect than those in the residence times on the sintered material properties of both CFA and SFA. As a conclusion, the best overall properties were achieved at the highest processing temperature for both samples. However, the optimization of strength and time should be done carefully to avoid low strengths resulted from the excessive residence time.

2. The following conclusions were drawn from pozzolanic reactivity studies given in three subcategories.

    i. The hydraulic classification technology used to separate ultrafine fractions from the as-received samples was resulted in promising results. The overflow products with average particle sizes of 5.2 μm for CFA and 4.4 μm for SFA were separated from the respective as-received samples with average particle sizes of 39 μm and 21 μm. The ultrafine fraction of CFA (CUFA) was separated with 10.75% yield and 53.28% recovery of -5 μm particles in the overflow product while 17.51% yield and 63.13% recovery were obtained for the ultrafine fraction of SFA (SUFA). Finer particle size could be obtained with this hydraulic classification technology. However, in this case, yield and recovery values would decrease. The results obtained from all the experiments conducted within the scope of classification indicate that the hydraulic classification technology developed at CAER gave good results for the recovery of very fine particles with enhanced chemical compositions in terms of pozzolanic reactivity.

    ii. The mortar tests indicate that CUFA and SUFA provided more than 10% reduction in water demand compared to the control sample for 30% PC replacement. The mortar cubes containing CUFA and SUFA samples exhibited also higher strength development rates after 14 days compared to the ones with as-received samples and PC only. At the end of 112 days, both CUFA and SUFA provided more than 40% increase in compressive strength compared to the control sample for the PC replacement ratios of higher than 20%. As a comparison,

SUFA gave better results than CUFA in both water demand and compressive strength tests. The mortar bars prepared with the both FA and UFA samples exhibited very low shrinkage and expansion values. These values decreased generally with increasing PC replacement ratio especially after 14 days. All of these results point out that compressive strength and dimensional stability will not be a barrier for the utilization of the ultrafine ash fractions as value added pozzolans.

iii. Thermogravimetric (TG) analyses of the paste specimens indicate that both UFA samples exhibited higher pozzolanic reactivity development rates compared to the respective as-received samples especially after 28 days. After 112 days, 68.56% and 62.68% $Ca(OH)_2$ content of PC only pastes were obtained with the pastes containing CUFA and SUFA samples, respectively, corresponding to 11% and 13% more $Ca(OH)_2$ consumptions in reference to the respective as-received samples. According to XRD analyses, portlandite content in PC/UFA pastes decreased significantly after 14 days compared to the PC only paste. These XRD and TG results were in well agreement with the ones obtained from the mortar tests.

All of these classification, mortar and paste experiments indicate that a highly reactive lower cost pozzolan with very fine particle size and high surface area can be produced from Çatalağzı and Sugözü fly ashes using a relatively simple hydraulic classification process.

3. According to the point-counting data, CFA and SFA samples originally contain 11.30% and 4.50% cenospheres, respectively. Results obtained from the float-sink tests and screening analyses point out that cenosphere contents decreased with decreasing size and increasing density for both samples. Based on the float-sink tests, CFA has much more floating products and more cenospheres than SFA for the same density interval. According to the air classification results, cenospheres were concentrated in the underflow products, and their contents increased with increasing air pressure and decreasing motor speed for both samples. All of these tests and analyses suggest that the most efficient cenosphere separation technique among the examined methods was screening. Cenosphere contents of CFA and SFA increased to 21.65% and 11.83%, respectively by only using simple screening through 38 μm. This cenosphere content was obtained with 90% recovery and 47% yield for CFA whereas SFA provided 81% recovery and 30% yield for 11.83% cenosphere content.

REFERENCES

Acar, I. and Atalay, M.U., *Characterization of sintered class F fly ashes*, Fuel, 2012, http://dx.doi.org/10.1016/j.fuel.2012.10.057.

Ahmaruzzaman, M., *A review on the utilization of fly ash*, Progress in Energy and Combustion Science, Vol. 36, pp. 327-363, 2010.

Aineto M., Acosta A., Rincon J.M., Romero, M., *Production of lightweight aggregates from coal gasification fly ash and slag*, World of Coal Ash (WOCA), 2005.

Alcala, J.F.C., Davila, R.M., and Quintero, R.L., *Recovery of cenospheres and magnetite from coal burning power plant fly ash*, Transactions of the Iron and Steel Institute of Japan, Vol. 27, No. 7, pp. 531-538, 1987.

Alkaya, D., *The investigation of fly ash use in soil improvement*, Electronic Journal of Construction Technologies, Vol. 5, No. 1, pp. 61-72, 2009.

Antiohos, S. and Tsimas S., *Investigating the role of reactive silica in the hydration mechanisms of high-calcium fly ash/cement systems*, Cement and Concrete Composites, Vol. 27, pp. 171-181, 2005.

Antiohos, S.K. and Tsimas, S., *Reactive silica of fly ash as an indicator for the mechanical performance of blended cements*, Measuring, Monitoring and Modeling Concrete Properties, Printed in the Netherlands, pp. 403-409, 2006.

ASTM C20, *Standard test methods for apparent porosity, water absorption, apparent specific gravity and bulk density of burned refractory brick and shapes by boiling water*, ASTM International, West Conshohocken, PA, USA, 2005.

ASTM C109, *Standard test method for compressive strength of hydraulic cement mortars (Using 2-in. or [50-mm] cube specimens)*, ASTM International, West Conshohocken, PA, USA, 2011.

ASTM C134, *Test methods for size, dimensional measurements, and bulk density of refractory brick and insulating firebrick*, ASTM International, West Conshohocken, PA, USA, 2005.

ASTM C157, *Standard test method for length change of hardened hydraulic-cement mortar and concrete*, ASTM International, West Conshohocken, PA, USA, 2008.

ASTM C230, *Standard specification for flow table for use in tests of hydraulic cement*, ASTM International, West Conshohocken, PA, USA, 2008.

ASTM C305, *Standard practice for mechanical mixing of hydraulic cement pastes and mortars of plastic consistency*, ASTM International, West Conshohocken, PA, USA, 2012.

ASTM C311, *Standard test methods for sampling and testing fly Ash or natural pozzolans for use in Portland-cement concrete*, ASTM International, West Conshohocken, PA, USA, 2011.

ASTM C326, *Standard test method for drying and firing shrinkages of ceramic whiteware clays*, ASTM International, West Conshohocken, PA, USA, 2003.

ASTM C490, *Standard practice for use of apparatus for the determination of length change of hardened cement paste, mortar, and concrete*, ASTM International, West Conshohocken, PA, USA, 2011.

ASTM C511, *Standard specification for mixing rooms, moist cabinets, moist rooms, and water storage tanks used in the testing of hydraulic cements and concretes*, ASTM International, West Conshohocken, PA, USA, 2009.

ASTM C618, *Standard specification for coal fly ash and raw or calcined natural pozzolan for use in concrete*, ASTM International, West Conshohocken, PA, USA, 2012.

ASTM C1437, *Standard test method for flow of hydraulic cement mortar*, ASTM International, West Conshohocken, PA, USA, 2007.

ASTM D3967, *Standard test method for splitting tensile strength of intact rock core specimens*, ASTM International, West Conshohocken, PA, USA, 2008.

Benavidez, E., Grasselli, C. and Quaranta, N., *Densification of ashes from a thermal power plant*, Ceramics International, Vol. 29, pp. 61-68, 2003.

Bentz, D.P. and Remond, S., *Incorporation of fly ash into a 3-D cement hydration microstructure model*, Building and Fire Research Laboratory, National Institute of Standards and Technology (NIST), Gaithersburg, Marryland, 20899, USA, Report No. NISTIR 6050, 48 pages, 1997.

Biernacki, J.J., Vazrala, A.K. and Leimer, H.W., *Sintering of a class F fly ash*, Fuel, Vol. 87, pp. 782-792, 2008.

Blissett, R.S. and Rowson, N.A., A review of the multi-component utilisation of coal fly ash, Fuel, Vol. 97, pp. 1-23, 2012.

BS EN 450-1, *Fly ash for concrete: Definition, specifications and conformity criteria*, BSI, London, UK, 2005.

BS 3892-1, *Pulverized-fuel ash: Specification for pulverized fuel ash for use with Portland cement*, BSI, London, UK, 1997.

Chandra, N., Sharma, P., Pashkov, G.L., Voskresenskaya, E.N., Amritphale, S.S. and Baghel, N.S., *Coal fly ash utilization: Low temperature sintering of wall tiles*, Waste Management, Vol. 28, pp. 1993-2002, 2008.

Chappex, T. and Scrivener, K., *Alkali fixation of C-S-H in blended cement pastes and its relation to alkali silica reaction*, Cement and Concrete Research, Vol. 42, pp. 1049-1054, 2012.

Cicek, T. and Tanriverdi, M., *Lime based steam autoclaved fly ash bricks*, Construction and Building Materials, Vol. 21, pp. 1295-1300, 2007.

Dunstan, E.R., *How does pozzolanic reaction make concrete "green"*, 2011 World of Coal Ash (WOCA) Conference, 2011.

Erol, M., Küçükbayrak, S. and Ersoy-Meriçboyu, A., *Characterization of coal fly ash for possible utilization in glass production*, Fuel, Vol. 86, pp.706-714, 2007.

Erol, M., Küçükbayrak, S. and Ersoy-Meriçboyu, A., *Characterization of sintered coal fly ashes*, Fuel, Vol. 87, pp. 1334-40, 2008a.

Erol, M., Küçükbayrak, S. and Ersoy-Meriçboyu, A., *Comparison of the properties of glass, glass-ceramic and ceramic materials produced from coal fly ash*, Journal of Hazardous Materials, Vol. 153, pp. 418-425, 2008b.

Electricity Generation Company (EUAS), *Electricity production report*, 2011, (online at: http://www.enerji.gov.tr/yayinlar_raporlar/Sektor_Raporu_EUAS_2011.pdf).

European Coal Combustion Products Association (ECOBA), *Production and utilization of CCPs in 2009 in Europe (EU 15)*, 2010.

European Commission (EC), *Electricity production, consumption and market overview*, Eurostat, September 2012, (available online at: http://epp.eurostat.ec.europa.eu/statistics_explained/index.php/Electricity_production,_consumption_and_market_overview).

Furlani, E., Brückner, S., Minichelli, D. and Mashio, S., *Synthesis and characterization of ceramics from coal fly ash and incinerated paper mill sludge*, Ceramics International, Vol. 34, pp. 2137-2142, 2008.

Gao, P., Lu, X., Lin, H., Li, X. and Hou, J., *Effects of fly ash on the properties of environmentally friendly dam concrete*, Fuel, Vol. 86, pp. 1208-1211, 2007.

German, M.R., *Sintering theory and practice*, Book, Printed by John Wiley & Sons Inc., 550 pages, 1996.

Ghosal, S. and Self, S.A., *Particle size-density relation and cenosphere content of coal fly ash*, Fuel, Vol. 74, No. 4, pp. 522-529, 1995.

Gurupira, T., Jones, J.L., Howard, A., Lockert, C., Wandell, T. and Stencel, J.M., *New products from coal combustion ash: Selective extraction of particles with density < 2*, International Ash Utilization Symposium, Center for Applied Energy Research, University of Kentucky, 2001.

Gutierrez, B., Pazos, C., and Coca, J., *Recovery of gallium from coal fly ash by a dual reactive extraction process*, Waste Management & Research, Vol. 15, pp. 371-382, 1997.

Hanehara, S., Tomosawa, F., Kobayakawa, M. and Hwang, K.R., *Effects of water/powder ratio, mixing ratio of fly ash, and curing temperature on pozzolanic reaction of fly ash in cement paste*, Cement and Concrete Research, Vol. 31, pp. 31-39, 2001.

Helmuth, R., *Fly ash in cement and concrete*, Portland Cement Association, Skokie, IL, USA, 203 pages, 1987.

Hernandez-Exposito, A., Chimenos, J.M., Fernandez, A.I., Font, O., Querol, X., Coca, P., and Garcia Pena, F., *Ion flotation of germanium from fly ash aqueous leachates*, Chemical Engineering Journal, Vol. 118, pp. 69-75, 2006.

Hirajima, T., Petrus, H.T.B.M., Oosako, Y., Nonaka, M., Sasaki, K. and Ando, T., *Recovery of cenospheres from coal fly ash using a dry separation process: Separation estimation and potential application*, International Journal of Mineral Processing, Vol. 95, pp. 18-24, 2010.

http://en.wikipedia.org/wiki/Cenosphere

http://en.wikipedia.org/wiki/File:Fly_Ash_FHWA_dot_gov.jpg

http://en.wikipedia.org/wiki/Pozzolan

http://en.wikipedia.org/wiki/Pozzolanic_reaction

http://iopscience.iop.org, *Automatic Point Counter*, James Swift and Son Ltd., Journal of Scientific Instruments, Vol. 32, pp. 123, 1955.

http://iti.northwestern.edu/cement/

http://mcc.lsu.edu/

http://www.apitco.org/Profiles/Cenospheres%20from%20fly%20ash.pdf

http://www.azom.com/article.aspx?ArticleID=1725

http://www.basf-yks.com.tr

http://www.catestermik.com/index/cates.html

http://www.ce.memphis.edu/1101/notes/concrete/PCA_manual/Chap03.pdf

http://www.cenoash.com/products.htm

http://www.cenosphereindia.com/grades.html

http://www.flyashcenosphereexportindia.com/

http://geoinfo.nmt.edu/staff/hoffman/flyash.html

http://www.ipmd.net/Introduction_to_powder_metallurgy/Sintering

http://www.isken.com.tr/tr/index.asp

http://www.quantachrome.com/

http://testinternational.co.uk/

Hubbard, F.H. and Dhir, R.K., *A compositional index of the pozzolanic potential of pulverized-fuel ash*, Journal of Materials Science Letters, Vol. 3, pp. 958-960, 1984.

Hutchison, C.S., *Laboratory Handbook of Petrographic Techniques*, University of Malaya, Kuala Lumpur, Malaysia, 1974.

Hwang, K., Noguchi, T. and Tomosawa, F., *Prediction model of compressive strength development of fly ash concrete*, Cement and Concrete Research, Vol. 34, pp. 2269-2276, 2004.

Ilic, M., Cheeseman, C., Sollars, C. and Knight, J., *Mineralogy and microstructure of sintered lignite coal fly ash*, Fuel, Vol. 82, pp. 331-336, 2003.

Islam, G.M.S., *Evaluating reactivity and sorptivity of fly ash for use in concrete construction*, Ph.D. Thesis in the Concrete Technology Unit, University of Dundee, 2012.

Iyer, R.S. and Scott, J.A., *Power station fly ash-a review of value added utilization outside of the construction industry*, Resources, Conservation and Recycling, Vol. 31, pp. 217-228, 2001.

Jala, S. and Goyal, D., *Fly ash as a soil ameliorant for improving crop production*, Bioresource Technology, Vol. 97, pp. 1136-1147, 2006.

Kang, S.J., *Sintering: Densification, Grain Growth and Microstructure*, Book, Printed by Butterworth Heinemann, 280 pages, 2004.

Khatib, J.M. and Mangat, P.S., *Influence of superplasticizer and curing on porosity and pore structure of cement paste*, Cement and Concrete Composites, Vol. 21, pp. 431-437, 1999.

Kolay, P.K. and Singh, D.N., *Physical, chemical, mineralogical, and thermal properties of cenospheres from an ash lagoon*, Cement and Concrete Research, Vol. 31, pp. 539-542, 2001.

Kruger, R.A., *The use of cenospheres in refractories*, Energeia, Vol. 7, No. 4, 1996.

Langan, B.W., Weng, K., and Ward, M.A., *Effect of silica fume and fly ash on heat of hydration of Portland cement*, Cement and Concrete Research, Vol. 32, pp. 1045-1051, 2002.

Li, T.X., Jiang, K., Neathery, J.K. and Stencel, J.M., *Triboelectrostatic process of combustion fly ash after carbon burnout*, International Ash Utilization Symposium, Center for Applied Energy Research, University of Kentucky, 1999.

Lilkov, V., Dimitrova, E. and Petrov, O.E., *Hydration process of cement containing fly ash and silica fume: The first 24 hours*, Cement and Concrete Research, Vol. 27, pp. 577-588, 1997.

Lingling, X., Wei, G., Tao, W. and Nanru, Y., *Study on fired bricks with replacing clay by fly ash in high volume ratio*, Construction and Building Materials, Vol. 19, pp. 243-247, 2005.

Lu, G.Q. and Do, D.D., *Adsorption properties of fly ash particles for NOx removal from flue gases*, Fuel Processing Technology, Vol. 27, pp. 95-107, 1991.

Mangialardi, T., *Sintering of MSW fly ash for reuse as a concrete aggregate*, Journal of Hazardous Materials, Vol. 87, pp. 225-239, 2001.

Naik, T.R., Ramme, B.W. and Tews, J.H., *Use of high volumes of class C and class F fly ash in concrete*, Cement, Concrete and Aggregates, Vol. 16, pp. 12-20, 1994.

Nisnevich, M., Sirotin, G., Eshel, Y. and Schlesinger, T., *Structural lightweight concrete based on coal ashes (containing undesirable radionuclides) and waste of stone quarries*, Magazine of Concrete Research, Vol. 58, pp. 233-241, 2006.

Nochaiya, T., Wongkeo, W. and Chaipanich, A., *Utilization of fly ash with silica fume and properties of Portland cement-fly ash-silica fume concrete*, Fuel, Vol. 89, pp. 768-774, 2010.

Paya, J., Monzo, J., Peris-Mora, E., Borrachero, M.V., Tercero, R. and Pinillos, C., *Early-strength development of Portland cement mortars containing air classified fly ashes*, Cement and Concrete Research, Vol. 25, pp. 449-456, 1995.

Paya, J., Monzo, J., Borrachero, M.V., Peris-Mora, E. and Amahjour, F., *Mechanical treatment of fly ashes: Part IV. Strength development of ground fly ash-cement mortars cured at different temperatures*, Cement and Concrete Research, Vol. 30, pp. 543-551, 2000.

Perez-Lopez, R., Nieto, J.M. and Almodovar, G.R., *Utilization of fly ash to improve the quality of the acid mine drainage generated by oxidation of a sulphide-rich mining waste: Column experiments*, Chemosphere, Vol. 67, pp. 1637-1646, 2007.

Petrus, H.T.B.M., Hirajima, T., Oosako, Y., Nonaka, M., Sasaki, K. and Ando, T., *Performance of dry-separation processes in the recovery of cenospheres from fly ash and their implementation in a recovery unit*, International Journal of Mineral Processing, Vol. 98, pp. 15-23, 2011.

Querol, X., Moreno, N., Umana, J.C., Alastuey, A., Hernandez, E., Lopez-Soler, A. and Plana, F., *Synthesis of zeolites from coal fly ash: an overview*, International Journal of Coal Geology, Vol. 50, pp. 413-423, 2002.

Rahaman, M.N., *Sintering of ceramics*, Book, Printed by Taylor & Francis Group LLC, 388 pages, 2008.

Ramamurthy, K. and Harikrishnan, K.I., *Influence of binders on properties of sintered fly ash aggregate*, Cement and Concrete Composites, Vol. 28, pp. 33-38, 2006.

Ramme, B.W., Noegel, J.J. and Rohatgi, W.B., *Separation of cenospheres from fly ash*, United States Patent Application Publication, No. US 2008/0190327 A1, 2008.

Rathbone, R., Robl, T., McCabe, M. and Tapp, K., *The effect of hydraulically classified ultrafine ash on mortar properties*, Cement Combinations for Durable Concrete Proceedings of the International Conference, University of Dundee, Scotland, UK, pp. 65-70, 2005.

Rathbone, R.F., *Superpozzolanic concrete for sustainable construction and CO_2 emissions reduction*, Project, University of Kentucky, Center for Applied Energy Research, 2004.

Robl, T.L. and Groppo, J.G., *Method for hydraulically separating carbon and classifying coal combustion ash*, United States Patent (Patent No: US 7,963,398 B2), 2011.

Robl, T.L. and Groppo, J.G., *Technology and methodology for the production of high quality polymer filler and super-pozzolan from fly ash,* United States Patent (Patent No: US 6,533,848 B1), 2003.

Siddique, R., *Performance characteristics of high-volume Class F fly ash concrete*, Cement and Concrete Research, Vol. 34, pp. 487-493, 2004.

Stevens, W., Robl, T. and Mahboub, K., *The cementitious and pozzolanic properties of fluidized bed combustion fly ash*, World of Coal Ash (WOCA) Conference, Lexington, KY, USA, 2009.

The American Coal Ash Association (ACAA), *2010 coal combustion product (CCP) production & use survey report*, 2011.

TS, *The regulation of hazardous waste in Turkish standard: Appendix 11-A. Storage criteria of solid wastes*, 2005.

TS EN 12457-4, *Characterization of waste-leaching-compliance test for leaching of granular waste materials and sludge: Part 4. One stage batch test at a liquid to solid ratio of 10 L/kg for materials with particle size below 10 mm*, Turkish Legislation for Standardization, 2004.

Tsuboi, I., Kunugita, E. and Komasawa, I., *Recovery and purification of boron from coal fly ash*, Journal of Chemical Engineering of Japan, Vol. 23, pp. 480-485, 1990.

Tsuboi, I., Kasai, S., Kunugita, E. and Komasawa, I., *Recovery of gallium and vanadium from coal fly ash*, Journal of Chemical Engineering of Japan, Vol. 24, pp. 15-20, 1991.

Tuzcu, E.T., *Removal of heavy metals in waste water by using coal fly ash*, Ms. Thesis at Middle East Technical University, 2005.

Tütünlü, F., *The utilization of fly ash in manufacturing of building bricks*, Ms. Thesis at Middle East Technical University, 2000.

US Energy Information Administration (USEIA), *EIA's latest short-term energy outlook for electricity*, 2012, (available online at: http://www.eia.gov/electricity/).

Uzal, B., Turanlı, L., Yücel, H., Göncüoğlu, M.C. and Çulfaz, A., *Pozzolanic activity of clinoptilolite: A comparative study with silica fume, fly ash and a non-zeolitic natural pozzolan*, Cement and Concrete Research, Vol. 40, pp. 398-404, 2010.

Vassilev, S.V., Menendez, R., Alvarez, D., Diaz-Somoano, M., and Martinez-Tarazona, M.R., *Phase-mineral and chemical composition of coal fly ashes as a basis for their multicomponent utilization*, Fuel, Vol. 82, pp. 1793-1811, 2003.

Vassilev, S.V., Menendez, R., Diaz, M., and Martinez, M.R., *Phase-mineral and chemical composition of coal fly ashes as a basis for their multicomponent utilization*, Fuel, Vol. 83, pp. 585-603, 2004.

Vassilev, S.V. and Vassileva, C.G., *A new approach for the classification of coal fly ashes based on their origin, composition, properties and behavior*, Fuel, Vol. 86, pp. 1490-1512, 2007.

Wandell, T., *Cenospheres, from wastes to profits*, American Ceramic Society Bulletin, Vol. 75, pp. 3, 1996.

Winter, N., *Understanding Cement*, the e-book, WHD Microanalysis Consultants Ltd., 2005, (available online at: http://www.understanding-cement.com).

Xenidis, A., Mylona, E. and Paspaliaris, I., *Potential use of lignite fly ash for the control of acid generation from sulphidic wastes*, Waste Management, Vol. 22, pp. 631-641, 2002.

Yamamoto T., Kanazu T., Nambu, M. and Tanosaki, T., *Pozzolanic reactivity of fly ash – API method and K-value*, Fuel, Vol. 85, pp. 2345-2351, 2006.

Yilmaz, A., *Relationship between compressive and chemical compositions of Portland and pozzolanic cements*, BAÜ Fen Bil. Enst. Dergisi, Vol. 5, No. 2, pp. 4-13, 2003.

Yoon, R.H., *Chapter 5: Triboelectric charging of coal and quartz by turbocharger*, Monpilai Hangsubcharoen, e-book, pp. 193-224, 1999, (available online at: http://scholar.lib.vt.edu/theses/available/etd-042999-164825/unrestricted/CH5.PDF)

Zeng, Q., Li, K., Fen-chong, T., and Dangla, P., *Determination of cement hydration and pozzolanic reaction extents for fly ash cement pastes*, Construction and Building Materials, Vol. 27, No. 1, pp. 560-569, 2012.

PERSONAL INFORMATION

Surname, Name: Acar, İlker
Nationality: Turkish (T.C.)
Date and Place of Birth: 14 July 1980, Bursa, Turkey
Marital Status: Single
Phone : +90 312 210 58 16
Fax : +90 312 210 58 22
Email : ailker@metu.edu.tr, acarilker16@gmail.com

EDUCATION

Degree	Institution	Year of Graduation
BS	Kocaeli University, Kocaeli, Turkey Faculty of Engineering, Department of Environmental Engineering GPA: 3.31 (Honor Student)	2003
High School	Demirtaşpaşa Technical High School, Department of Industrial Electronic	1997

WORK EXPERIENCE

Year	Place	Enrollment
2003-Present	Middle East Technical University Department of Mining Engineering Ankara, Turkey	Research Assistant
2011-2012	University of Kentucky Center for Applied Energy Research Environmental and Coal Tech. Group Lexington, KY, USA	Visiting Researcher
August, 2002	Bursa Metropolitan Municipality Wastewater Treatment Plant Bursa, Turkey	Summer Practice

July, 2002	Bursa Metropolitan Municipality Drinking Water Treatment Plant Bursa, Turkey	Summer Practice
August, 2001	Bursa Environmental and Urban Development Institution Bursa, Turkey	Summer Practice
1996-1997	Oyak Renault Car Factory Bursa	High School Internship

FOREIGN LANGUAGES

- English

PUBLICATIONS

BOOKS

- Gülsün M., Özün S., Sivrikaya O., Lüle M., Aydın G., Kaya R., Acar C., **Acar İ.**, Pekpak E., Sözeri H., Camalan M., Çırak, M., *"Mineral Processing Laboratory Manual",* METU Printing House, Ankara, Turkey, 2010.

ARTICLES (published in peer reviewed journals covered by SCI, SSCI, AHCI or other indices core lists)

- **Acar, I.** and Atalay, M.U., *Characterization of sintered class F fly ashes*, Fuel, 2012, http://dx.doi.org/10.1016/j.fuel.2012.10.057 (In Press).

PAPERS (presented at published in the proceedings of refereed international congress and symposiums regularly held by international organizers)

1. **Acar, I.**, Atalay, M.U., *Sintering characteristics of the two bituminous coal fly ashes*, XIV. Balkan Mineral Processing Congress, Vol. 1, pp. 420-424, 2011, Tuzla, Bosna Herzegovina.

2. Sivrikaya, O., **Acar, I.**, Atalay, M.U., *Cleaning possibility of Çırpılar coal for power plant feed*, Proceedings of The XIII Balkan Mineral Processing Congress, pp. 333-336, Edited by Krausz S., Ciobanu L., Cristea N., Ciocan V., Cristea G., Bucharest-Romania, 14-17 June 2009.

3. **Acar, I.**, Sivrikaya, O., Atalay, M.U., *Washability charecteristic of Mihalıççık coal*, Proceedings of 11th International Mineral Processing Symposium, pp. 719-725, Edited by Özbayoğlu G., Arol A.İ., Hoşten Ç., Atalay Ü., Belek-Antalya, Turkey, 21-23 October 2008.

ACADEMIC AWARDS

1. *Academic Course Performance Award in Ph.D. Education*, Department of Mining Engineering, Middle East Technical University, 2007.

2. *Honor student in Undergraduate Education*, Department of Environmental Engineering, Kocaeli University, 2003.

SCHOLARSHIPS

1. TUBİTAK-BİDEB, *2214-Yurt Dışı Araştırma Bursu*, Visiting Scholar, Center for Applied Energy Research (CAER), University of Kentucky, 9-month, December 2011-September 2012.

2. TÜRK EĞİTİM VAKFI, *Successful student scholarship*, Undergraduate Student, Department of Environmental Engineering, Kocaeli University, 4-year, 1999-2003.